Summer 2010

Fluvial erosion measurements of streambank using Photo-Electronic Erosion Pins (PEEP)

Fabienne Bertrand
University of Iowa

FLUVIAL EROSION MEASUREMENTS OF STREAMBANK USING PHOTO-ELECTRONIC EROSION PINS (PEEP)

by

Fabienne Bertrand

A thesis submitted in partial fulfillment
of the requirements for the Master of
Science degree in Civil and Environmental Engineering
in the Graduate College of
The University of Iowa

July 2010

Thesis Supervisor: Professor Athanasios N. Papanicolaou

Graduate College
The University of Iowa
Iowa City, Iowa

CERTIFICATE OF APPROVAL

_____

MASTER'S THESIS

_____

This is to certify that the Master's thesis of

Fabienne Bertrand

has been approved by the Examining Committee
for the thesis requirement for the Master of Science
degree in Civil and Environmental Engineering at the July 2010 graduation.

Thesis Committee:

_____
Athanasios N. Papanicolaou, Thesis Supervisor

_____
William Eichinger

_____
Paul Hanley

To my parents

Do not be afraid, I am your shield; your reward shall be very great.

Genesis 15:1

ACKNOWLEDGMENTS

First and foremost, I would like to thank God for His grace and blessings during this journey. He has granted me with the adequate talents and abilities to be successful. I thank my parents for investing so much in my education and for always pushing me to go beyond my limits. I want to express my gratitude to my research advisor Dr Thanos Papanicolaou for his guidance, criticism, extensive support for the success of this project. During my stay at IIHR, Dr Papanicolaou helped me to grow as an engineer, develop my critical thinking, and to seek for high quality research. I extend my thanks to my thesis committee members Drs William Eichinger and Paul Hanley for dedicating their valuable time in completing this project. Dr Christopher Wilson has devoted his time on this project. For this I am grateful.

The cooperation of local farmers in South Amana and the Beeghly-Farrell families have devoted their lands for this bank erosion study. Without their cooperation, this study would have not been possible. Finally, I thank my family and friends for their support during my stay at the University of Iowa. Last, but not least, I thank my Sediment Transport's family who devoted their expertise and assistance in the field work including the following: Kevin Denn, Ken Wacha, and Tommy Sutarto.

TABLE OF CONTENTS

LIST OF TABLES

LIST OF FIGURES

LIST OF NOMENCLATURE

º	Angle in degree
ºC	Celcius
CL	Median
DIFF	Differential
DL	Data logger
E	Fluvial bank-erosion rate
HB	Half bridge
L	Erosion length for photovoltaic PEEP
LB	Left bank
LL	Lower limit
M	Erodiblity coefficient
m	Exponent
R^2	Coefficient of determination
RB	Right bank
R_{pp}	Photovoltaic ratio
SE	Single-ended
UL	Upper limit
x	Ratio between voltage of measuring PEEP over voltage of reference PEEP
y	Erosion length for photo-resistance PEEP
τ_{cr}	Critical shear stress
τ_s	Shear stress

CHAPTER 1. INTRODUCTION

1.1 Study rationale

Bank erosion causes significant damage in infrastructure (e.g., bridge crossings, pipes), which is estimated to be nearly $1.1 billion in the Midwest during the last decade (Papanicolaou et al., 2008). Bank erosion, also, results to losses of fertile agricultural soil with averaged loss rates of about 0.5 ft/yr (Thoma et al., 2005). In Iowa, bank erosion has been exacerbated by the conversion of nearly 80% of prairies to agricultural fields (Burkart et al., 1994), which resulted to increased streambank failure and channel downcutting both of which contribute to half of the annual sediment load in a typical mid-size, Midwestern river (stream that is ~100 ft wide) (Schilling and Wolter, 2000). Along the same lines, Odgaard (1987) reported that 40% of the suspended sediments found in streams came from the riverbanks.

Increased bank erosion can also have deleterious effects on the stream water quality and residential fish species. Excessive streambank erosion is associated with large amounts of suspended sediments which block light penetration, affect the photosynthesis process, and lead to ecosystem food reduction(Yusoff, 1989). In a nutshell, bank erosion constitutes an intricate physical, socio-economical, and ecological problem requiring an improved understanding of the key processes governing bank erosion. This improved understanding can lead to the development of new technology for performing improved monitoring and policies which are needed for minimizing loss of land, agriculture productivity, and damage in infrastructure.

1.2 Critical Literature Review of Streambank erosion processes

Naturally, much research has already been devoted to bank erosion. These contributions include a number of excellent (Grissinger, 1982; Lawler, 1993b; Lawler et al., 1997b; Thorne, 1982). A comprehensive literature review has been recently carried out by Papanicolaou et al. (2006) and Thorne (1982).

As result of this review, a comprehensive list of all papers dealing with river banks is compiled in Figure 1.1. Figure 1.1 outlines the available literature, by plotting the numbers of papers divided for 4 main topic categories as function of years of publication. These 4 main categories, namely, "mass erosion and bank stability" and "fluvial erosion", "vegetation", and "others" are described below in some detail.

1.2.1 Mass erosion and bank stability category

Several authors (Casagli et al., 1999; Harmel et al., 1999; Hooke, 1979; Lindow et al., 2009; Simon et al., 2000; Thorne, 1980) have investigated the role of mass and fluvial bank erosion processes, although most of the observations are limited to non-cohesive bank soils, lack continuous data recordings, and are of limited scale.

Mass failure or known interchangeably as mass wasting is defined as the process triggered by the collective action of gravity and fluid forces (e.g.,Thorne and Tovey (1981), Duan (2005)) and mainly occurs during and right after the recession of high flow events. For this reason, Duan (2005), among others, have correlated the frequency of mass failure to the frequency of floods. Millar and Quick (1998) depicted mass failure as the process when blocks of materials collapse ("en masse" failure). According to Millar and Quick (1998) slumps of bank soil collapse when a critical bank height is exceeded. Later, Papanicolaou et al. (2007) has suggested that for mass failure to occur not only the bank critical height should be reached or surpassed but also the bank angle with the stream bed must be greater than a critical value (Figure 1.2). Mass failure has been predominantly found to occur at the bank crest (Papanicolaou et al., 2006) although during high flow events severe bank toe undercutting can lead to the destabilization of the upper bank.

Bank stability literature classifies into two groups: granular loose material; and cohesive material.

Granular loose material stability is modeled using the threshold channel profile approach. The most commonly used method for analyzing the threshold channel profile is the tractive force approach given by Glover and Florey (1951), which results in a cosine profile. Parker (1978), Ikeda et al. (1988), and Pizzuto (1990) also endorsed the cosine profile. On the other hand, Mironenko et al. (1984) proposed a parabolic profile and the exponential profile was put forward by Ikeda (1981), Diplas (1990), and Diplas and Vigilar (1992). More investigations on mobile-bed channels are reported elsewhere (Cao and Knight, 1997; 1998; Ikeda and Izumi, 1991; Parker, 1979; Yu and Knight, 1998). An experimental study was carried out by Stebbings (1963).

Bank stability of cohesive riverbanks depends on numerous controlling variables such as soil properties and structure (Arulanandan, 1975; Van Klaveren and McCool, 1998), soil moisture conditions (Simon et al., 2000), and complex electrochemical forces between cohesive particles and flow and vegetation (Pizzuto et al., 2010; Wynn and Mostaghimi, 2006). Therefore, stability analysis of cohesive banks is a challenge. Little knowledge is available about the complex electrochemical forces between cohesive particles and the water flow.

1.2.2 Fluvial erosion category

Compared to mass failure which is mostly triggered by high flow events, fluvial entrainment is a continuous process and commences when the hydraulic forces exceed in magnitude the resistance force (Millar and Quick, 1998; Papanicolaou et al., 2007). For non-cohesive soils the resistance force is dependent on the submerged weight and friction angle (angle of repose) and for cohesive soils is function of the cohesion strength (Papanicolaou et al., 2007; Thorne and Tovey, 1981).

Fluvial erosion, comparatively to mass failure results to less erosion on an event scale (measured in terms of sediment mass per area per unit time) and for this reason has received much less attention compared to mass failure. There has been recently a

recognition that mass failure is strongly affected by other processes, including, fluvial erosion. As fluvial erosion at the toe bank takes place with the continuous removal of bank material, a change in the bank slope occurs with bank overdeepening and alteration of the bank angle. Similar effects have been encountered with the formation of cantilevers (Duan, 2005; Papanicolaou et al., 2007).

Cohesive banks at the crest are more resistant to fluvial entrainment unless they have been through subaerial processes (e.g. freeze-thaw cycle) which weaken the soil strength (Thorne and Tovey, 1981; Wolman, 1959). Most likely, fluvial erosion is predominant at the lower portion of the bank which is subject to the significant excess or apparent shear stress at the toe (Fox et al., 2007; Prosser et al., 2000; Simon and Collison, 2001). In summary, the seasonal contributions of fluvial erosion on sediment yield, however, can be significant over time and thus fluvial erosion should be considered in bank stability analyses (Papanicolaou et al., 2007; Thorne and Tovey, 1981).

1.2.3 Vegetation

The removal of the riparian vegetation affects the bank soil properties (e.g., moisture, porous structure) and reduces the critical erosional strength of soil by a factor of 3 making the bank soil more susceptible to the action of the hydraulic forces (i.e., drag and lift forces) (Millar, 2000; Papanicolaou and Hilldale, 2001). It is the pioneering work of Wolman (1959) which demonstrated the interconnection between bank vegetation and soil properties. The modification of the vegetation patterns affects the soil properties of banks (such as soil wetness) and makes the impacts of the freeze/thaw cycle (discussed in section 1.2.4) on the reduction of soil strength more pronounced (Van Klaveren and McCool, 1998). Figure 1.3 shows cantilever blocks reinforced by the presence of roots in the Cecina River (Italy).

1.2.4 Other processes

Subaerial processes (e.g. frost/thaw cycle, swelling, soil moisture) are processes which profoundly influence directly or indirectly the erosion activity at the banks (Wolman and Brush, 1959). Mass failure is also triggered by temporal changes in pore water pressures within the bank soil continuum (Hooke, 1979). Reduction in pore water suction and loss of the river confining pressure during sudden recession of the hydrograph undermines bank strength with the introduction of seepage stresses (Casagli et al., 1999).

Subaerial processes (illustrated in Figure 1.4 and Figure 1.5) have significant contribution to bank retreat starting from the midsection of the bank and extending to the bank crest (Lawler et al., 1999). The last two decades, subaerial processes have gained a lot of attention. Several investigations (Couper and Maddock, 2001; Lawler, 1993a; Prosser et al., 2000; Wynn and Mostaghimi, 2006) have been devoted to the subject. Van Klaveren and McCool (1998) reported that freeze/thaw cycle can significantly reduce the critical erosion strength in some cases by a factor of 10. In summary, subaerial processes are mainly seen as preparatory processes which makes the bank vulnerable to fluvial entrainment or/and mass-wasting processes.

1.3 Research focus of this thesis

Based on the critical literature review performed earlier, it became apparent that less attention has been given on fluvial erosion of cohesive soil banks comparatively to other processes. The focus of this research is on fluvial erosion of cohesive river banks, which is a topical issue for most of the streams in the Midwest. There are several challenges associated with the determination of the rate of cohesive bank fluvial erosion with the most notable being the determination of the critical erosional strength (which is a surrogate measure of soil cohesion strength), the limited number of continuous field

observations pertinent to fluvial erosion, and lastly, the determination of the bed shear stress magnitude exerted by the flow on the bank profile.

The rate of fluvial erosion at a bank is related to the excess shear stress (Arulanandan et al., 1980; Partheniades and Kennedy, 1966):

$$E = M\left(\frac{\tau_s}{\tau_{cr}} - 1\right)^m \tag{1.1}$$

where E denotes the fluvial bank-erosion rate (Kg/m^2/s), M is defined as the erodibility coefficient and has the same units as E, τ_s (Pa), and τ_{cr} (Pa). Similar to τ_{cr}, M also depends upon the sediment properties affecting interparticle forces (e.g., bulk density, sediment composition, organic content, soil age). Both M and τ_{cr} are known in the literature as erodibility parameters and are site-specific (Kandiah, 1974). The exponent m is generally considered unity (van Ledden et al., 2004).

To accurately estimate bank erosion rate, one needs to accurately predict the critical shear stress τ_{cr}. For cohesive materials, the critical shear stress is difficult to be predicted (Lawler et al., 1997a), depends on the soil composition (e.g. clay and organic matter content), and it is difficult to be directly estimated. Little information is available in the literature about the erodibility behavior of cohesive soils which depends on the hydrodynamics forces, electrochemical forces between particles and flows, as well as the biological forces (Papanicolaou et al., 2006). Also errors (which can be significant) are introduced in the prediction of the side-wall shear stress τ_s by using the uniform flow approximation. Little progress (Papanicolaou and Hilldale, 2002; Roca et al., 2009; Tamburrino and Gulliver, 1999) is done to incorporate into the bank erosion models the induced action of the turbulent flow structure on the bank fluvial erosion.

Major efforts should be devoted for methods to directly estimate the rate of fluvial erosion. This will minimize the sources of errors induced by the parameters used in equation 1.1. The following sections elaborate further on some of these issues and

provide insight into the available methods (i.e., analytical, experimental, and field) used to quantify fluvial erosion of cohesive banks and pending research needs.

1.3.1 Laboratory observations of the rate of fluvial erosion E

The erosional strength of a soil, has been measured using annular (rotating) or straight flumes (Aberle et al., 2003; Hilldale, 2001; Lau et al., 2001; McNeil et al., 1996; Mitchener and Torfs, 1996; Parchure and Mehta, 1985; Roberts et al., 2003; Westrich et al., 1997; Zreik et al., 1998), a rotating cylinder (Arulanandan, 1975), and a specialized jet device (Tolhurst et al., 1999). A detailed review of these devices can be found in Black and Paterson (1997) and is beyond the scope of this thesis. Tests have been conducted *in situ* and *ex situ*, and researchers have compared effects of compaction, clay/sand proportions, clay type, organic content, pH, salinity, flora and fauna, and various other chemical and compositional parameters. In general, in situ flumes may be subdivided into two groups: (1) benthic re-circulating flumes (Amos et al., 1992; Black and Cramp, 1995; Houwing and van Rijn, 1998; Maa et al., 1993; Pierce et al., 1970; Widdows et al., 1998) and benthic straight flow-through flumes (Aberle et al., 2003; Gust and Morris, 1989; Ravens and Gschwend, 1999; Young, 1977), and (2) miscellaneous devices (Paterson, 1989; Schünemann and Kühl, 1993).

1.3.2 Analytical work

Analytical work complemented with experimental measurements has focused on the estimation of τ_s (Pa). Most of the available studies provided a correction for the side wall shear stress by accounting for the effects of secondary currents on the shear stress distribution. Guo and Julien (2005) have introduced a relationship to estimate the side-wall shear stress that is applicable to a rectangular channel cross-sections. Later, Papanicolaou et al. (2007) has proposed a more general approach with can be applied to estimate the side-wall shear stress for non-prismatic channels. Duan (2005) has also suggested an analytical approach to estimate the rate of bank retreat associated to the

coupled effect of mass failure and fluvial erosion. Fluvial erosion was treated with a probabilistic approach and bank retreat was considered to occur when fluvial entrainment rate is greater than deposition rate.

1.3.3 Field measurements

1.3.3.1 Conventional methods

Erosion pins and repeated cross-sectional survey techniques are the most conventional methods used to directly estimate fluvial entrainment rates (Lawler, 1993b) at a site. Erosion pins are most likely used for short-term scale studies. The technique has been employed for decades (Wolman, 1959) and remains a popular approach as it is cheap and easily operable. Typically, the pins are combined with stage data to estimate streambank fluvial erosion magnitude (Casagli et al., 1999; Hooke, 1979; Hooke, 1980; Wolman, 1959). This technique has also been used to investigate the effect of freezing and thawing cycle on bank stability (Lawler, 1993a), and other subaerial processes (Prosser et al., 2000). Erosion pins are usually combined with other techniques such as repeated cross-section surveys, aerial photographs or more advanced techniques such as Photo-electronic erosion pins to estimate fluvial erosion rates and/or deposition rates at a study site (Bartley et al., 2008; Couper et al., 2002; Couper and Maddock, 2001; Hancock et al., 2010; Keesstra et al., 2009; Lawler et al., 1999; McDermott and Sherman, 2009; Mitchell et al., 2003; Prosser et al., 2000; Saynor and Erskine, 2006).

The conventional methods present some significant disadvantages as they do not provide continuous measurements of fluvial erosion but instead provide snapshots of erosion between periods of measurements and do not allow the accurate identification of the critical events triggering fluvial erosion. Although progress is made to estimate the rate of bank erosion over time, automated techniques are still in needed for more high resolution erosion data. A consequence of this limitation is a lack of available data for

bank retreat change over a period especially during critical flow events, which shape the bank profile. Newly and more reliable techniques are needed to address this limitation.

1.3.3.2 Newly developed techniques

Newly techniques are available in the literature to estimate fluvial erosion rate or the erodibility parameters. Can be found in the literature, the jet testing device (Thoman and Niezgoda, 2008), the LIDAR technology and Airborne Laser Scanning (Korpela et al., 2009; Pizzuto et al., 2010; Thoma et al., 2005), and the Photo-electronic Erosion Pin so called PEEP (Lawler, 1991; Lawler, 1992). A modified version of the PEEP sensors is also available and described in Lawler (2005b).

Clark and Wynn (2007) used a modified version of the submerged jet test device developed by Hanson (1991) to estimate the resistance for cohesive soil and to compare the results with other methods available in the literature. The operational principle consists of an applied jet acting on the bank surface at a uniform velocity. The experiment is performed until equilibrium conditions for the scour hole are reached, viz., when the rate of scouring does not vary with time. The scour depth divided by the time constitutes the erosion rate at the bank (Hanson, 1991). The erodibility parameter is estimated by fitting the scour data from the jet test device to the excess shear stress from equation 1.1. Clark and Wynn (2007) used data for a local stream and compared this techniques with other empirical relationships available in the literature (Hanson and Simon, 2001; Julian and Torres, 2006; Thorne and Osman, 1988). The predictions differed and confirmed that τ_c and k_d are site specific and should be measured in-situ. One limitation associated to this technique is the uniform jet velocity. The effect of turbulence and soil roughness are not considered (Clark and Wynn, 2007).

More recently Light Detection and Ranging (LIDAR) has been used in remote sensing mapping, and surveying. In fluvial geomorphology, this tool was employed to quantify channel dynamics, to delimitate bank cross-section, and to estimate the bank

erosion rate. Notebaert et al. (2009) studied the channel variability and estimated the total riverbank erosion using a LIDAR imagery technique. Pizzuto et al. (2010) investigated the interaction of trees on cohesive riverbanks using repeated bi-annual LIDAR surveys. (Thoma et al., 2005) used an airborne laser technique to evaluate the sediment contribution from the banks at a river in Minnesota. Several sources of errors can be introduced with this technique, which are outlined in (Thoma et al., 2005). In addition, this technique is relatively expensive and will be more efficient for large scale fluvial erosion studies.

A proposed alternative technique is the Photo-Electronic Erosion Pin (PEEP system). A relatively new device, the PEEP system (Lawler, 1991; Lawler, 1992) is used to monitor erosion and deposition rates in several catchments. This technique has been used by few authors (Couperthwaite et al., 1998; Lawler, 1991; Lawler, 2005b; Lawler, 2008; Mitchell et al., 1999; Prosser et al., 2000). The instrument which is described in details in Chapter 3 is light-dependent. The instrument was tested to monitor bed deposition and fluvial erosion of cohesive and non-cohesive materials. Although, reliable with some improvements needed in the data analysis, Lawler (1992) reported the limitations of the system. Data were lost when the instrument is cover with snow, vegetation and highly turbid water. However, the Thermal Consonant Timing Concept (TCT) could be exploited for an indication of erosion even when the light could not reach the instrument (Lawler, 2005a; Lawler, 2005b; Lawler, 2008).

The PEEP sensors have been used in coastal engineering and fluvial geomorphology studies. Couperthwaite et al. (1998) studied the tide effect on sediment dynamics. The PEEP system was used to collect the deposition and erosion measurements. The Lawler group reported the effectiveness of the instrument. Mitchell et al. (1999) monitored how the waves affect a mud bank in River Trent (UK) and the contribution of the wind in the erosion and deposition processes. Mitchell et al. (1999) such as Couperthwaite et al. (1998) analyzed where the effect of the wind was significant

leading to high magnitude erosion rates. Another study conducted in Austria measured the change in bed elevation in a swash zone (Horn and Lane, 2006).

The PEEP sensors are efficient for small scale erosion measurements, cheap and straightforward technique. Although they require further testing PEEPs can be used to provide continuous datasets for bank retreats.

1.4 Summary and Critical needs

Substantial developments have occurred over the last decade in bank erosion research. As Figure 1.1 shows, there is a growing number of bank erosion investigations (38% of the publications appear since 1997) and a shift in the pattern of 'hot' topics in the discipline. Thus, new research has elucidated the role of riparian vegetation (Abernethy and Rutherfurd, 1998; 2000; Simon and Collison, 2002) and bank hydrology (Casagli et al., 1999; Rinaldi and Casagli, 1999; Rinaldi et al., 2004) as key controlling influences on bank stability. In contrast, few studies have been concerned with the process of fluvial erosion (i.e. the removal of bank sediments by the direct action of the flow), and little progress has been made in understanding fluvial bank erosion of cohesive sediments since the contributions of Arulanandan et al. (1980) and Grissinger (1982). Notable exceptions to this trend include some work that has sought to quantify entrainment thresholds and process rates (Dapporto et al., 2001; Lawler et al., 1997a; Simon et al., 2000).

Although major efforts (Fox et al., 2007; Langendoen and Alonso, 2008; Langendoen et al., 2009; Lawler, 1991; Papanicolaou et al., 2007) have been completed to monitor bank retreat in a channel reach, there is still a lack of available techniques in the literature to assess the erosion rate of banks comprised of cohesive materials in frequent intervals (Couperthwaite et al., 1998; Darby et al., 2007; Julian and Torres, 2006; Millar and Quick, 1998; Papanicolaou et al., 2007; Pizzuto, 2009; Prosser et al., 2000; Simon et al., 2000; Wolman, 1959).

This research will quantify the fluvial erosion process of cohesive soil banks in a small stream in Eastern Iowa by providing continuous records of bank erosion rates, measured in-situ with PEEPs, and relating this information to changes in the stream stage and discharge. If so, this will lead to a more accurate prediction of the temporal and spatial change of the streambank and will provide for the first time the entrainment thresholds and process rates.

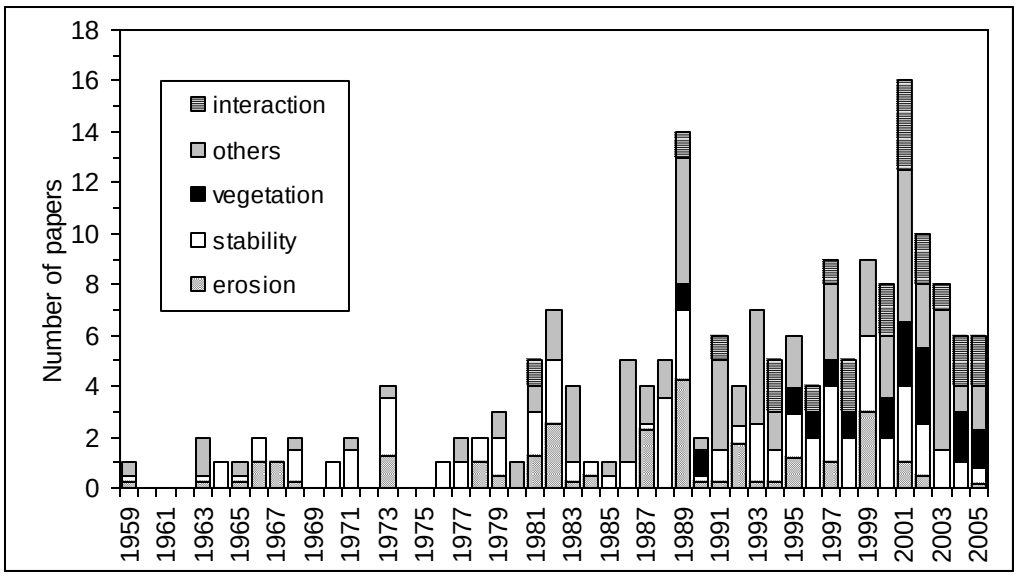

Erosion: papers focused on fluvial entrainment; Stability: papers on mass failures and bank stability; Vegetation: papers focusing on the role of vegetation; Others: papers on other issues related to bank erosion (e.g. measurement of bank retreat, variables controlling rates of retreat, sediment delivery from bank processes, influence of bank processes on channel geometry, etc); Interaction: papers on modelling width adjustments and channel migration, and including to some extent the interaction between fluvial erosion and mass failures.

Figure 1.1: Summary of the bibliographic review on riverbank erosion processes (from Rinaldi & Darby, in press, modified).

Figure 1.2 : Planar failure (Thorne et al., 1997)

Figure 1.3: Cantilever blocks reinforced by roots in Cecina River Italy (Papanicolaou et al., 2006)

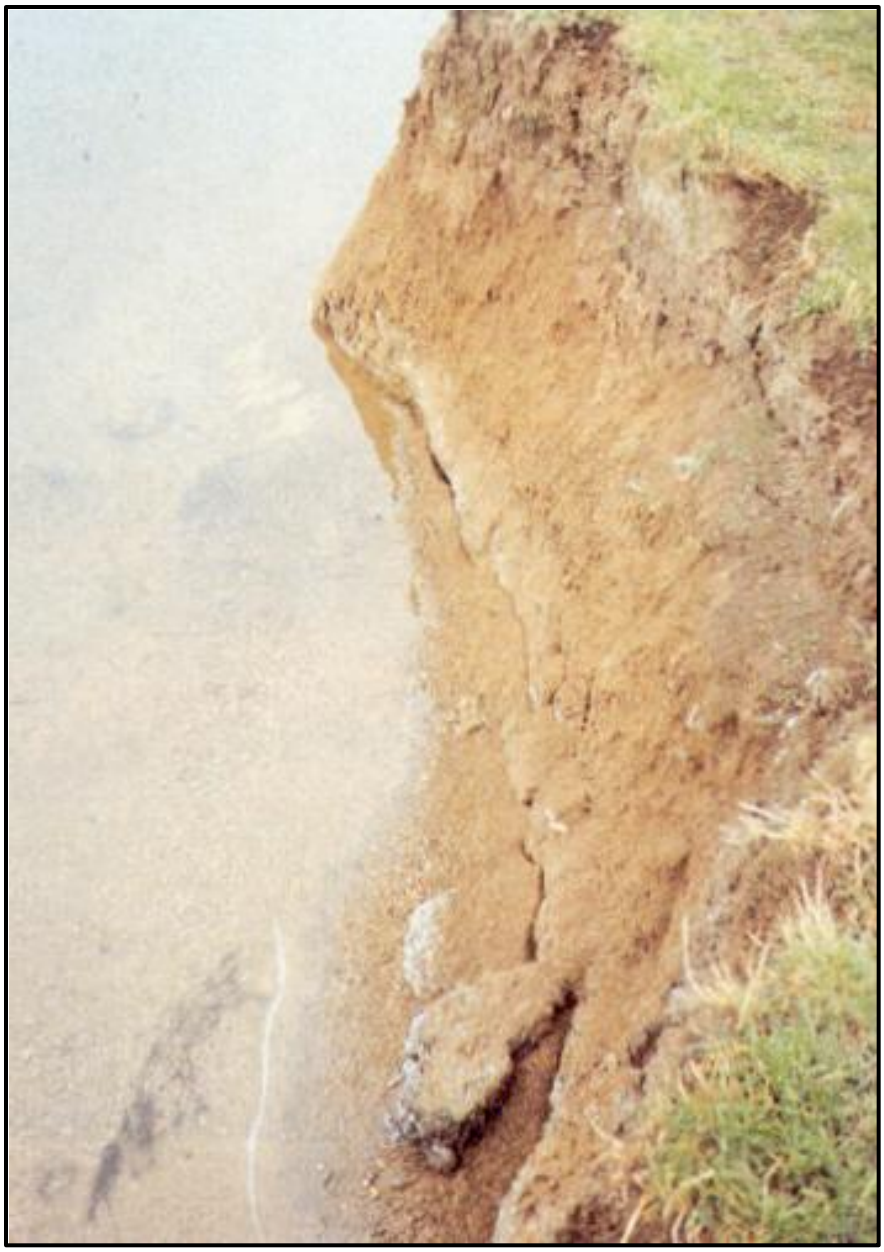

Figure 1.4: Sub-aerial processes: freeze/thaw (Thorne et al., 1997)

Figure 1.5: Pop-out failure in a cohesive lower bank (Midwestern US) (Papanicolaou et al., 2006)

CHAPTER 2. OBJECTIVES

The two main objectives of this study were (1) to monitor bank erosion in different parts of a watershed in hopes of identifying the dominant erosion processes affecting reaches with different stream orders and (2) to evaluate a state-of-the-art, automated instrument for continuously monitoring bank erosion, namely the Photo-Electric Erosion Pin, or PEEP.

Past research (Hooke, 1980; Wolman, 1959) has shown that streambank erosion is influenced by several factors including land-use, soil characteristics (such as texture), stream morphology, and subaerial processes (e.g., soil moisture and temperature). The relative influence of each controlling factor will vary at different locations along a stream channel and it is hypothesized that this will result in different erosion processes affecting those reaches. In this study, two sites were selected along an Eastern Iowa stream based on their location in a watershed, their distinguishing flow conditions, and visual evidence of bank erosion. One site was in the headwaters of the system at the confluence of two first order streams. This area is prone to extremely flashy flow conditions. The second site was located in the lower reaches of the watershed where the stream is a fourth order system. This area experiences more sustained, higher flows during runoff events.

The goal of the study was to evaluate the relative importance of fluvial erosion (compared to mass failure) at each site. It was expected that the dominant erosion mechanism would be different at each site. Mass erosion was expected to dominate in the flashy headwater system, while fluvial erosion was expected to dominate at the downstream site.

In order to quantify fluvial erosion at each site, the performance of a state-of-the-art, automated, monitoring instrument, the PEEP, was evaluated and compared to more traditional erosion measurements (channel surveys and standard erosion pins). The advantage of the PEEP over the traditional methods is its ability to continuously monitor

bank retreat, which will better pinpoint the exact timing and magnitude of small to moderate erosion events (i.e., fluvial erosion). The periodic measurements through the traditional methods provide only a net value between measurements.

Indeed, the knowledge of the periodicity of bank change during individual runoff events, both large and small, as well as better correlation between bank erosion and the subaerial/ flow conditions occurring at the time of erosion will greatly enhance the understanding of bank erosion.

CHAPTER 3. METHODOLOGY

3.1 Methods overview

This chapter is organized into two main sections, which describe the study reaches, or sites, and the instruments used to monitor bank erosion.

The first part of this Methodology section describes the two experimental reaches in the Clear Creek, IA Watershed (CCW; Figure 3.1) used in this study. The sites were selected based on their position in the watershed and evidence of previous bank erosion.

The first reach (hereafter referred to as "Site 1") is located below an agricultural headwater system of the CCW where two 1st order streams meet. It is expected that mass failure is the dominant erosion mechanism here due to the flashiness of the system. The second reach in the CCW (hereafter referred to as "Site 2"), which at this point is a 4th order stream, is situated near the mouth of the watershed. The area surrounding this reach is mainly urbanized. Fluvial erosion is expected to be the main erosion process at Site 2.

The period of observation began on May 18, 2009 with the installation of the monitoring equipment at the two sites. Monitoring ended at Site 1 on June 22, 2009 after a destructive flash flood. At Site 2, monitoring continued until December 1, 2009. Two major storm events (June 19 and August 27, 2009) during this period were selected for more detailed statistical analysis.

Bank erosion at the two sites was monitored using traditional methods such as channel surveys and erosion pins. In addition, a newly-developed, automated instrument (i.e., the PEEP), which is described herein in detail including its principles of operation, physical description, installation, and set-up, was also used in this study. The measurements of bank erosion from the PEEPs were compared and validated against the more traditional methods of monitoring bank. Finally, the data processing and statistical

methods used to evaluate the performance of the PEEPs and to identify trends of the data are described in this Methodology section.

3.2 Experimental site description

3.2.1 Clear Creek Watershed: General description

The Clear Creek Watershed (CCW), which is a HUC-10 watershed (0708020904) that drains approximately 270 km^2 of east-central Iowa to the Iowa River (Figure 3.1). The CCW is representative of watersheds in the Midwest especially regarding climate (humid-continental), soil type/order (Alfisols and Mollisols), and land use (predominantly agricultural). In addition, the CCW is well instrumented by IIHR Hydroscience & Engineering at the University of Iowa to monitor rainfall, streamflow, soil moisture, and infiltration/runoff, as well as other water quality parameters.

Clear Creek is approximately 40 river km long with a sinuosity between 1.27 and 1.49. The channel has been straightened significantly to facilitate the movement of water through the system (Rayburn and Schulte, 2009). The average slope of the main channel from the headwaters to the mouth of the stream is 0.001 (Loperfido et al., 2009).

Row crop agriculture (i.e., corn and soybean) is the predominant land use (55 %) with the remaining surface area comprised of grasslands (33 %), deciduous forests (7 %), and a growing urban area (5 %). Since 1940, there has been a decline in the percentage of agricultural land coupled with an augmentation in urban areas (Rayburn and Schulte, 2009).

Soils in this watershed are mainly loess-derived and highly erodible. The soil texture varies from sandy loam to clay loam in the CCW. Moving downstream, the dominant soil texture changes from a silty-clay loam in the headwaters to a silty-loam near the mouth. Approximately 65% of the upland slopes in the CCW range between 2 and 9%. The combination of extensive agricultural activities, increased urbanization,

highly erodible soils, and steep slopes within CCW have influenced the fluvial processes and stream bank erosion in the watershed (Abaci and Papanicolaou, 2009).

3.2.2 Climate

The CCW is characterized by cold winters and hot summers with wet springs. Warm, humid air masses from the Gulf of Mexico influence the summer climate. Conversely, winter is dominated by dry air from Canada. The average temperature is 9^{o}C with a maximum temperature of 31^{o}C in July and a low temperature of -26^{o}C in January. Thus freeze-thaw cycles are present annually. The estimated mean annual rainfall is 889 mm with a snowfall water equivalent (SWE) of 76.2 mm/yr (Papanicolaou and Abaci, 2008). High intensity thunderstorms are common from April to September with a peak in June.

During the study period (May 18-December 1, 2009), the CCW experienced multiple storm events (Table 3.1). The event of June 19, 2009 was significant in terms of runoff (and bank erosion) producing a flash flood, where stage in the stream increased 4 m in 1 hour. Although the cumulative rainfall was not significant in terms of magnitude, the precipitation intensity was the sixth highest 5-minute precipitation on record (Denn, 2009) and the hydrograph experienced a long period of high flow (Figure 3.2). Significant soil losses and bank collapses were observed throughout the CCW.

3.2.3 Site 1: Headwater reach

The first study reach, "Site 1", (Figure 3.3) is a 76-m, second order stream, located downstream of the 190th Street bridge near U.S. Highway 151 in Iowa County. The reach drains a 26-km^2, agricultural sub-watershed of the CCW. The mean annual stream flow discharge for this reach is 5.9×10^6 m^3 / yr with an annual sediment discharge is 5×10^3 tons (Abaci and Papanicolaou, 2009).

Six cross-sections were established every 15 m within the reach to determine the reach geometry and for extensive monitoring (Figure 3.3). The average bank height of each cross section is 3.3 m and the average bank angle was 23^0.

The headwater sub-watershed upstream of this reach contains 80% row crop agriculture with the remaining area being grassed land. The dominant soil texture within this catchment is silty-clay loam and is highly erodible. The elevation in the catchment ranges from 235 m to 274 m above sea level with upland slopes varying from 1% to 10% with an average declination of 4%. Due to the intense agriculture, erodible soils and high slopes, this sub-watershed has some of the highest erosion rate in CCW (Abaci and Papanicolaou, 2009) making this watershed a key spot to study the effects of long-term anthropogenic disturbance on land-uses.

3.2.4 Camp Cardinal Study Reach

The second study reach, "Site 2", is located at Camp Cardinal Rd. in Coralville, Iowa near the CCW confluence with the Iowa River. At this point, the reach is a fourth order stream flowing through an urban environment. Flow at Site 2 is less flashy than site 1 and the sustained high flows facilitate fluvial erosion. The average bank height was 5.8 m and the average bank angle was 47^0. The reach is at a bend in the river, so the study was focused on the right bank (looking downstream), which receives the impinging flow. The average annual flow is 7.2×10^7 m^3 / yr and the sediment discharge from this site is 7.8×10^4 tons. Figure 3.4 shows the bank height is steep and greater than 2 m. This bank had obvious signs of bank erosion.

3.3 Experimental Instruments

Multiple monitoring instruments were established at Sites 1 & 2 to evaluate flow and bank erosion. Pressure transducers were used to measure the stage and quantify discharge. Channel surveys were used to determine bank profiles and, coupled with traditional erosion pins, provided a verification of the bank erosion rates determined

using the PEEPs. The installation of the instruments occurred on May 18, 2009 and monitoring continued until December 1, 2009.

3.3.1 Stage Measurements

Water level sensors (Global Water WL16) consisting of a vented pressure transducer and attached datalogger were used to monitor the stage at Site 1 every 15 minutes. The transducer has an accuracy of ±0.2% for a temperature range of 1.7^0C to 22.2^0C (Global Water Instrumentation, 2009). The pressure transducers were installed in a stilling well at each cross-section along the reach to minimize the effect of waves and currents (Abaci and Papanicolaou, 2009). Three T-Posts were placed upstream of the pressure transducer (Figure 3.5) to protect the sensor against debris. The stage for this site has previously been correlated to discharge using a rating curve developed through standard methods (Abaci and Papanicolaou, 2009; Kennedy, 1984).

At Site 2, pressure transducers were not installed. The stage was monitored at the USGS gage station (#05454300) approximately 100 m upstream of the monitoring site. Discharge was determined through established USGS rating curves.

3.3.2 Total station-surveys of channel cross sections

Cross-sections of the reaches at Sites 1 and 2 were regularly surveyed (Figure 3.6) using a Leica Total Station to determine any change in the bank profile. The angular accuracy of the instrument is 5″ and point measurements are taken and the coordinates calculated in 3 s. Consecutive surveys were conducted mainly after large runoff events. At Site 1, surveys of the six cross-sections were conducted before and after the June 19, 2009 flood event, as well as on April 9, 2009; May 28, 2009; June 23, 2009 and June 24, 2009. At Site 2, the first survey was conducted on July 17, 2009, while subsequent surveys were conducted on July 30, 2009; September 30, 2009. The horizontal bank retreat can be calculated using pre and post-event surveys data. This bank erosion length was compared to erosion lengths from the erosion pins and PEEPs for validity.

3.3.3 Standard erosion pins

Traditional erosion pins have been used extensively to estimate bank erosion at small, local scales (Bartley et al., 2008; Hancock et al., 2010; Harden et al., 2009; Hooke, 1979; Lawler, 1993a; Lawler et al., 1999; Thorne, 1980). In this study, the erosion pins consisted of 30-cm steel nails. The pins were inserted into the bank face in a gridded pattern. Pins were in-line from the top of the bank to the toe, as well as parallel to the water surface. A total of 30 erosion pins were installed at Site 1 with a higher density of erosion pins (45) installed at Site 2 (Figure 3.7). Initially, the head of the nail was flushed to the bank face. As the bank retreated, the exposed length of the nails was measured carefully using a measure tape. The erosion pins data were used as a verification of the bank erosion monitored by the PEEPs.

3.3.4 Photo-Electronic Erosion Pin (PEEP)

A primary goal of this study was to evaluate state-of-the-art, automated instruments for continuous bank erosion measurements, namely the Photo-Electronic Erosion Pins (or PEEPs). Two different models of PEEPs were used in this study. The principles of operation, physical descriptions, calibration, installation, and set-up of both PEEP models are described in this section. In addition, the processing and statistical analysis of the data are explained in the following sections.

3.3.4.1 Principles of Operation

The Photo-Electronic Erosion Pin, which was originally described in Lawler (1991), which provides automated and continuous monitoring of erosion and deposition. The PEEPs are essentially a series of photovoltaic/ photo-resistance cells (or diodes) encased in transparent waterproofed acrylic tube (Lawler, 1991; Lawler, 1992). Thus, the PEEPs are light dependent. The photovoltaic PEEP provides a voltage as light (e.g., from the sun) strikes the diodes. The voltage is sent along a cable and is recorded on a datalogger. With the photo-resistance PEEP, an external voltage is supplied to the PEEP

but is stopped when reaching the photo-resistors. As light strikes the photo-resistors, their resistance drops, which allows a higher voltage to pass through to the datalogger, where the value is recorded. Figure 3.8 illustrates the principle of the PEEP sensors.

Essentially for both PEEP models, an increase in the number of exposed diodes (i.e., struck by light) corresponds to a higher voltage sent to the datalogger. When the PEEPs are initially inserted into the bank face parallel to the water surface, all the diodes are covered by the bank sediment and the voltage received by the datalogger is low. However, as the bank face retreats, more diodes are exposed and the voltage received by the datalogger increases. This voltage is normalized against a reference value, which corresponds to the voltage if all PEEP diodes are exposed. This ratio is then related to an erosion length. The ratio between the reference voltage and the voltage received by the datalogger is considered to account for the fluctuations of sunlight or temporary shadows.

3.3.4.2 Description of the instrument

For this study, two PEEP models were used (i.e., a photovoltaic PEEP and a photo-resistance PEEP). The photovoltaic PEEP is a PEEP 200 series by Hydro Scientific Limited (Figure 3.9 a). The model consists of 20 photovoltaic cells in series over a 20-cm section that constitutes the active length of the sensor. The diodes are encased in an acrylic tube. The whole instrument is 66 cm long and is terminated by a 15-m cable, which can be connected to a datalogger. The outer diameter of the protective acrylic tube is 16 mm. Two of the diodes located at either end of the active length are considered reference cells. The other eighteen diodes are used to evaluate the location of the bank face. The accuracy of the instrument is ± 2 – 4 mm with a 95 % confidence level (Hydro Scientific, 2004). Two PEEPs of this model were used in this study and identified as L230 and L231.

The second PEEP model is produced by Rickly Hydrological Company and are based on the principle proposed by Lawler (1991). However, these PEEPs use photo-

resistors. In addition, these PEEPs are shorter with only 13 diodes (Figure 3.9 b). The diodes are encased in an acrylic tube. These PEEPs require an additional, fully exposed PEEP for the reference values. Ten PEEPs of this model were used in this study and identified as A1, A2, A3, A4, A5 and B1, B2, B3, B4, B5.

Two Campbell Scientific data loggers (CR 800 and CR 1000) were used to store the data. The dataloggers were set to receive voltages in the range of 0-225 mV every 15 minutes (Lawler, 2005b). A computer was used to download the data. The dataloggers use solar power to operate. The power of the datalogger is sufficient to send the initial voltage required by the Rickly PEEPs.

3.3.4.3 Calibration

A calibration process was required before installing the PEEPs that relates the exposed active length of the PEEP and the voltage received by the datalogger. An outdoor, site-specific calibration is recommended (Lawler, 1991)therefore, a field calibration was conducted at both Sites 1 & 2 for the PEEPs on a sunny day with some fluctuations of the light intensity. Initially, the PEEPs were laid horizontally adjacent to one another on floodplain at each site in alignment with the sun (Figure 3.10). Steel wire stakes were used to fix the PEEPs to the ground to prevent tilting of the PEEPs, which would produce invalid data.

A dark tube was placed over all the diodes of each PEEP. The tube was moved back at defined intervals exposing the diodes, which simulated bank erosion. The interval between the exposure of subsequent diodes was 4 minutes and the measurement window for each diode was every fifteen seconds. The calibration process lasted about 2 hours. The corresponding voltage recorded by the datalogger after each consecutive movement of the tube was correlated to the measured exposed length for the calibration. The exposed length was measured using a measure tape.

However, this method proved insufficient when recorded voltages after installation were lower than the calibrated values. It was assumed that the tubes did not block all the light reaching the diodes and was not accurately simulating the field situation. Therefore, a second calibration was conducted by incrementally sliding the PEEPs out of the pre-drilled holes in the stream bank (Figure 3.11). This calibration proved successful since all subsequent values were within the calibration range.

To determine the relationship between the exposed length of the PEEP and the received voltage (i.e., the bank retreat), the exposed length was plotted on a graph against the ratio of the voltage received by the datalogger normalized against the reference value. A linear relationship was used for the photovoltaic PEEPs and a polynomial equation was used for the best fit line of the photo-resistance PEEPs.

For the photovoltaic sensor, the ratio between the voltage of any cell "i" to the voltage of the front reference cell was calculated (Equation 3.1) and termed the photovoltaic ratio (R_{pp}), which is expressed as a percentage.

$$R_{pp} = \frac{\text{voltage cell i (mV)}}{\text{voltage front referencecell(mV)}} \tag{3.1}$$

The erosion length of the PEEP was then determined using a linear egression (Equation 3.2) that relates the R_{pp} (%) and measured exposure length:

$$L = c + d \times R_{PP} \tag{3.2}$$

where c = 17.83 and d = 2.1743 are coefficients determined from the PEEP User Guide (2004).

For the photo-resistance PEEPs, the ratio between the reference PEEP and the measuring PEEP was initially determined from the data (Equation 3.3) and the applied to a polynomial equation (Equation 3.4) namely the 2D NIST HAHN Model, to calculate the erosion length. The coefficients: a, b, c, d, e, f, and g were obtained for each sensor

using the commercially free, web-based software at (http://zunzun.com/Equation/2/NIST/NIST%20Hahn/).

$$x = \frac{\text{voltage measuring PEEP (mV)}}{\text{voltage referencePEEP (mV)}} \tag{3.3}$$

$$y = \frac{a + bx + cx^2 + cx^3}{1 + ex + fx^2 + gx^3} \tag{3.4}$$

After calibration, the values from the dataloggers can be converted to erosion lengths using Equations 3.2 and 3.4; however, visual confirmation is recommended.

3.3.4.4 Installation

The recommended procedure for installing the PEEPs calls for drilling two 16-mm diameter holes. The first hole is into the bank face, parallel to the water surface. The second hole must be vertical from the top of bank some distance from the edge to avoid disturbing the bank. The two holes must intersect perfectly so that the PEEP cable can be passed through the holes. This technique proved difficult and was modified.

The modified procedure for installing the PEEPs required auguring a 16-mm hole parallel to the water surface only about 1 m into the bank face. The hole was carefully drilled to avoid significant disturbance to the surrounding bank soils (Figure 3.13 a). Moreover, the diameter of the hole was kept close to the outer diameter of the sensor itself (Figure 3.11).

Before inserting the PEEP into the hole, the cable at the end of the sensor was attached to the side of acrylic tube using plastic cable ties. Care was taken not to cover the diodes with the cable. In addition, sufficient slack was maintained at the tube/ cable interface to avoid snapping the cable. The PEEP and attached cable were then inserted in the bank so that only one diode was initially exposed (Figure 3.13 b, c). This configuration allowed the cable to exit the front of the hole so that the cable may travel up the bank face to the

datalogger. The cable along the bank face was inserted into a garden hose for additional protection and the hose was fixed to the bank surface using bent steel wire stakes.

The data loggers were attached to 3-m aluminum poles that were driven at least 1 m into the ground. These poles were positioned approximately 2 m from the bank edge to avoid slumping. The cables were wired into the dataloggers and the remaining slack wire was bound to these poles (Figure 3.13 d).

At Site 1, five photo-resistance PEEPs (B1, B2, B3, B4, and B5) and one photovoltaic PEEP (L230) were installed on May 18th. For the photo-resistance PEEPs, B5 was considered as the reference PEEP and secured at the flood plain as shown in Figure 3.13 d. On the right bank (looking downstream), PEEPs B2, L230, and B4 were respectively inserted into the bank face from the top of the bank to the toe, while on the left bank B1 and B3 were installed at the top and bank toe, respectively (Figure 3.12).

These PEEP sensors were removed shortly after the June 19th event. The left bank experienced significant mass failure and PEEPs B1 and B3 were completely exposed. No data were recorded for these PEEPs due to a substantial battery drain. The PEEPs on the right bank remained in-place, but significant erosion had also occurred. The reference PEEP, B5, was moved from its original location due to over bank water flow.

At Site 2, four photo-resistance PEEPs (A1, A2, A4, and A5) and 1 photovoltaic PEEP (L231) were installed. Three transects were established on only the right bank (looking downstream), which is the side that received the impinging flow around the bend. PEEP A2 was installed in Transect 1 (T1), PEEP L231 in Transect 2 (T2), and PEEPs A1 and A4 in Transect 3 (T3). T1 was the most upstream transect followed by T2 and T3 moving downstream. The sensors A4 and A1 were installed, respectively, at the toe and mid bank section. L231 and A1 were installed, respectively, at mid and top bank.

3.3.4.5 Set up and Programming

The dataloggers required specific programs in order to receive and record the voltage signals from the PEEPs. The programs were created using the Short Cut software provided by Campbell Scientific. For the photovoltaic PEEPs, a differential voltage reading was used; however, with the photo-resistance PEEPs, a half bridge program was used, which allowed for an excitation voltage to be sent across the wires through the resistors. The specifications of both programs (differential and half bridge programs), as well as the wiring schematics are provided respectively in Appendices A, B, and C.

3.3.4.6 Data processing

Flow stage from the pressure transducers and the USGS website, as well as the PEEP data were downloaded weekly at both sites. Data were collected from May 18, 2009 to June 22, 2009 at Site 1 and from June 4, 2009 to December 1, 2009 at Site 2. Using the calibration relationships, the recorded voltages from the PEEP data (in mV) were converted to erosion length (in mm).

The data collected during darkness (i.e., at night) were filtered from the dataset because no artificial light was used in this study. A limitation of the PEEPs is that they only provide valid data in daylight. The daily period of observation was from 7 am to 7 pm during the summer and from 8 am to 5 pm during fall and winter seasons. Information about daily sunrise and sunset were found at the "U.S. Naval Oceanography website: http://aa.usno.navy.mil/data/docs/RS_OneDay.php".

The data were further filtered to remove values outside the calibrated range (e.g., negative numbers). In addition, values recorded while the PEEPs were submerged were removed from the dataset. The lack of data accuracy while the instrument is submerged is reported in the literature (Lawler, 1991; Lawler, 2005b; Lawler et al., 1997a; Lawler et al., 1999; Lawler et al., 2001). This filtering is commonly done especially in coastal engineering applications (Couperthwaite et al., 1998; Mitchell et al., 1999; Mitchell et al.,

2003) where these authors filtered the original dataset and smoothed the remaining values with a daily mean approximation.

During the period of observation, both sites experienced high flow events, which produced significant erosion exposing many of the PEEP diodes. This required the PEEPs to either be reset into the bank or completely removed. The flash flood event of June 19th facilitated the removal of the PEEPs at Site 1. At Site 2 on July 7, 2009 all PEEPs were reset into the bank. Finally on August 27, 2009 another flash flood event occurred at Site 2, which required PEEP A2 to be reset. After the resetting of a PEEP, the absolute erosion length was calculated by adding the previous daily mean value of erosion to the newly recorded data after the instrument was reset. This explains why the recorded erosion lengths are greater than the active length of the PEEP.

3.3.4.7 Statistical analysis

The results provided by the PEEPs were evaluated using different statistical methods including the following: moving averages, Shewhart Control charts, and autocorrelation. For the moving averages, five different intervals (1.25-hour, 3.75-hour, 6.25-hour, 11.25-hour, and 24 hour) were used to identify any trends in the dataset. In addition, the moving averages provided a means for analyzing the variability of the erosion processes at the sensors locations. The technique smoothed the high fluctuation within the dataset and permitted an improved visualization of the erosion patterns at the sensors locations. Therefore, the most predominant erosion processes were detailed for each sensor. The intervals were chosen such as the most prominent features within the original dataset remained. The Shewhart Control Charts provide information regarding the effects of the extreme events on the dataset, as well as the time series of the real data, the central limit (CL), and upper/ lower control limit (UL/LL). The CL is the median while the upper and lower control limits are the median plus a baseline variation triggered by the physical processes (e.g., erosion). The autocorrelation is the correlation of the data

to themselves. The lag time was usually taken to be up to a quarter of the number of observations (Chatfield, 1984). The autocorrelation function was calculated using Minitab (version 15) and plotted against the time lag. These statistical methods permitted to distinguish extreme events from frequent events. They also gave information about the effect of seasonality on the erosion dataset.

A regression analysis was done to verify the accuracy of the instrument when submerged under water. All the data (including inundated data) were plotted against the dataset when the inundated data are removed. Using Minitab (Version 15), the regression analysis was conducted between the two datasets for each sensor at Site 2. The period of observation at site 1 was too short to conduct this analysis. The same technique was done at site 2 to compare the physical measurements of the sensors with a measure tape and the automated data estimated by the sensors.

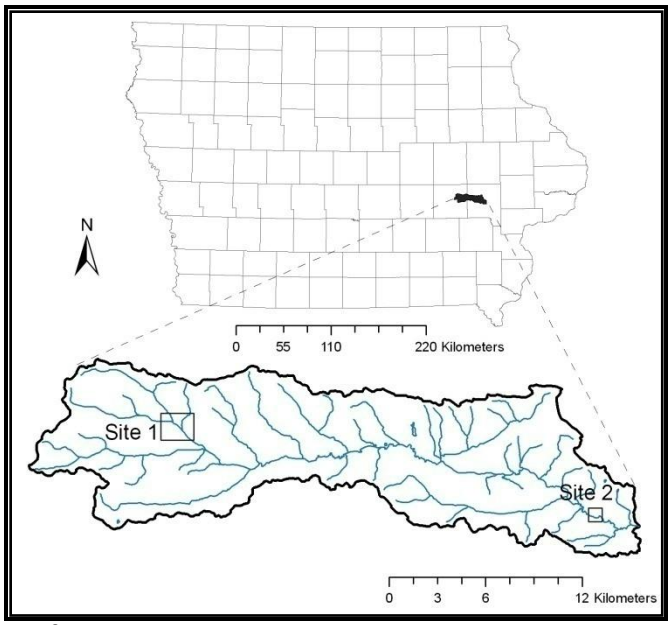

Figure 3.1: Location of the Clear Creek, IA Watershed and the study sites. Site 1 is located in the headwaters and Site 2 is situated near the mouth.

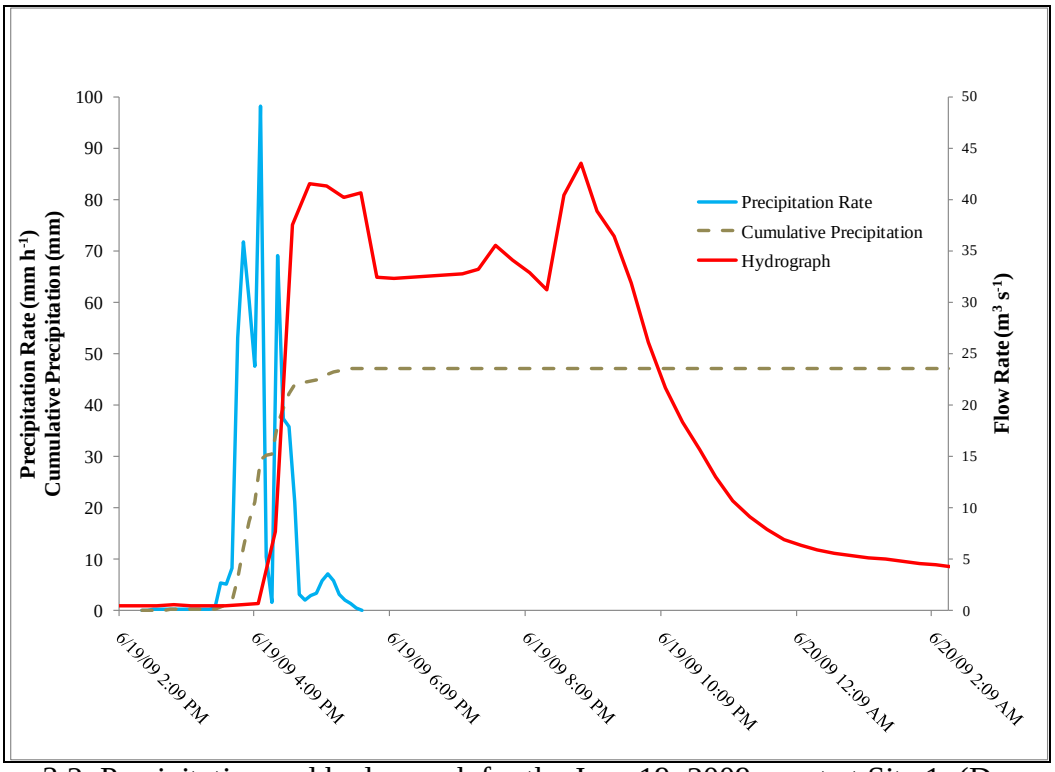

Figure 3.2: Precipitation and hydrograph for the June 19, 2009 event at Site 1 (Denn, 2009)

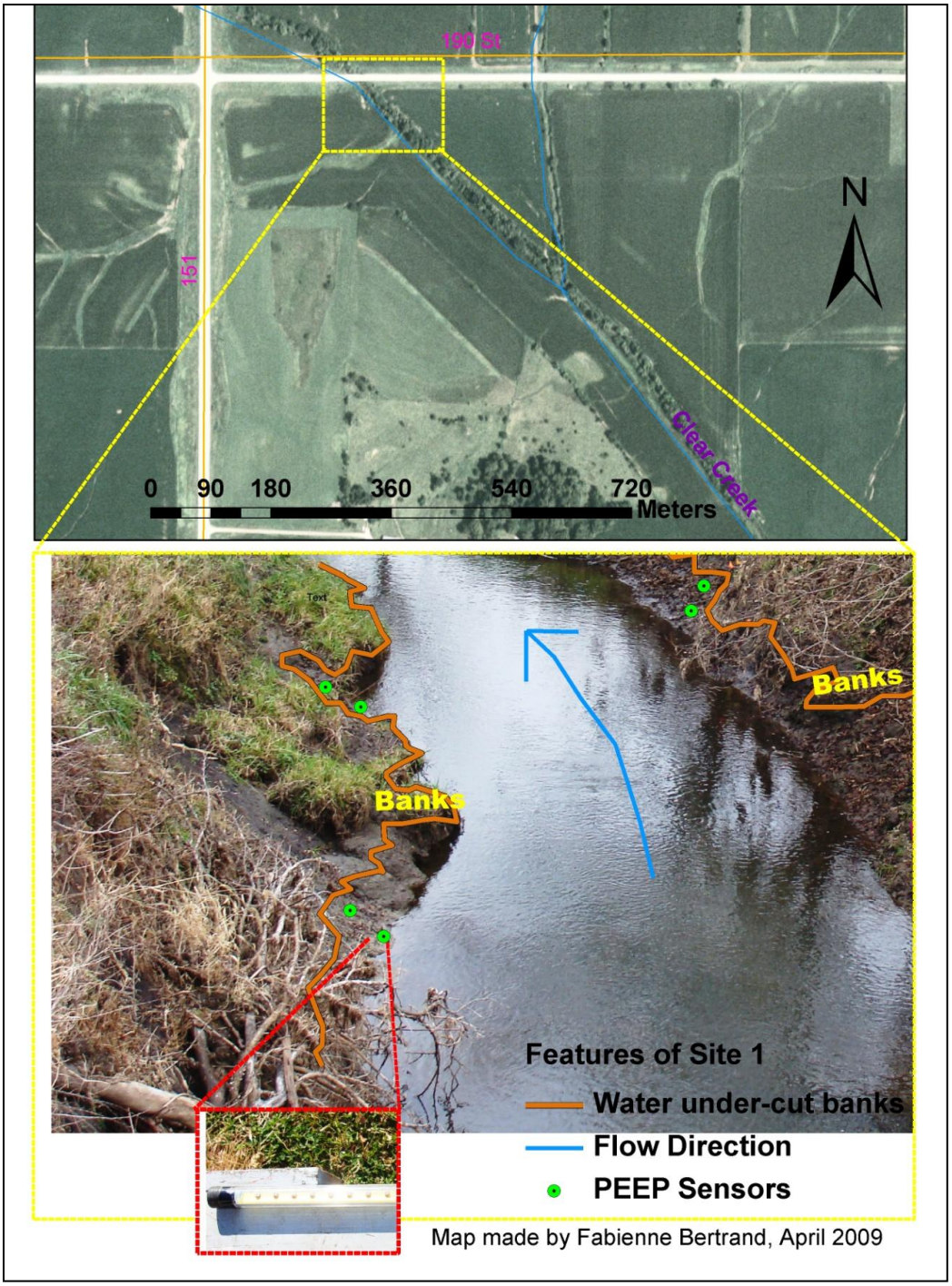

Figure 3.3: Site 1 Study Reach

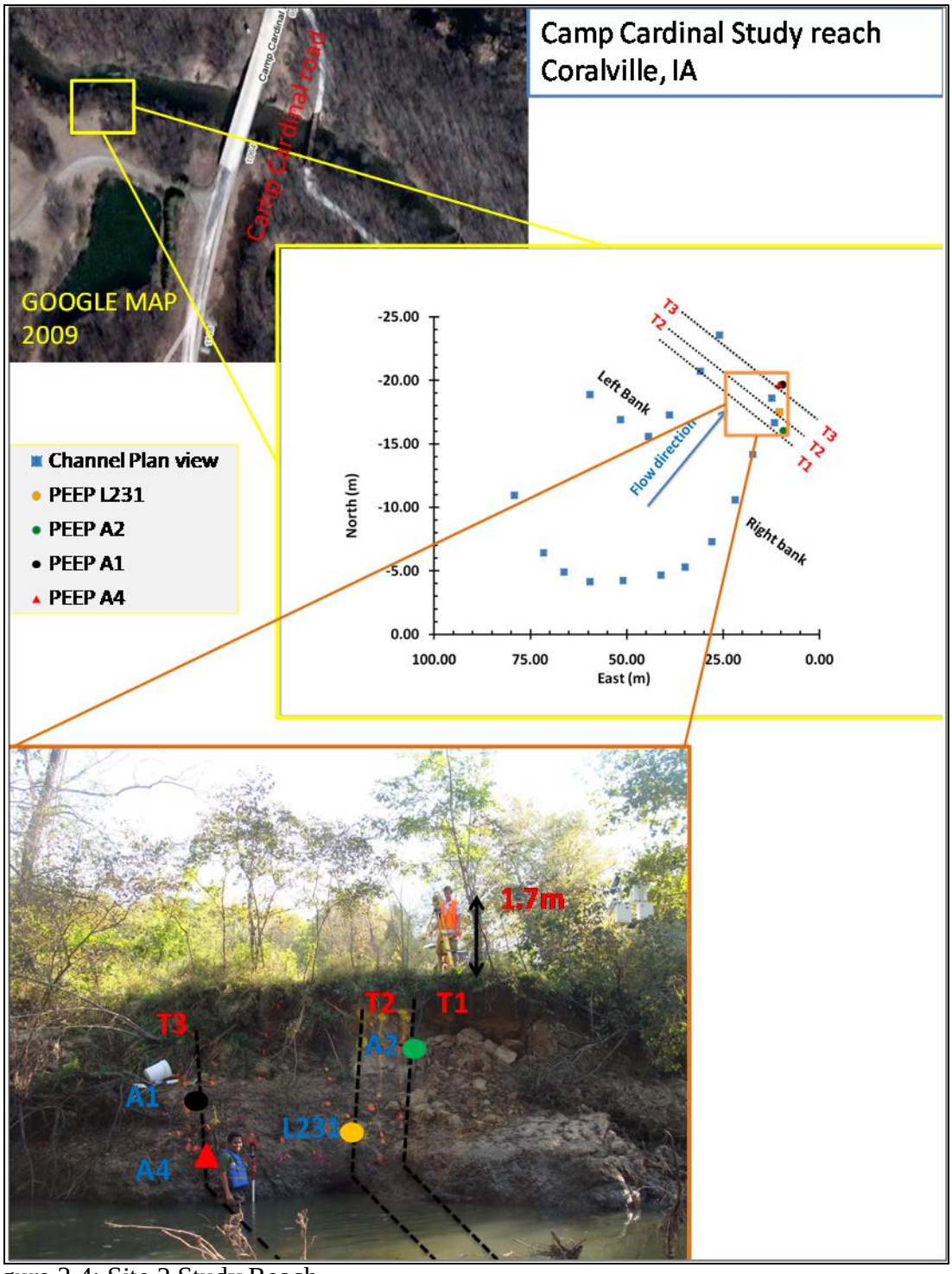

Figure 3.4: Site 2 Study Reach

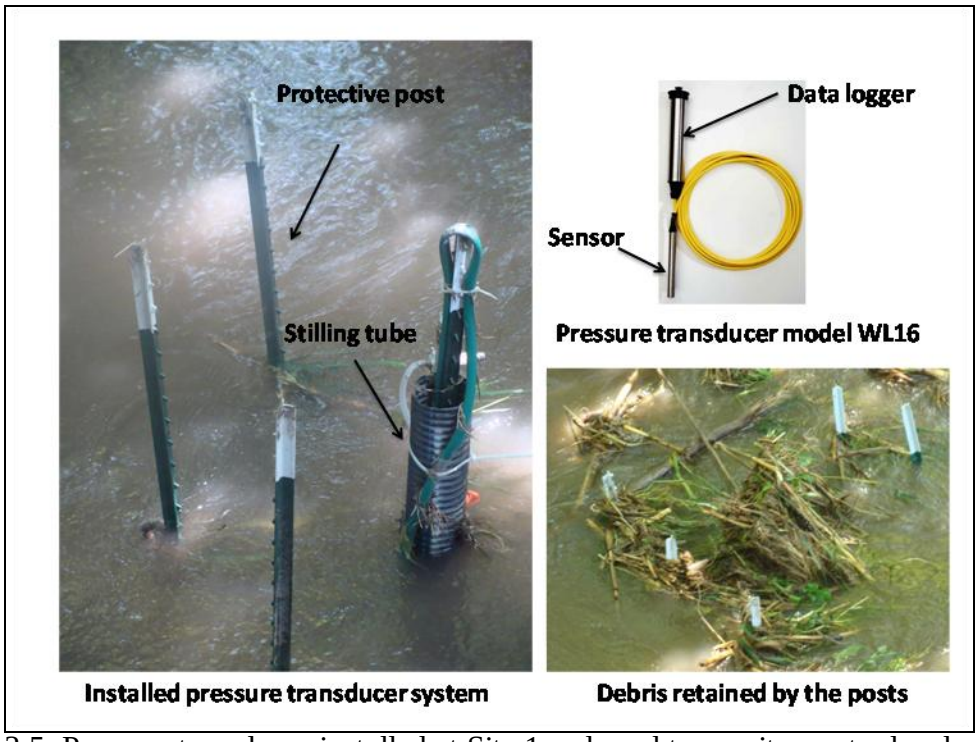

Figure 3.5: Pressure transducer installed at Site 1 and used to monitor water level.

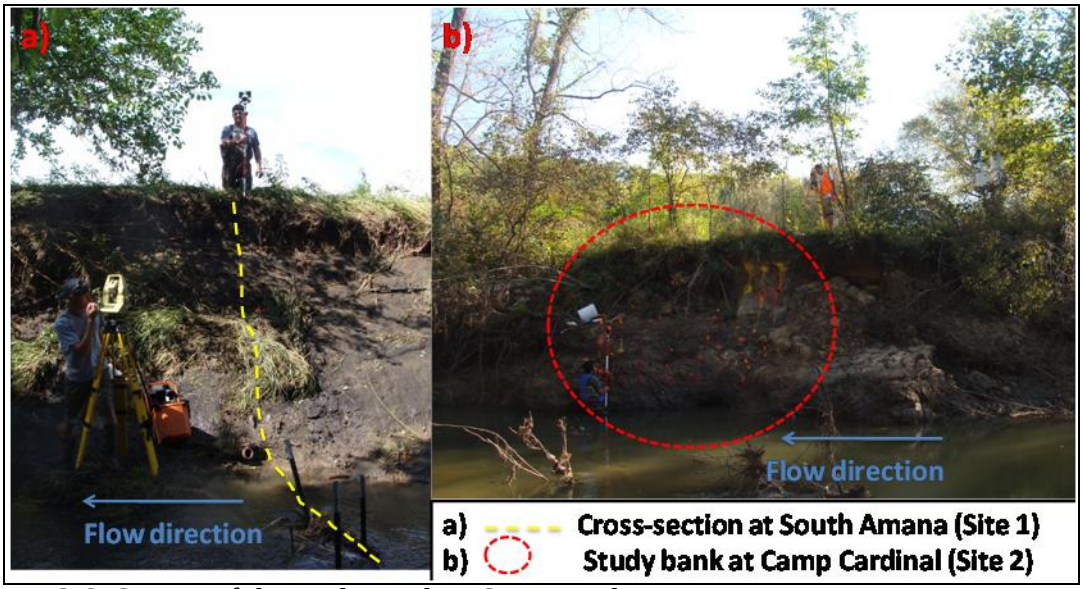

Figure 3.6: Survey of the study reach at Sites 1 and 2.

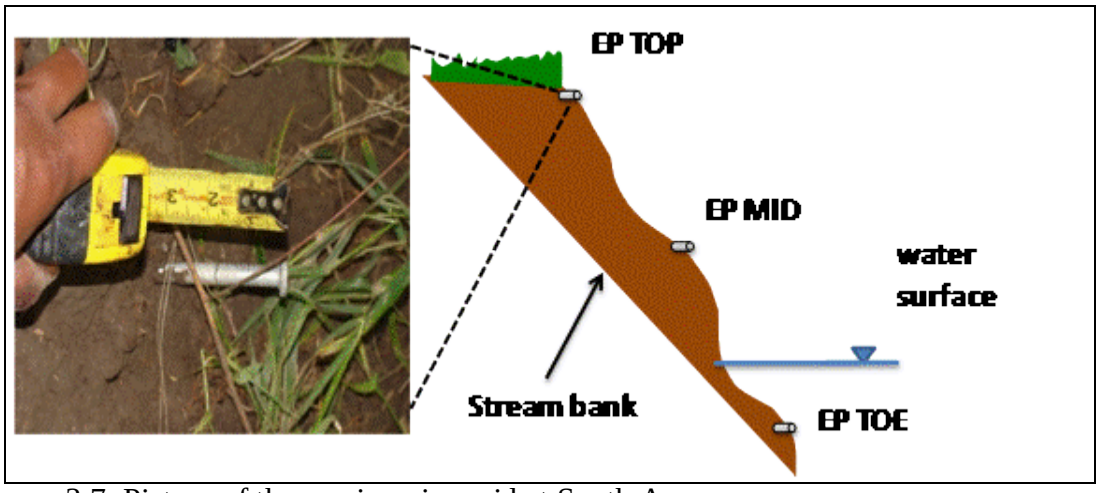

Figure 3.7: Picture of the erosion pins grid at South Amana.

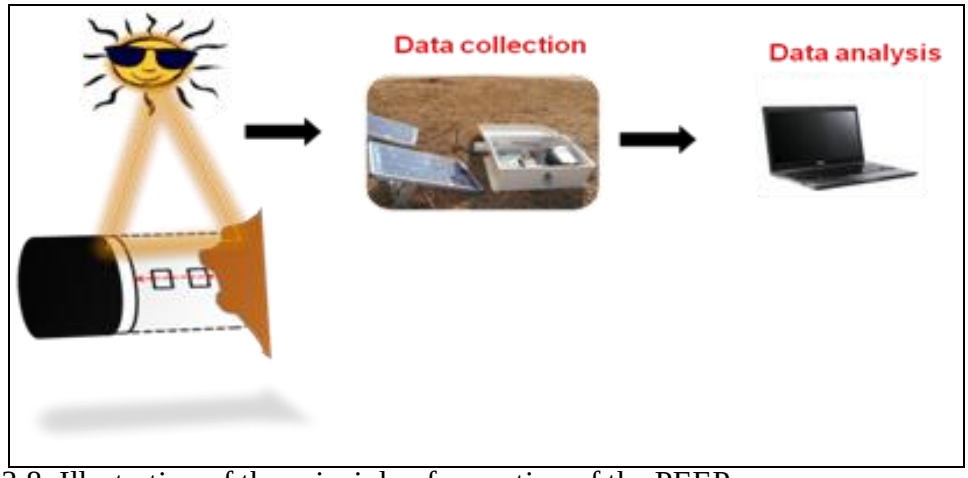

Figure 3.8: Illustration of the principle of operation of the PEEP.

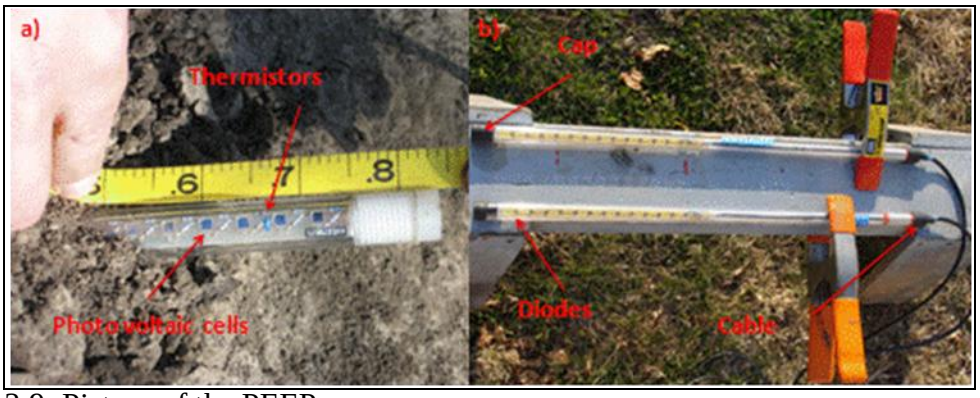

Figure 3.9: Picture of the PEEP sensors.
(a) Photovoltaic sensor
(b) Photo resistance sensor

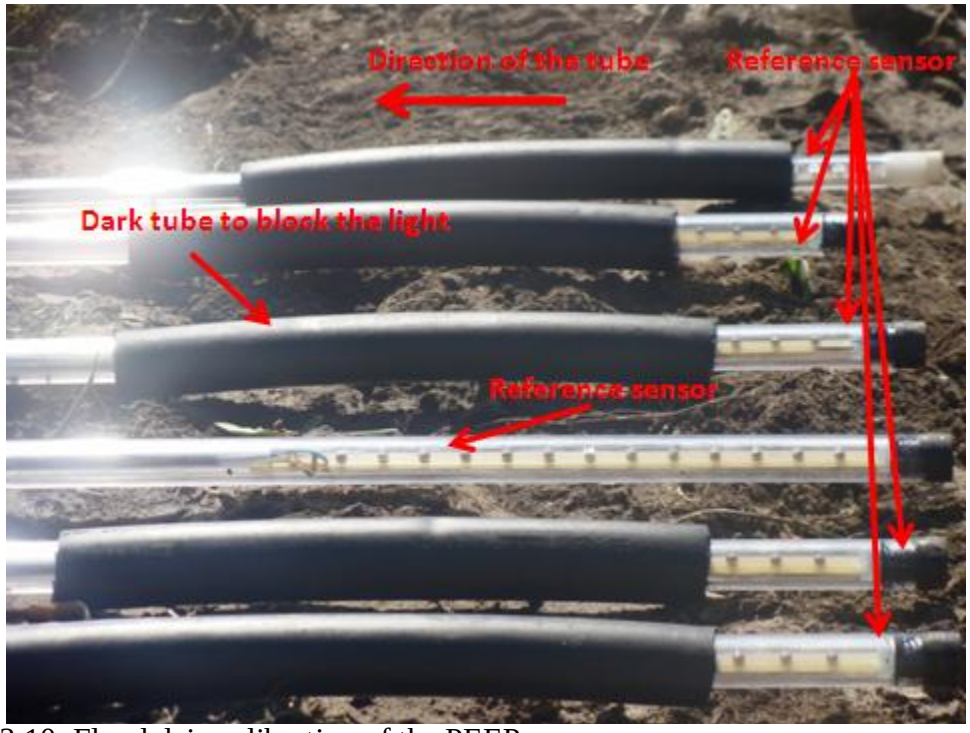

Figure 3.10: Floodplain calibration of the PEEPs.

Figure 3.11: In-bank calibration of the PEEP.

Figure 3.12: Site 1 study reach showing the location of the PEEPs.

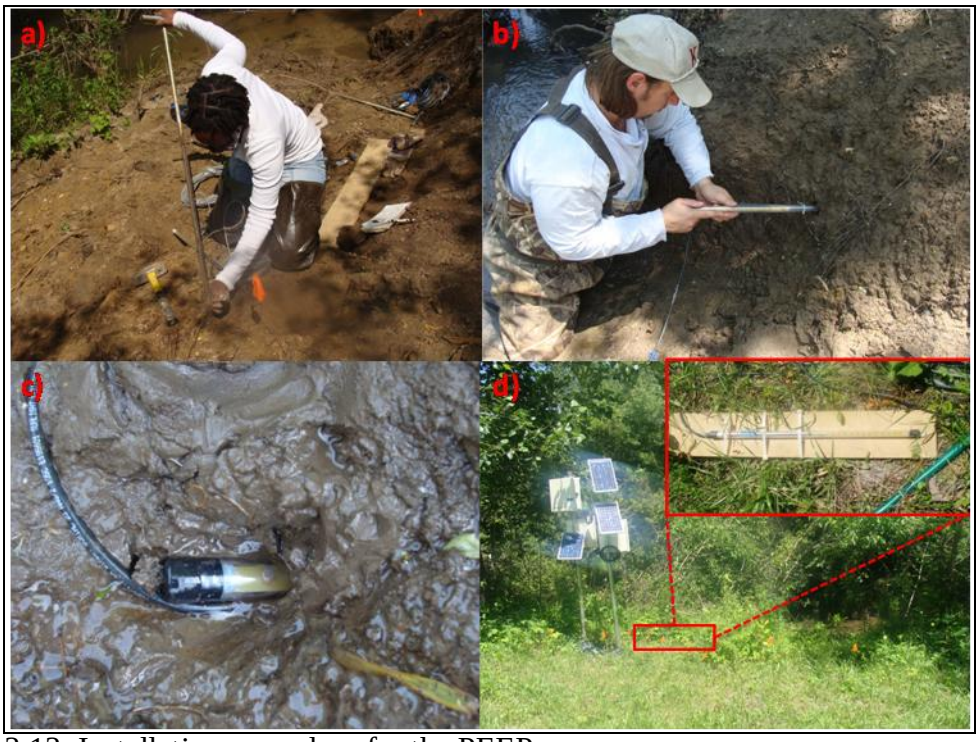

Figure 3.13: Installation procedure for the PEEPs.

Table 3.1: Storm characteristics for the June 19th event (Denn 2009)

Historic of the storm event in CCW	
Date	**Location**
June 16, 2009	Site 1
June 18, 2009	Site 1
June 19, 2009	Site 1 and 2
June 21, 2009	Site 1
August 27, 2009	Site 2

CHAPTER 4. RESULTS

The results chapter is organized as follows. First, we provide the time series data (15-minute intervals) obtained with the Photo-Electronic Erosion Pins (PEEPs) at Site 1. We continue with the statistical analysis of the data at Site 1. The statistical analysis includes the performance of the moving average approach in the 15-minute interval time series data. The selected intervals are 1.25-hour, 3.75-hour, 6.25-hour, 11.25-hour, and 24-hour. The moving average analysis is complemented with the performance of the Shewhart method to identify the trends of the 15-minute interval data by comparing the recorded observations with the mean value and the upper and lower control limits. The Shewhart analysis is used to identify if there is a systematic variation of the data in comparison to their mean value and isolate critical erosional events that are near or beyond the control limits. Finally, a correlogram is performed to identify the autocorrelation of the PEEPs signals at different locations atop the bank interface at Site 1. The autocorrelations will serve as a method for detecting seasonal variability, non-stationarity vs. stationarity of the data, and short-term correlation of data at the different locations. Then, suggestions about the physical processes that ensue at Site 1 can be made. Comparison of the PEEP data is made against traditional methods namely, erosion pins or flags, geodetical surveys, and direct measurements of the PEEP's exposure length with a tape. The latter approach will be referred to hereafter as "measure tape" traditional method.

An identical analysis is performed for Site 2. This analysis is complemented with an investigation of the effects of light on sensor accuracy, the role of water clarity, and the degree of light penetration in case the PEEPs are fully submerged in water. The performance of the PEEPs is evaluated at different locations as their location with respect to the bank crest affects the degree of lighting received by the voltaic photodiodes and the percentage of time the PEEPs remain emergent through the water surface. A regression

plot between the PEEP results and the measure tape observations is also performed at Site 2. A similar analysis has been performed at Site 1 but due to space limitations and lack of long-term data these data are not presented here. The last section of Chapter 4 provides an intercomparison of the data between Sites 1 and 2. This intercomparison includes values of average magnitudes of erosion at the two sites, discussion of trend analysis, and discussion on the governing physical mechanisms for the observed erosion processes at the two sites. This discussion is complemented with a preliminary analysis of the bank shear stress distribution at Site 1. The determined bank shear stress distribution is compared to the critical erosion strength of the bank soil.

4.1 Site 1

4.1.1 Time Series

The time series data for the 15-minutes interval are presented concommently with the stage measured at Site 1. Figure 4.1 presents the data for period of May 18th – June 22nd, 2009. Figure 4.2 provides a much more detailed depiction of the erosion rates for a narrower time window focused on the historic event of June 19th, 2009. At glance, Figure 4.1 shows continuous toe erosion activity for the period of observation. Bank toe erosion has been observed to occur on a continuous basis and presents high variability that is attributed to the variability in the stress exerted by the flow. According to Simon and Collison (2001), Papanicolaou et al (2007), and Fox et al. (2007), bank toe erosion is triggered due to significant excess or apparent shear stress, which can lead to bank undercutting near the toe region. Therefore, it is most probable that bank toe erosion at Site 1 is triggered by the fluvial shear stress.

Near the bank crest (location of sensor B2), bank erosion presents less variability comparatively to the near bank toe location; however, the mean magnitude of erosion near the crest is higher in magnitude for most of the period of observation. It is not worthy to state that for the period of May 21st to May 26th, 2009, which coincides with a

drop in the stage, high variability is shown near the crest comparatively to the remaining period of observation. This variability is attributed to subaerial processes and potentially to the swell that occurs at this location. A similar behavior has been reported in the literature by Lawler et al. (1999) and more recently by Pizzuto (2009). In short, the time series data at the toe and crest reveal, that at the toe fluvial erosion is the dominant mode of erosion whereas at the crest there is a cumulative action of fluvial erosion and subaerial processes. This finding agrees with the observations by Prosser et al. (2000) that stated 80% of the time, bank erosion at the toe is dominated by fluvial hydraulic forces. Similarly Lawler et al. (1999) postulated through decadal observations that subaerial processes have a significant contribution to bank erosion starting from the midsection of the bank and extending to the bank crest.

Another contributing factor to the variability of bank erosion shown at the site is the effects of the freeze thaw cycle observed in the study location(Gilley et al., 1993). The freeze/thaw cycle can significantly reduce the critical erosion strength in some cases by a factor of 10 (Van Klaveren and McCool, 1998).

The mid section of the section L230 experiences the highest erosion comparatively to the other two locations (crest and toe) for the period the activity has been recorded. It is not unusual for bank midsections to exhibit the highest erosion rate as those are the locations where the bank experiences a change in its overall gradient. This rather typical behavior has been reported in the literature (Harden et al., 2009; Simon et al., 2003).

As the stage increases and we approach closer to the June 19th event, the erosion rates increase at all locations. A maximum retreat of 20.5 – 22 cm is recorded to occur along the bank face (Figure 4.2). This is an indication that mass failure occurs during the rising and falling limbs of the hydrograph. In other words, the erosion process at the bank boundary loses its spatial randomness and occurs simultaneously at the same rate for all locations.

In addition, Figure 4.2 provides unique information about the time lag between the peak of the hydrograph and the highest erosion rate for all locations. The maximum retreat is observed roughly 21 hours after the occurrence of the hydrograph peak. Although, there is some uncertainty in the PEEP measurements due to potential dislocation of the sensors during the June 19th event. It is clear that swelling and subsurface flow within the bank soil have attributed to the delayed response of the bank to the June 19th event. Both subsurface flows and swelling are key components of subaerial processes reconfirming our earlier suggestion that mass erosion remains the controlling agent during and after the June 19th event at Site 1. This suggestion is similar to the observation made by Mitchell et al. (1999).

Figure 4.3 summarizes the effects of fluvial and mass erosion at Site 1 before and after the June 19th event. On an average, the survey data (Figure 4.3a) confirms the PEEP's observations. Table 4.1 provides a summary of the bank retreat at the PEEP cross-section and includes information about net erosion and deposition measured with roughly about 10 flags. Table 4.2 summarizes the bank retreat at 5 cross-sections measured with the erosion pins. Figure 4.3b provides a plan view of the study reach before and after the June 19th event. There are discernable differences between the pre- and post-event cross-sectional areas in Site 1. The pictures strongly confirm the mass erosion triggered by the June 19th event with the widening of the channel and the removal of the pre-existing vegetation along the bank face. Please note that the pre-event picture was only taken 2 hours before the initiation of the June 19th, while the post-event picture was taken the day after the event.

4.1.2 Statistical and Trend Analysis

A significant component of the statistical analysis is the moving average technique. The moving average technique is a filtering approach that is utilized to visually identify dominant trends within a time series. Moving average approaches have

been used in signal processing of air, water, and solid phase transport (Tennekes and Lumley, 1972). More recently, Fox et al. (2005) and Tamburrino et al. (1999) have utilized the moving average technique to discern large flow eddies from small eddies.

We have performed the moving average by considering five different intervals, namely 1.25-hour, 3.75-hour, 6.25-hour, 11.25-hour, and 24-hour. The selection of these intervals was made for deciphering the most prominent erosion-related events for the bank toe, mid-section, and crest. There are no discernable differences between the original time series and the moving average time series of 1.25 hours. For this reason and due to space limitations, we do not present the detailed data for the first time window of 1.25 hours.

Figure 4.4 a, b and 4.5 demonstrate a similar erosion pattern during the period of observation. As the moving time interval increases, the variability in erosion tends to be filtered out; however, the most prominent features remain. For the period May 18 – June 4, 2009 and for the time interval of 6.25 hours (Figure 4.4a), bank crest erosion dominates over bank toe erosion, as expected. For the remaining period of observation, the mid-section erosion obtains the highest values. This trend is consistent for all moving average time intervals presented here. This is not the case with the degree of variability exhibited at the three locations (i.e., toe, mid-section, and crest). For the 6.25-hour moving average window (Figure 4.4a), the recorded erosion presents a relatively high degree of variability for the three locations. This variability gradually reduces with an increase in the time average period. There are insignificant differences between Figure 4.4 b and 4.5, which suggest that the 11.25-hour window of observations preserves the highest fluctuations in the recorded erosion or equivalently the highest erosion events. This window coincides with the daylight period for the spring and summer months. During spring and summer, daylight was between 7 am and 7 pm; during fall and winter the daylight was between 8 am and 5 pm.

The practical importance of the moving average results has to do with recommendations about the sampling interval of PEEPs. Figure 4.4a, b reveal that a sampling interval varying between 6.25 hours and 11.25 hours may be suited for capturing the most erosive events for the banks at Site 1. This interval as noted earlier describes the most dominant events triggering both forms of erosion (fluvial and mass failure). Fluvial erosion ensues in the period between May 18 and June 18, 2009, whereas mass failure is clearly depicted by the June 19th event. Table 4.3 summarizes the averaged PEEP data obtained from the original time series and the 1.25-hour, 3.75-hour, 6.25-hour, and 11.25-hour, moving average interval time series. The table confirms our visual observation that there is negligible difference between 6.25 and 11.25 hours.

Figure 4.6 presents the Shewhart charts for hundreds of observations performed per location (toe, mid-section, and crest) at Site 1. The charts provide the time series of the real data and the median (or central limit, CL), as well as the upper and lower control limits (UL/ LL). The UL and LL are nothing more than the median plus a baseline variation triggered by the physical processes (e.g., erosion). At the bank crest, the actual erosion observations expressed in terms of erosion length present a downward trend with respect to CL indicating a non-stationarity (Chatfield, 1984). The downward trend implies that the original erosion observations are followed with observations of a comparatively smaller magnitude or equivalently the distribution of the real data is represented by a negatively skewed, log normal distribution. All observations in Figure 4.6 a (bank crest) have a conforming behavior, i.e., all data are within UL and LL and tend to cluster about CL, other than the data points corresponding to the June 19th event. These points exhibit a non-conforming behavior attributed to the intensity of erosion for this particular event.

Figure 4.6 b illustrates the control limits for the bank mid-section at Site 1. Again all points exhibit a conforming behavior except those points corresponding to the June 19th event. However, there are two distinct differences between Figure 4.6 a and 4.6 b.

The real data in the latter case cluster about the center line but equally above and below it indicating an alternating observation pattern with successive observations about the overall median. In addition, in Figure 4.6 b the number of non-conforming observations increases comparatively to the crest. This behavior suggests that the number of observations approaching the UL increases due to application of high magnitude bank shear stress for a longer period. A similar behavior about the number of non-conforming data is noted for the bank toe location. The difference between the bank toe and the other two locations is that observations above the median tend to be followed by further observations above the median, and similarly for observations below the median. The variability in erosion illustrated Figure 4.6 c is of intermittent nature suggesting that episodic erosion triggered by the complex interaction between flow and the bank profile occurs at the bank toe (Thorne and Osman, 1988). Contrary to the downward trend shown in Figure 4.6 a, the time series in Figure 4.6 c demonstrates an upward trend. The upward trend implies that most of the observations are of higher magnitude relative to the median and that the distribution of the data can be adequately described by a positively skewed, log normal distribution.

The correlograms developed for the three locations at Site 1 confirm the Shewhart chart findings. Figure 4.7 shows that at the crest short-term correlations between the observations are present. This is the outcome of a non-stationary time series. At the mid-section, a correlogram reflecting an alternating time series is developed. At the toe, the correlogram exhibits short-term correlation, which means values of the autocorrelation coefficient for longer lags tend to be approximately zero.

In addition to the statistical analysis, we have performed a comparison between the PEEP data at site 1 with data obtained based on two methods: (a) manual measurements of the PEEP exposed length via the measure tape and (b) survey measurements. All comparisons are made for the pre- and post-event of June 19th (Table 4.4). The comparisons show that there is a good agreement between all measurement

techniques. The maximum error was observed between manual and automated measurements of the exposed length of the PEEPs and this error was less than 27%. The error between the survey and the automated PEEP measurements was less than 14%. Potential sources of the disagreement between the measurement devices included light angle orientation with respect to the PEEP location, shading provided by the presence of clouds and trees in the proximity of PEEPs, and Magnus spin lift acting on the PEEP sensors when they were protruding into the flow, which may have caused the displacement of the PEEPs along their longitudinal axis due to increased rotational velocity. Not meaningful comparisons can be made between B1 and B3 due to the wash out of the PEEPs by the flow.

4.2 Site 2

4.2.1 Time Series

A similar procedure is adopted here to present the results for the absolute erosion length for Site 2 with the one considered for Site 1. Due to the spatial variability in surface bank erosion and anomalies found at the bank face at Site 2, three transects were considered, namely transect 1 (PEEP A2), transect 2 (PEEP L231), and transect 3 (PEEPs A1 and A4) (Figure 4.8). Contrary to the short time window of observation for Site 1, at Site 2 the period was extended from June 4, 2009 all the way to December 1, 2009. Emphasis was also placed on observation on and after the June 19th event and August 27th event. Likewise to Site 1, the time series data are presented within a 15-minute time interval. Figure 4.9 and 4.10 depict the stage-discharge variability and the absolute erosion length. A quick comparison between Figure 4.1and 4.2 with 4.9 and 4.10 reveals a discernable difference in the stage recorded at Sites 1 and 2, respectively. Other than the June 19th event that triggered a historic upper limit value of 300 cm and above, most of the stage values at Site 1 are of a single or at best double order of magnitude. At Site 2, the minimum observed stage (or baseflow) was of a three orders of magnitude,

nearly 100 cm. This comparison suggests that Site 2 must be more active in terms of continuous erosion than Site 1. This at-a-glance conclusion is well reflected by the absolute erosion lengths shown in Figure 4.9 and 4.10. Clearly there is continuous fluvial erosion occurring at the site. This fluvial erosion is complemented with mass failure triggered at various instances within the period of observation. A geomorphological outcome of the mass erosion is the over-steepening of the upper top half of the bank (Figure 4.8). In addition, this phenomenon results to over-hanging segments of the upper crest of the bank well illustrated in Figure 4.8. Ubiquitous forbays of protruding bank notches form near the toe. These forbays alternate in space revealing the cumulative impacts of increased shear stress, rainfall event wet conditions, as well as seepage on bank failure. These alternating bankform features have been observed in several sites around the world where semi-cohesive banks are present (Mitchell et al., 1999; Papanicolaou et al., 2007; Simon et al., 2000).

The time series data shown in Figure 4.9 and 4.10 confirm the visual observations made in Figure 4.8. Fluvial erosion was accompanied sporadically by mass erosion. As a result, the PEEP sensors had to be removed and reset due to their significant exposure to the flow and instabilities stemming from this exposure. For example, other than location A4 found at a relatively stable notch at Site 2, all other PEEPs had to be reset. This explains the "staircase shape" of the time series shown in Figure 4.9 and 4.10. The discontinuities found in the time series clearly correspond to the sensor reset. A review of Table 4.3 shows that the mean absolute erosion length at Site 2 is at least 3 to 4 times larger in magnitude than Site 1.

Figure 4.11 encapsulates the effects of the June 19th event at Site 2. Due to the extreme and flashy nature of the June 19th event, Sites 1 and 2 exhibit comparable absolute erosion rates. It is the August 27th event, which recorded the highest erosion rates at Site 2. Figure 4.12 presents a consistent bank erosion behavior for most mid-sized streams. There is a distinct difference between pre- and post-event bank erosion

features for this stream size. Bank erosion exacerbates during post-event, which typically corresponds to the falling limb of the hydrograph. The excess bank erosion is believed to be the cumulative impact of the rapid drawdown of the hydrograph, a similar observation has been made by Mitchell et al.(1999) in UK Streams and Darby et al. (2007) in the Sieve River, Italy. All the pre-described features were not observed at Site 1.

Figure 4.13 and 4.14 provide the summary of the before and after conditions for all three transects at Site 2. At Transect 1 the stream is active near the bed and the left bank where impingement of the incoming flow takes place. A similar behavior is shown in Transect 2. In Transect 3, the stream migrates towards the left bank.

4.2.2 Evaluation of PEEP Performance

Figure 4.15 summarizes the statistical tests performed for PEEPs A1, A2, and A4 located at the three transects at Site 2. On the vertical axis are plotted all the data, which include data when the PEEPs were submerged and unsubmerged. To determine the impact of submergence on the instrument performance, we correlated all data defined earlier with unsubmerged data. Figure 4.15 reveals that there is a positive correlation between unsubmerged and all data with the poorest performance exhibited by PEEP A4. Figure 4.15 incorporates regression lines and confidence intervals for the best fit lines of the real data. The closer the PEEPs are to the free water surface, the poorer the performance of the PEEP is. This is reflected with the R^2 value recorded for the three PEEP transects. The higher the elevation of the sensor, the higher the R^2 obtained from the best fit analysis. We believe PEEPs located near the toe of the bank perform poorer than the remaining PEEPs for the following reasons: (1) light availability and penetration corresponding to the submergence period of the PEEPs and (2) disturbance caused by the bank inundation and the formation of forbay areas in the proximity of the bank toe.

In terms of light availability, several authors (Effler, 1988; Effler et al., 2007; Lin et al., 2009) noted and quantified the role of water transparency on light penetration.

They demonstrated that suspended sediment triggers light scattering and, in some case, absorption. As a result the light penetrating the water may not reach the photovoltaic cells of the instrument. Transparency measurements performed by Loperfido (2009) in Clear Creek show that the average transparency is less than 40 cm. Therefore it is safe to say that attenuation of light due to traveling in the water phase is further amplified by the presence of suspended material, which affects water transparency.

Table 4.5 offers a comparison of the automated bank measurements with the traditional measurements (i.e., tape measure and surveys) at Site 2. The surveys were performed on July 30th and September 30th. There is an excellent agreement between the measurements for PEEP A2. The maximum error observed was about 20% and was recorded for PEEP L231. Figure 4.16 complements the results summarized in Table 4.4, and demonstrates the performance of all PEEPS against the measure tape measurements referred in the horizontal axis as manual measurements. The closer to the bank toe, the higher the departure is between the automated and manual measurements. Several authors in the literature have attributed this trend to the intense inundation that takes place near the toe. Vibration caused by the potential induced spiral motion of the impinging flow must also be considered (Couperthwaite et al., 1998; Lawler, 1991; Lawler, 1992; Lawler, 2005b; Lawler, 2008; Lawler et al., 2001; Mitchell et al., 1999; Prosser et al., 2000).

4.2.3 Statistical and Trend Analysis

Similar to Site 1, statistical analysis involved the performance of moving averages by considering five intervals (namely 1.25-hour, 3.75-hour, 6.25-hour, 11.25-hour, and 24 hour). Figure 4.17 demonstrates the moving average absolute erosion length for the 6.25-hour and 11.25-hour intervals. As expected the variability in Figure 4.17 b (11.25-hour interval) is smaller comparatively to the variability shown in the Figure 4.17 a (6.25-hour interval). Regardless of the differences in the degree of variability between the two

figures, both figures preserve the key features of erosion at Site 2. These features are described by the "staircase" type distribution following, with some time lag, the occurrence of the peak events. Similar to Site 1, it is concluded that a sampling interval varying between 6.25 and 11.25 hours is suitable for recording the most erosive events for the banks at Site 2.

Figure 4.18 provides the time series at a daily time step. By far, transects 1 and 2 exhibit the highest erosion, which corresponds with the formation of the forbay and where the incoming flow impinges into the inner bend section of the bank. The Shewhart control limits (Figure 4.19, Figure 4.20) reveal very interesting information regarding the mechanisms of erosion at Site 2. Despite the increased erosion length when compared to Site 1, the absolute erosion length at Site 2 resides within the upper and lower control limits indicating that no rare, or extreme, occasion events have occurred during the period of observation. This finding confirms the common knowledge within the hydraulic and geomorphologic community that bank erosion at the lower segments of a mid-sized stream is, for the most part, dictated by fluvial erosion and to a lesser extent by mass failure (Papanicolaou et al., 2006). Other than PEEP A4, which exhibits a relatively seasonal behavior, the erosion observations at the remaining PEEP locations exhibited an upward trend demonstrating the active nature of erosion at Site 2.

Figure 4.21 is the correlogram for the 15-minute data recorded at the four PEEP locations. The correlograms demonstrate the effect of seasonality on bank erosion. A sinusoidal pattern is observed with all observations being pretty much in phase for the first 100 minutes. Observations at A2 tend to become out of phase with the remaining of observations for time lags greater than 100 minutes. This finding is not unexpected considering that the dominant mechanism of erosion for PEEPS A1, A4, and L231 is fluvial whereas the dominant mechanism of erosion at A2 is both fluvial erosion and mass failure. When Figure 4.21 is compared to Figure 4.7, one can recognize the distinct nature of erosion between Sites 1 and 2. Site 1 is described by intermittent fluvial

erosion interjected by episodic mass erosion events whereas Site 2 is mostly governed by seasonal fluvial erosion variability.

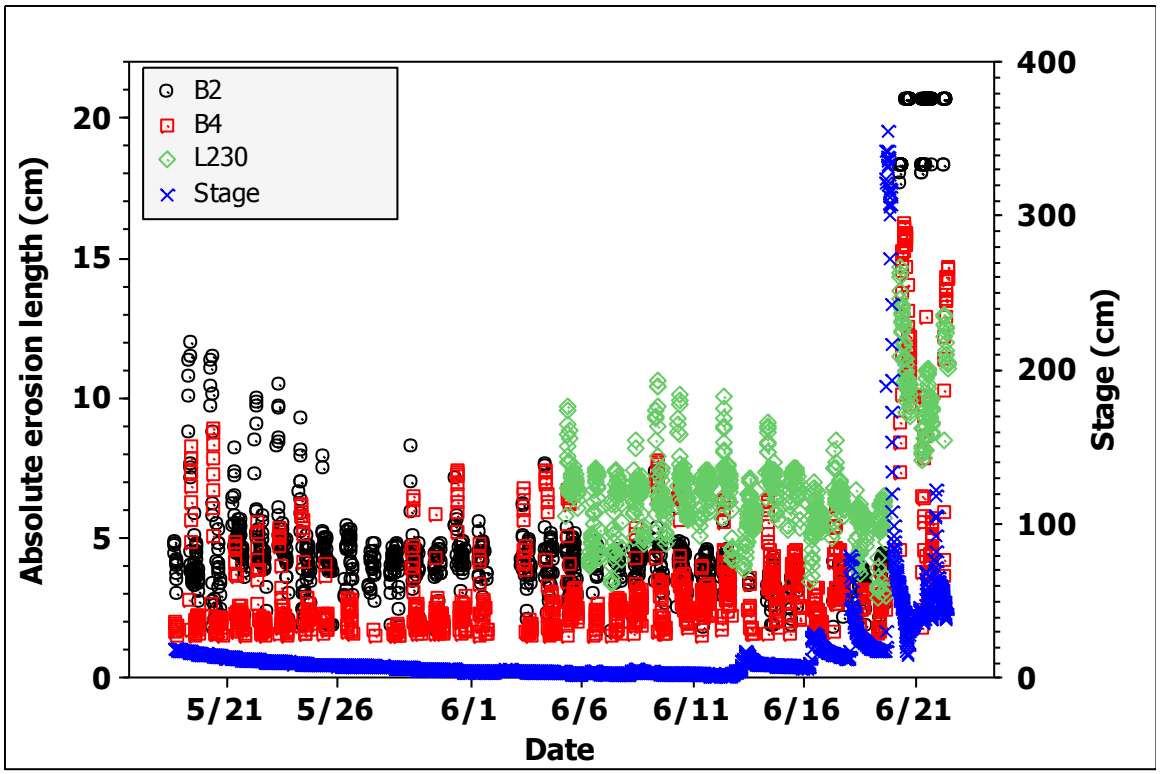

Figure 4.1: Times series of 15-minutes interval, stage and bank erosion measurements using the sensors B2, B4, L230 at South Amana (Site 1).

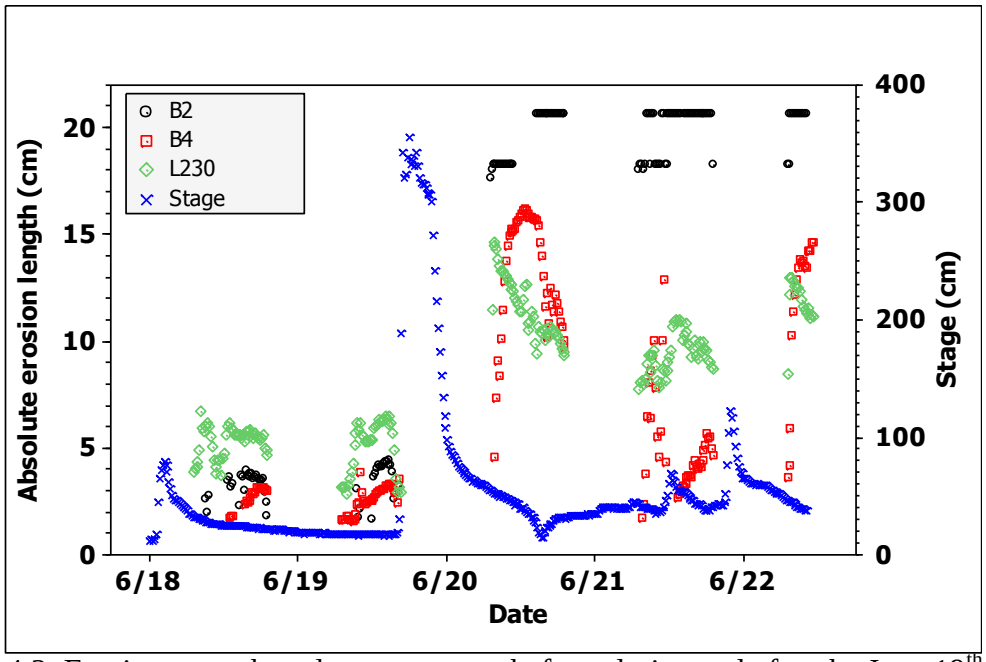

Figure 4.2: Erosion event-based measurement before, during and after the June 19th storm event at South Amana. The x-axis is the 15-minute interval, the primary y-axis is the absolute erosion measurements in cm and the secondary y-axis is the water stage in cm.

a) PEEP cross-section before and after the June 19th event

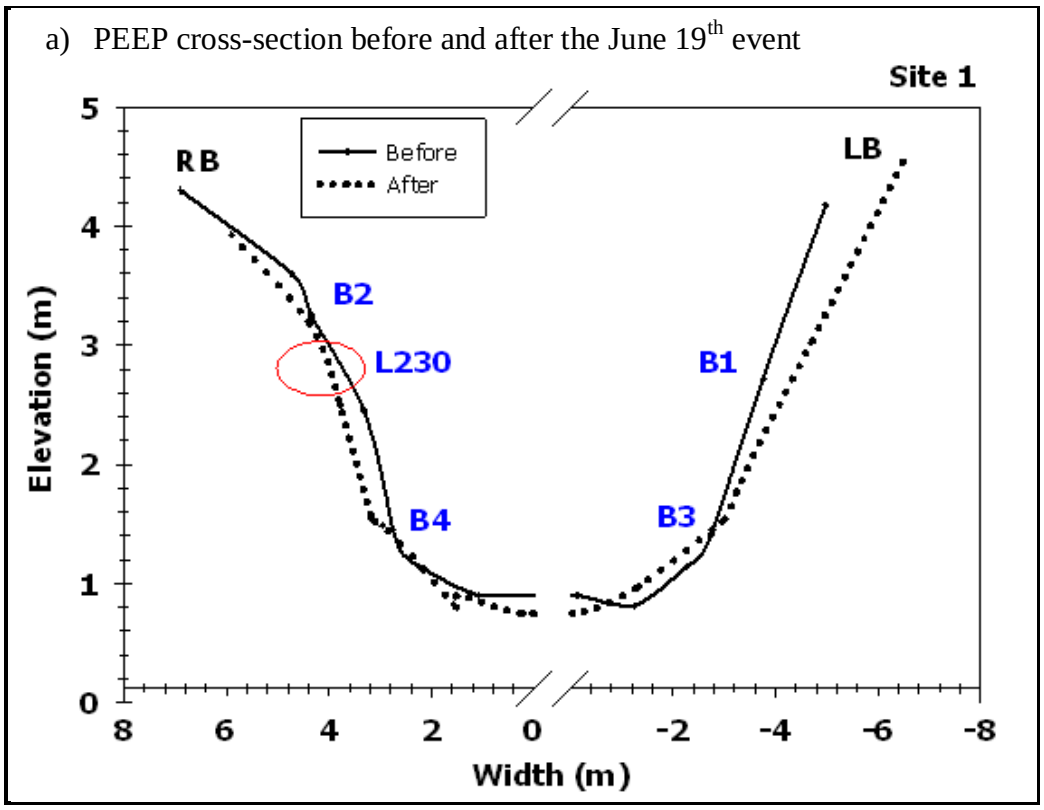

b) Picture of the PEEPs cross-section pre- and post event

Figure 4.3: South Amana before and after the June 19th event.
(a) PEEP cross-section pre-event and post-event. The bank profile is delimitated using the survey data of May 28th and June 23rd 2009.
(b) Plan view of the study reach pre-event and post- event. Facing downstream, "RB" stands for Right bank and "LB" for left bank.

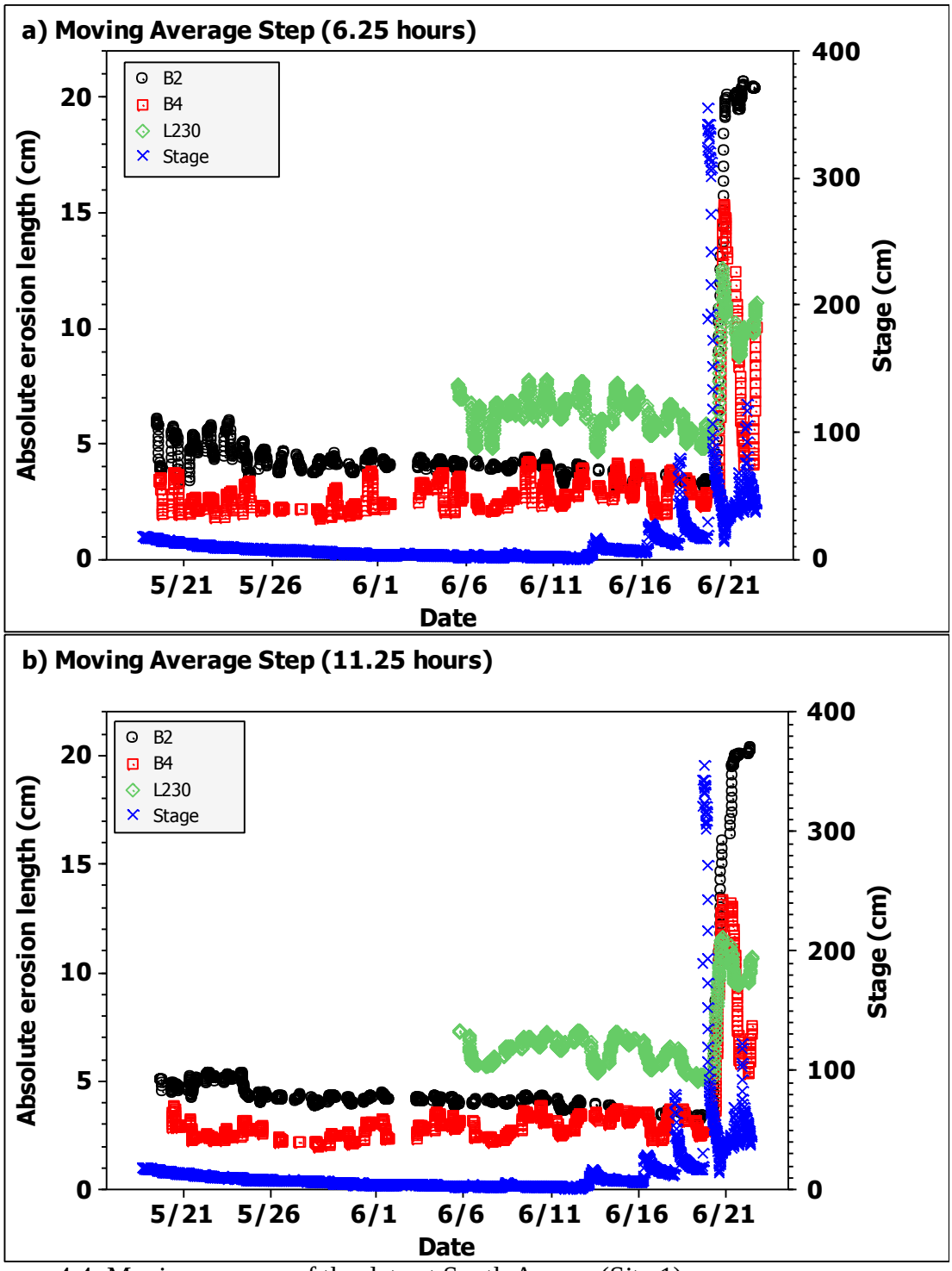

Figure 4.4: Moving average of the data at South Amana (Site 1)
(a) Moving average length: 6.25 hours
(b) Moving average length: 11.25 hours.

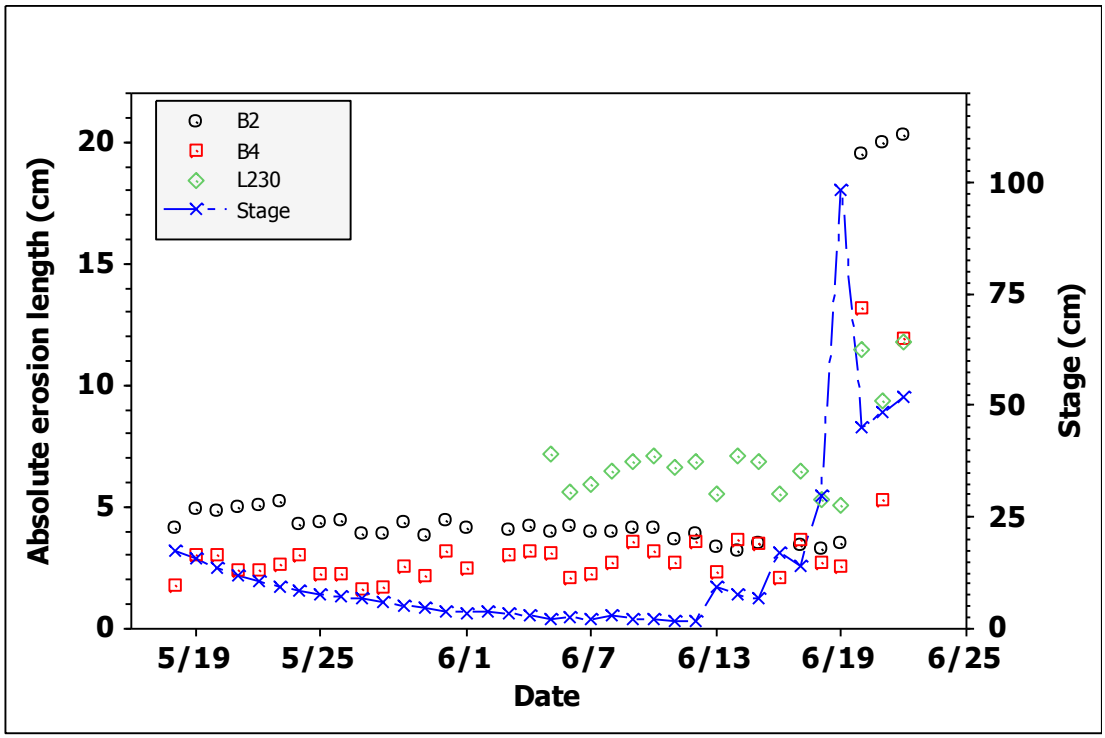

Figure 4.5: Times series of daily interval, stage and bank erosion measurements using the sensors B2, B4, L230 at South Amana (Site 1).

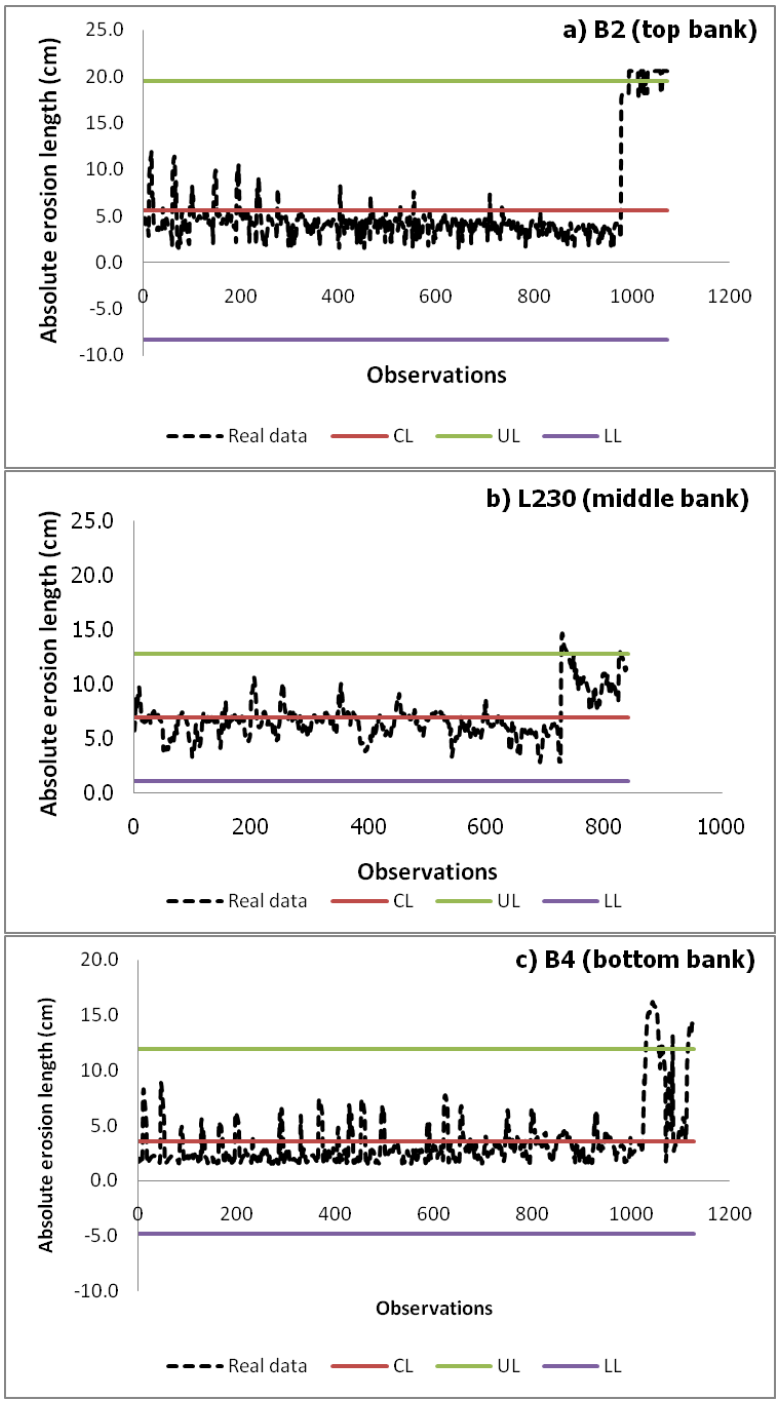

Figure 4.6: Shewhart control limits chart of the measurements data against the order of observations for the sensors at South Amana (Site 1).

(a) B2 (Top bank),
(b) L230 (middle bank)
(c) B4 (bottom bank)

In this graph, UL states for Upper control limit, LL for Lower control limit and CL for Center line.

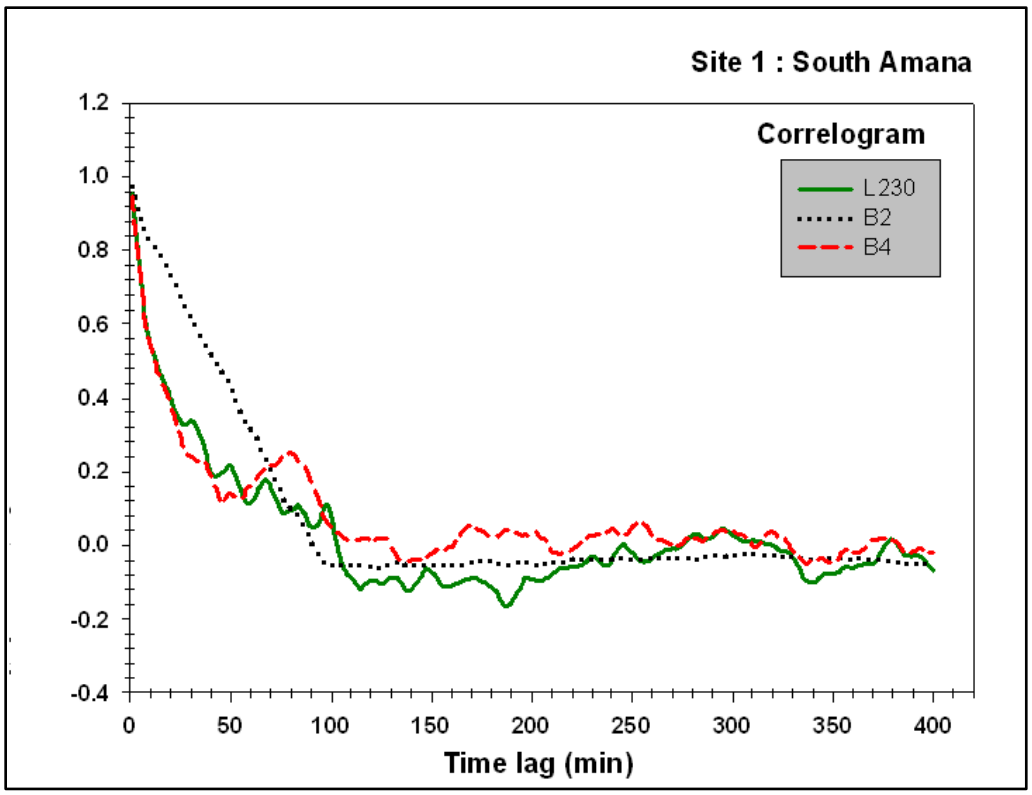

Figure 4.7: Correlogram of the 15-minutes interval time series using the PEEP sensors erosion data at South Amana (Site 1).

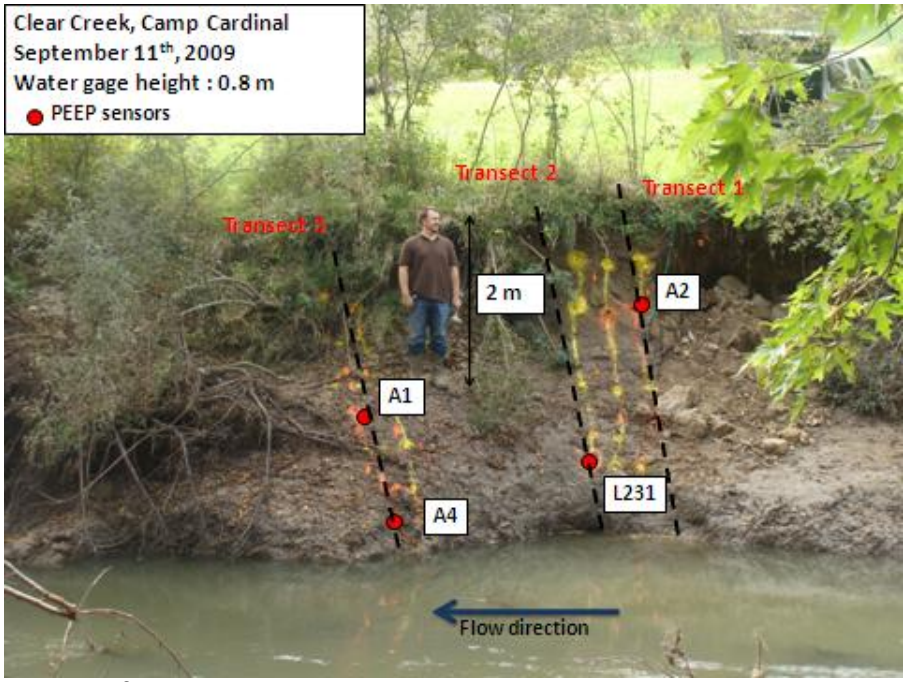

Figure 4.8: View of the three transects considered in Camp Cardinal (Site 2): Transect 1 (PEEP A2), transect 2 (PEEP L231), transect 3 (PEEP A1, and A4).

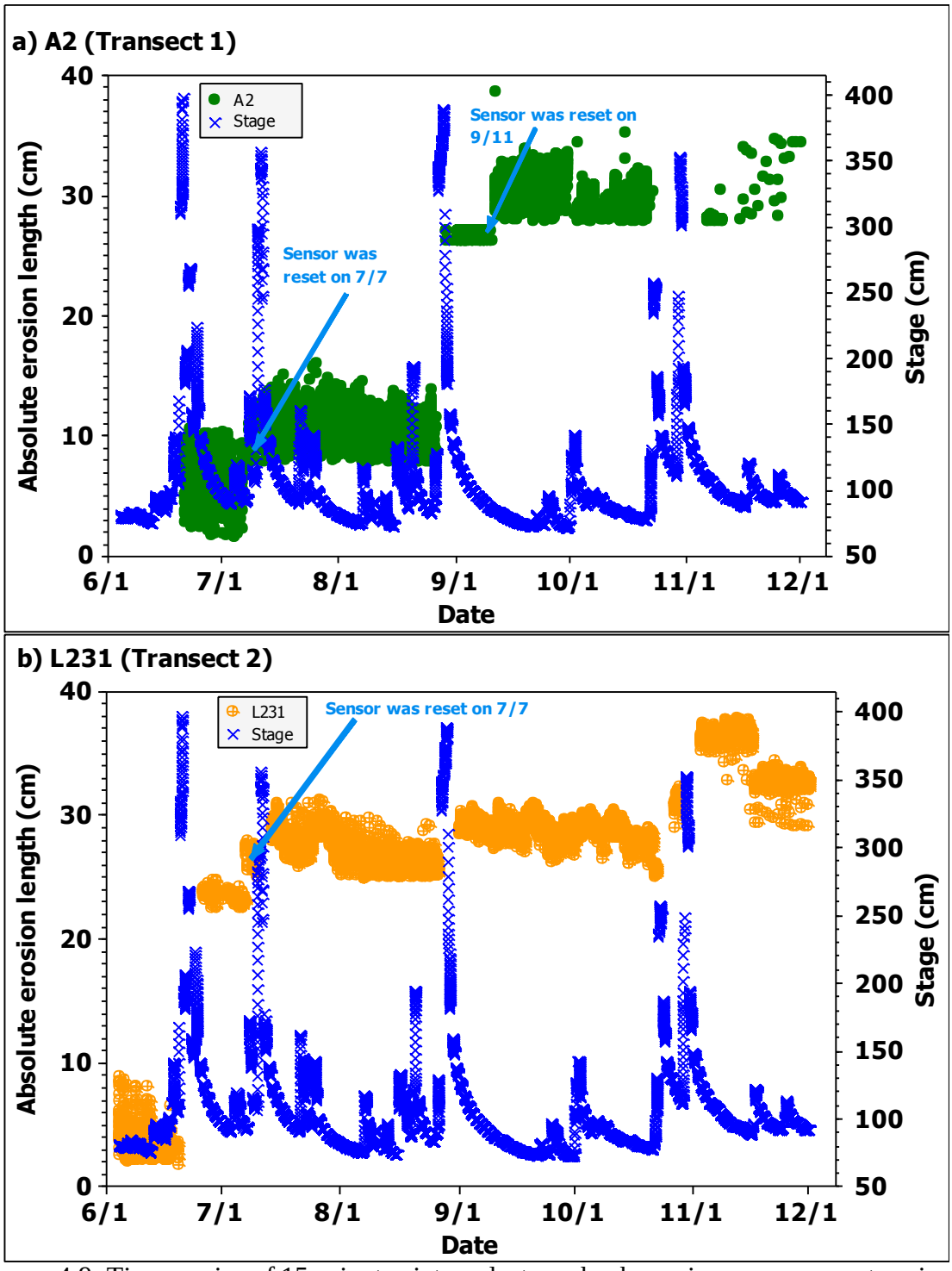

Figure 4.9: Times series of 15-minutes interval, stage, bank erosion measurements using the sensors at Camp Cardinal (Site 2)
(a) A2 (upper bank – Transect 1)
(b) L231 (middle bank – Transect 2)

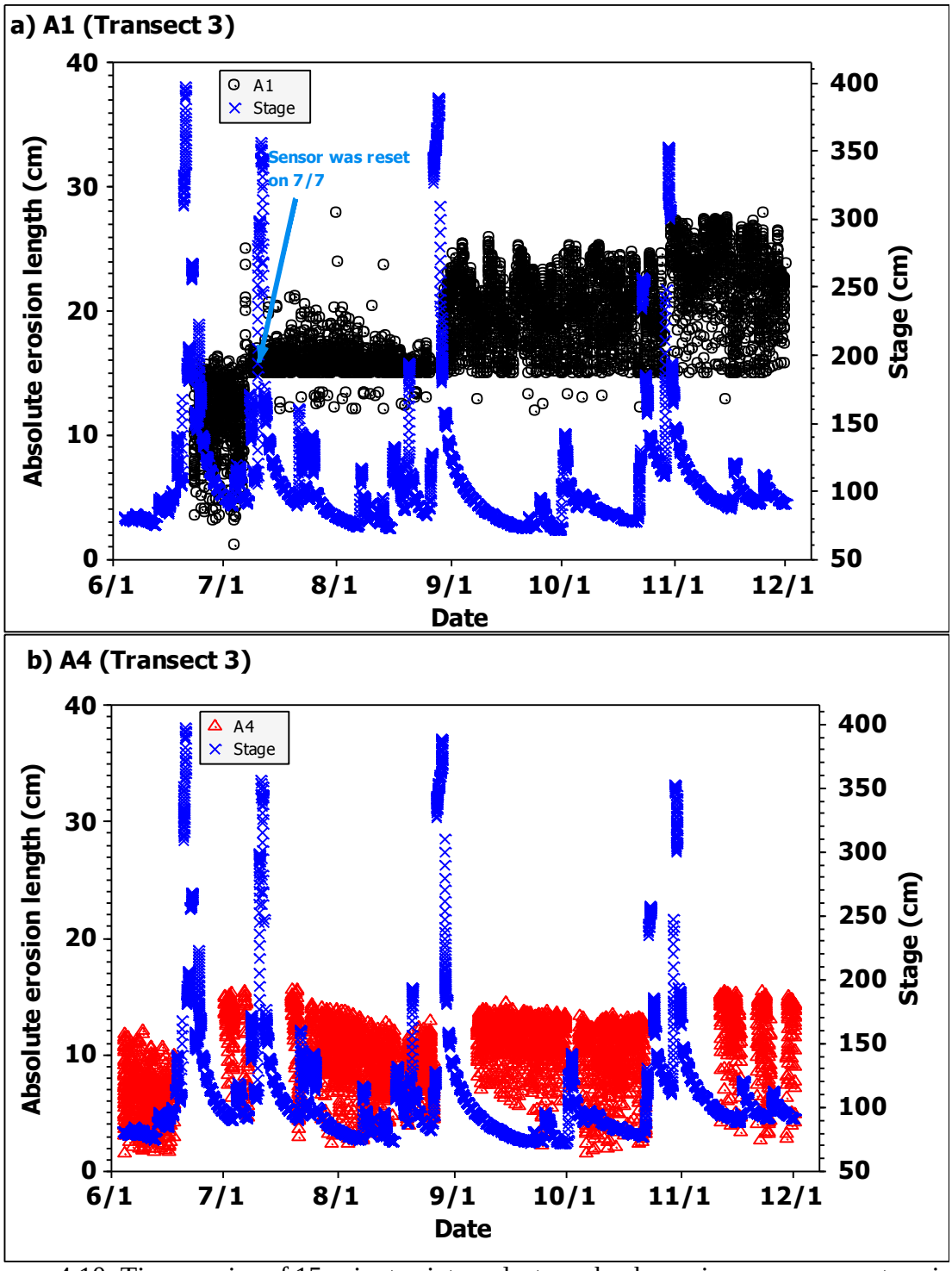

Figure 4.10: Times series of 15-minutes interval, stage, bank erosion measurements using the sensors at Camp Cardinal (Site 2)

(a) A1 (middle bank – transect 3)

(b) A4 (bottom bank – Transect 2)

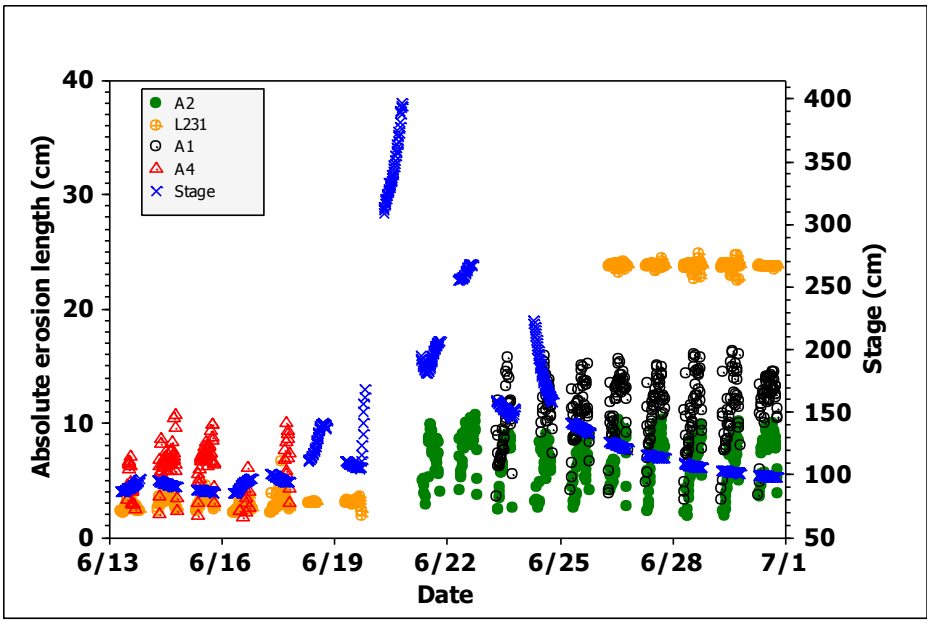

Figure 4.11: Erosion event-based measurement before, during and after the June 19th storm event at Camp Cardinal. The x-axis is the 15-minutes interval, the primary y-axis is the absolute erosion measurements in cm and the secondary y-axis is the water stage in cm.

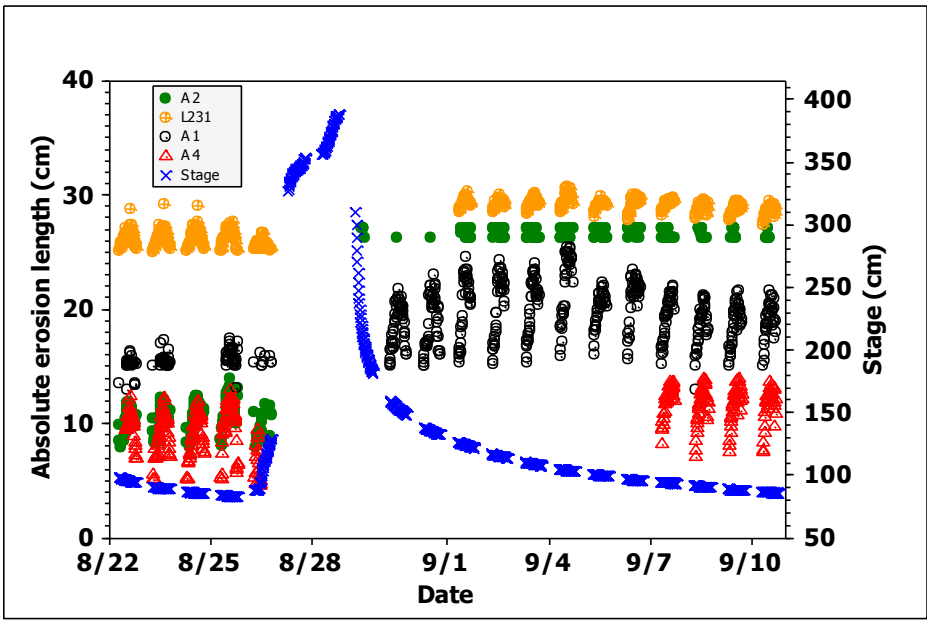

Figure 4.12: Erosion measurements at an event scale before, during and after the high flow event of August 27th at Camp Cardinal. The x-axis is the 15-minutes interval, the primary y-axis is the erosion measurements in cm and the secondary y-axis is the water stage in cm.

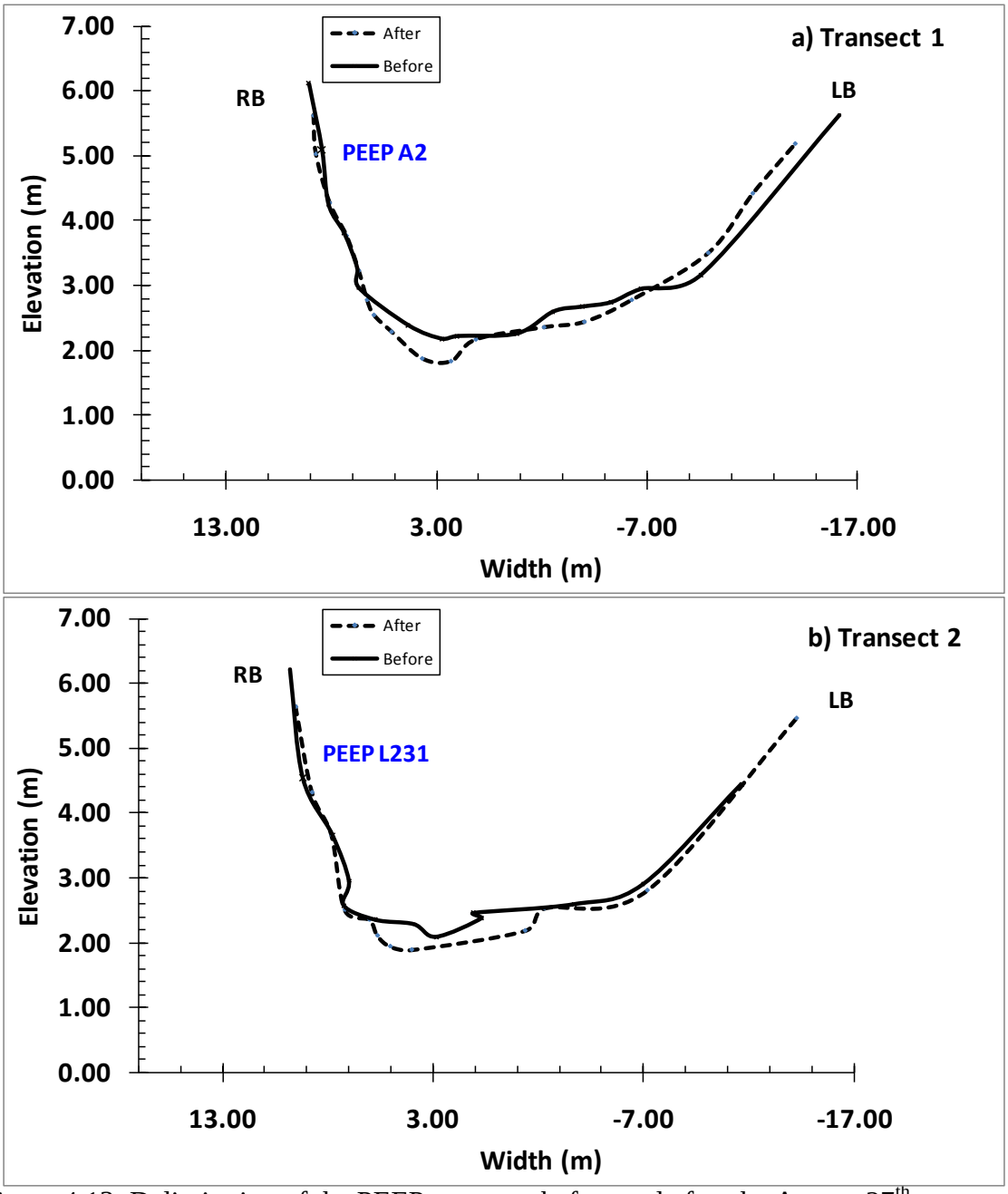

Figure 4.13: Delimitation of the PEEP transects before and after the August 27th event. The bank profile is delimitated using the survey data of July 30th and September 30th 2009. Facing downstream, "RB" stands for Right bank and "LB" for left bank.
(a) Transect 1
(b) Transect 2

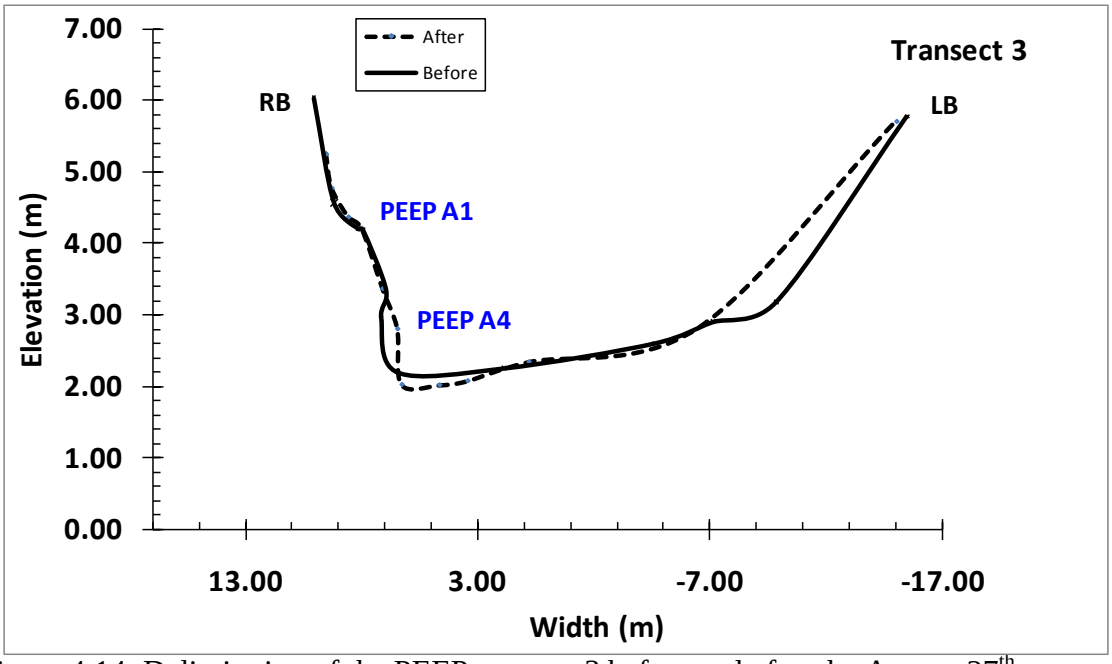

Figure 4.14: Delimitation of the PEEP transect 3 before and after the August 27th event. The bank profile is delimitated using the survey data of July 30th and September 30th 2009. Facing downstream, "RB" stands for Right bank and "LB" for left bank.

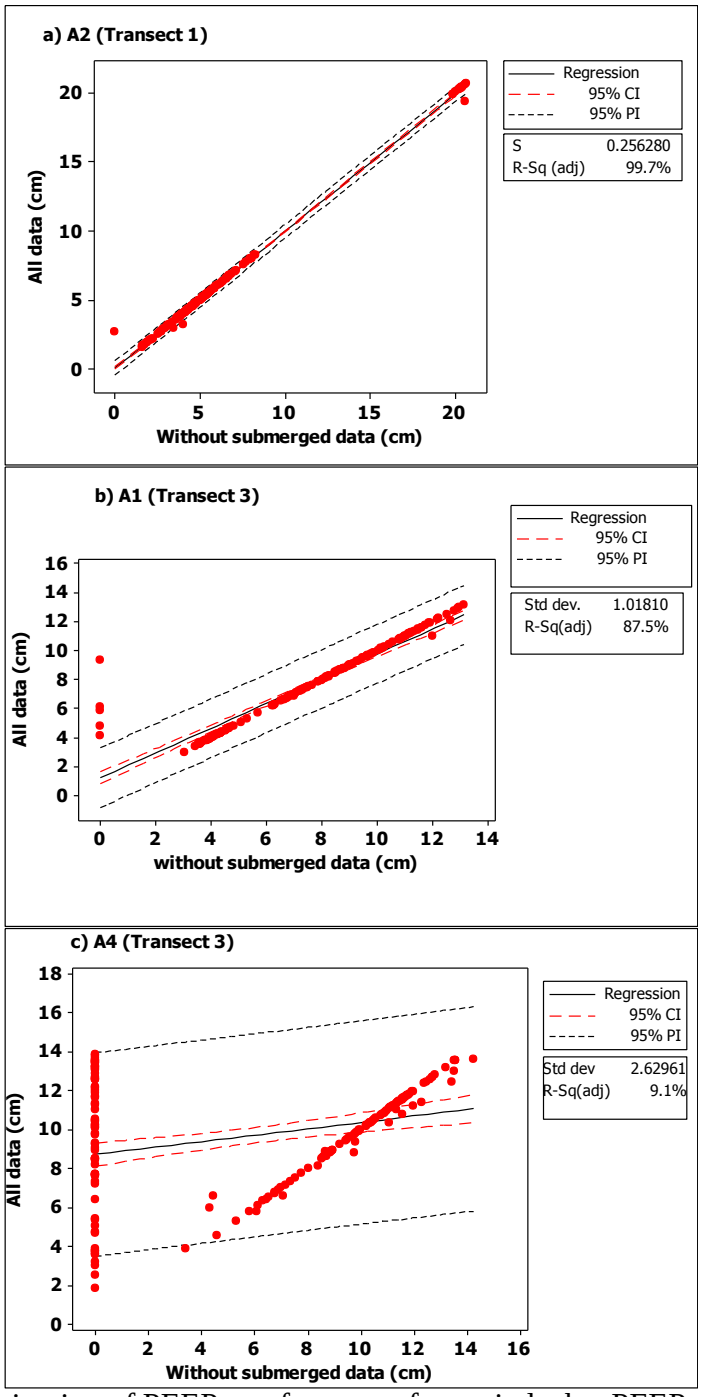

Figure 4.15: Examination of PEEPs performance for periods that PEEPs are submerged to the flow and unsubmerged at Camp Cardinal (Site 2). The x-axis includes data when PEEPs are fully submerged. The y-axis includes all the data without removing the data when submerged.

(a) Data recorded with PEEP A2
(b) Date recorded with PEEP A1
(c) Data recorded with PEEP A4

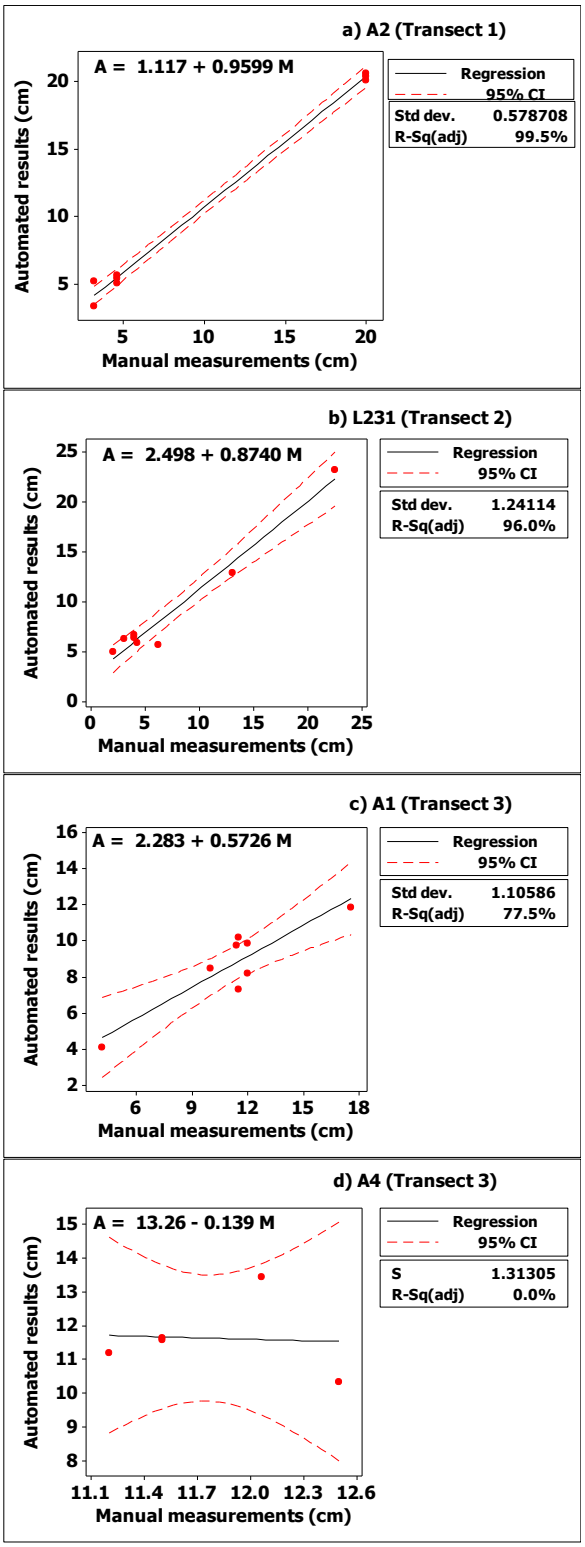

Figure 4.16: Regression plot between the PEEP results and measure tape measurements.
(a) A2
(b) L231
(c) A1
(d) A4 for the same date.

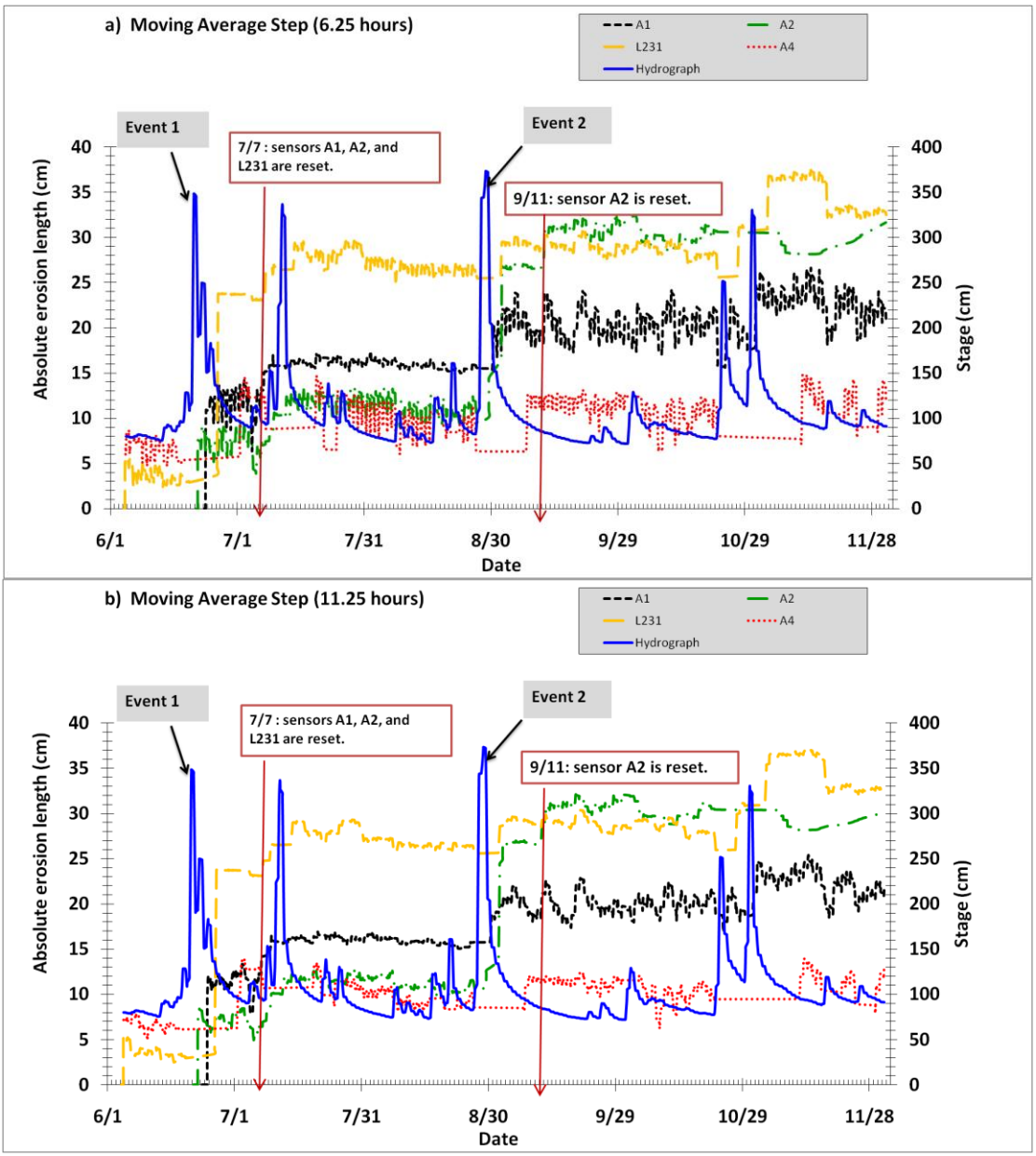

Figure 4.17: Moving average of the data at Camp Cardinal (Site 2)
(a) Moving average length: 6.25 hours
(b) Moving average length: 11.25 hours.

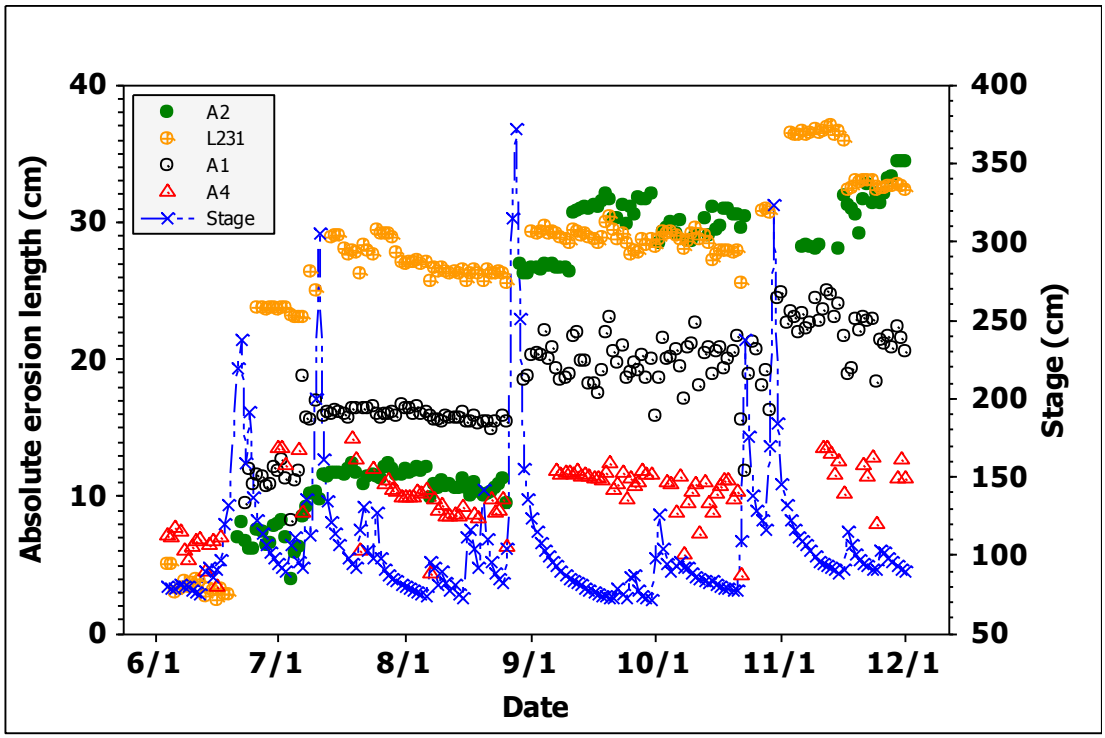

Figure 4.18: Times series of daily interval, stage and bank erosion measurements using the sensors A2, L231, A1, and A4 at Camp Cardinal (Site 2).

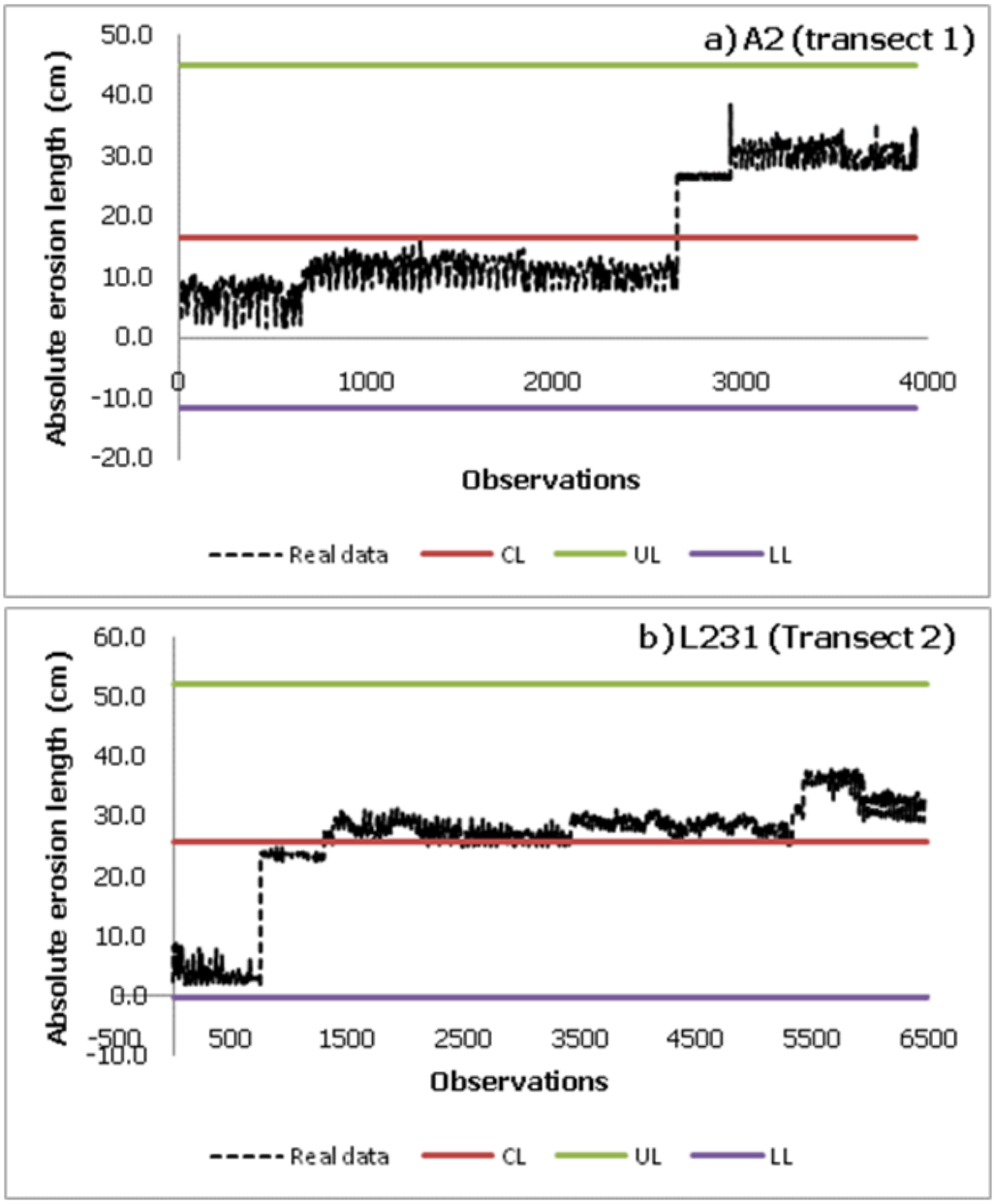

Figure 4.19: Shewhart Control limits chart of the measurements data against the order of observations for the sensors at Camp Cardinal (Site 2)

(a) A2 (Transect 1)

(b) L231 (Transect 2

In this graph, UL states for Upper control limit, LL for Lower control limit and CL for Center line.

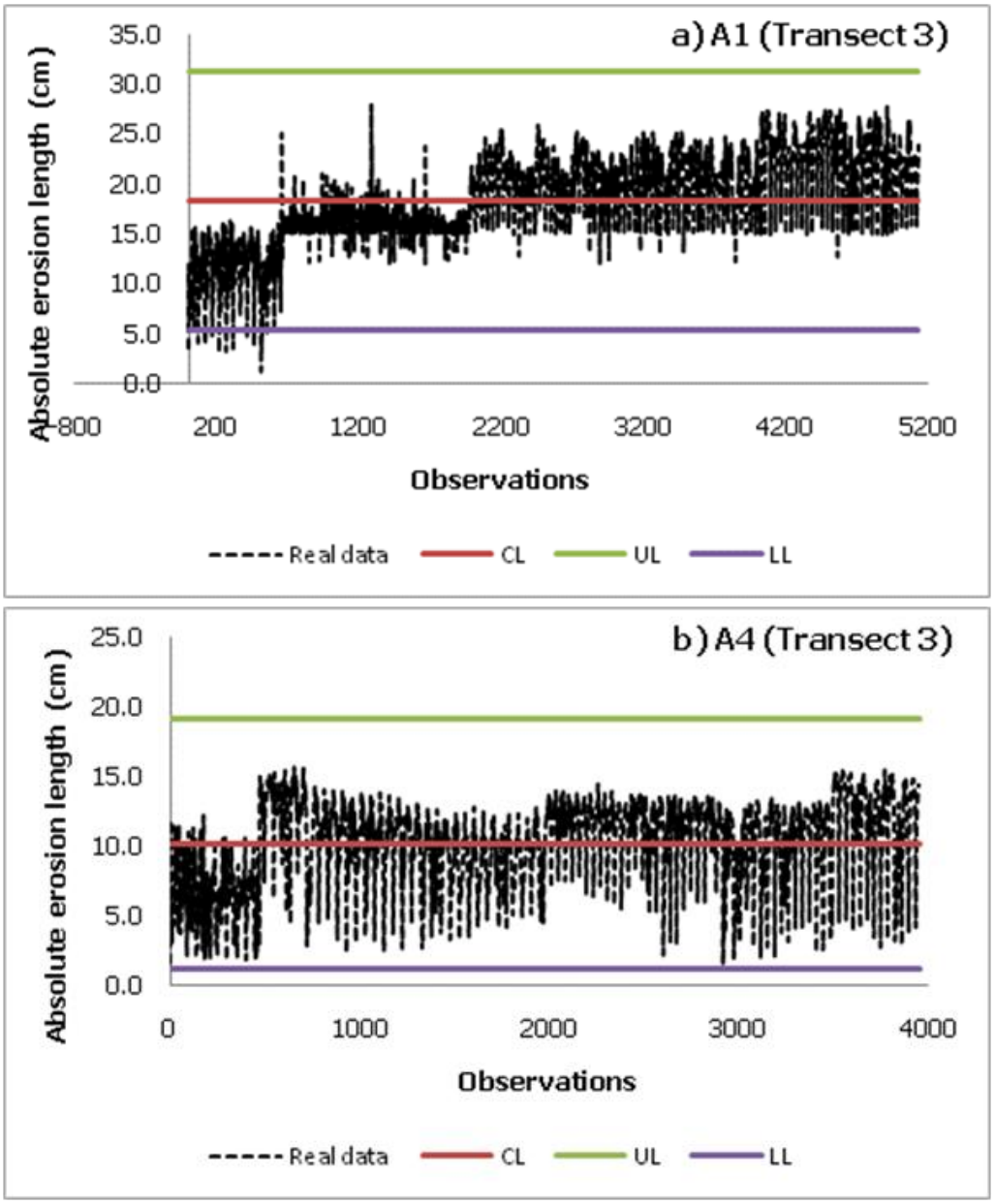

Figure 4.20: Shewhart Control limits chart of the measurements data against the order of observations for the sensors at Camp Cardinal (Site 2)

(a) A1 (Transect 3)

(b) L231 (Transect 3)

In this graph, UL states for Upper control limit, LL for Lower control limit and CL for Center line.

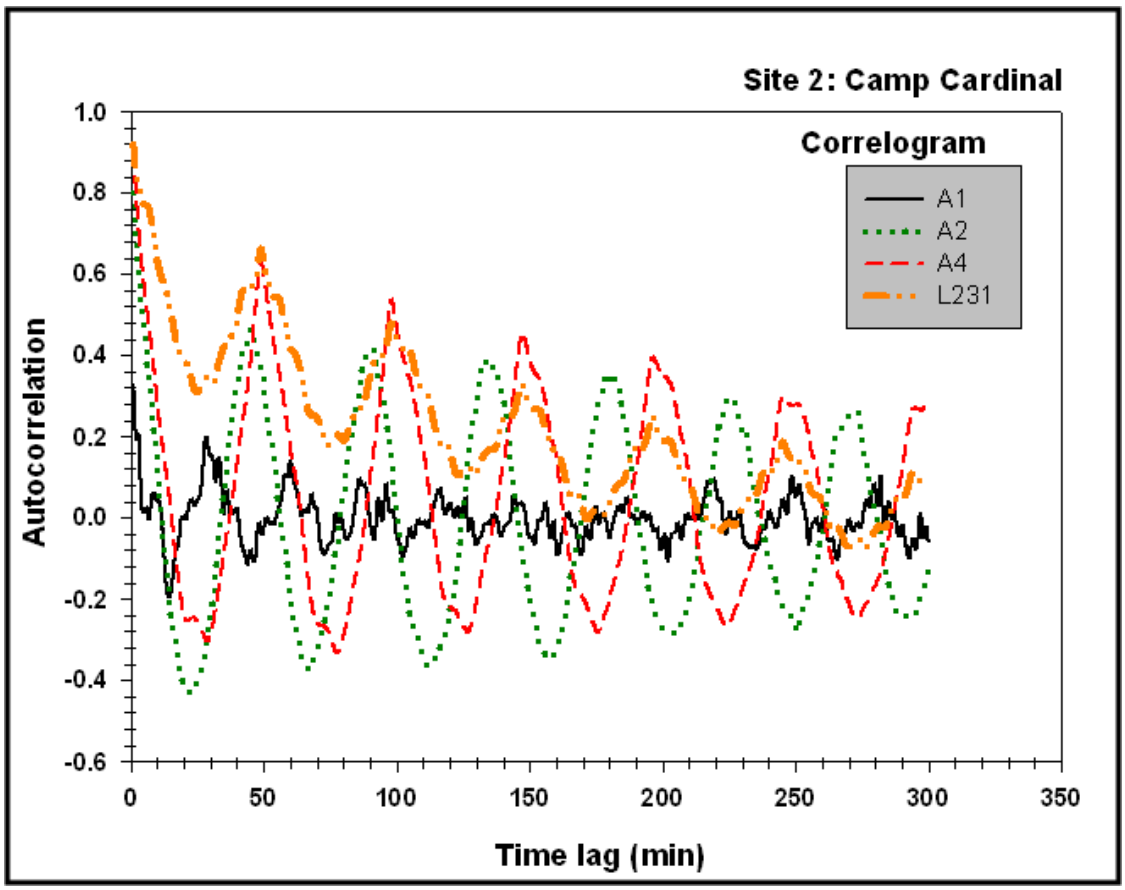

Figure 4.21: Correlogram of the 15-minutes interval time series using the PEEP sensors erosion data at Camp Cardinal (Site 2).

Table 4.1: Erosion pin measurements at Site 1 for the PEEP cross-sections before and after the June 19th event.

Cross-Section	Bank	Bank Location	June 12th, 2009	June 24th, 2009	Change ["+" erosion and "-" deposition]
			Exposed Length (cm)	Exposed Length (cm)	
PEEP	Left	B-1	NA	*	NA
PEEP	Right	B-2	5.1	27.9	22.9
PEEP	Left	B-3	4.8	*	NA
PEEP	Right	B-4	6.2	9.5	3.3
PEEP	Right	L230	0	8.9	8.9

Table 4.2: Erosion pin measurements at Site 1 from cross-section 1 to cross-section 5 before and after the June 19th event.

Cross-Section	Bank	Bank Location	June 12th, 2009 Exposed Length (cm)	June 24th, 2009 Exposed Length (cm)	Change ["+" erosion and "-" deposition]
1	East	Top	*	*	NA
1	East	Middle	1.7	30.5	28.7
1	East	Bottom	1.1	30.5	29.4
1	West	Top	*	*	NA
1	West	Middle	2.9	30.5	27.6
1	West	Bottom	1.3	30.5	29.2
2	East	Top	7.3	30.5	23.2
2	East	Middle	0.6	30.5	29.8
2	East	Bottom	0.6	5.1	4.4
2	West	Top	0.6	30.5	29.8
2	West	Middle	1.3	30.5	29.2
2	West	Bottom	0.5	30.5	30.0
3	East	Top	1.1	17.8	16.7
3	East	Middle	1.7	3.8	2.1
3	East	Bottom	0.3	19.2	18.9
3	West	Top	0.6	3.3	2.7
3	West	Middle	0.6	7.5	6.8
3	West	Bottom	1.6	24.8	23.2
4	East	Top	2.2	30.5	28.3
4	East	Middle	3.5	30.5	27.0
4	East	Bottom	3.7	0.0	-3.7
4	West	Top	0.8	3.7	2.9
4	West	Middle	0.6	2.4	1.7
4	West	Bottom	1.1	3.3	2.2
5	East	Top	3.2	7.6	4.4
5	East	Middle	0.8	7.0	6.2
5	East	Bottom	1.9	3.7	1.7
5	West	Top	0.6	0.2	-0.5
5	West	Middle	0.8	19.7	18.9
5	West	Bottom	4.9	7.1	2.2

Table 4.3: Averaging of the original time-series and the time series moving average of 1.25, 3.75, 6.25, and 11.25 hours interval.

Mean value of PEEPs absolute erosion length at site 1 and 2 (cm)					
	Original	Moving average step (hrs)			
PEEPS	time	1.25	3.75	6.25	11.25
B2	5.59	5.57	5.50	5.42	5.28
B4	3.51	3.50	3.45	3.42	3.40
L230	6.91	6.90	6.86	6.83	6.78
A1	18.38	18.38	18.39	18.40	18.41
A2	16.57	16.57	16.56	16.55	16.54
A4	10.14	10.14	10.14	10.14	10.14
L231	25.88	25.89	25.90	25.91	25.93

Table 4.4: Comparison of the automated bank measurements to the traditional methods (manual measurements and resurvey bank lines) at Site Amana.

Erosion length (cm) after the June 19th event (cm) at Site 1			
		PEEP SENSORS	
	Survey	Automated	Manual measurement with tape
PEEP B2	17.4	20.3	27.9
PEEP L230	Missing flag	11.8	8.9
PEEP B4	12.7	11.9	9.5
PEEP B1	58.7	Instrument washout by the flow	
PEEP B3	Deposition	Instrument washout by the flow	
Bank cross-section survey before the event : May 28th			
Bank cross-section survey after the event : June 23rd			

Table 4.5: Comparison of the automated bank measurements to the traditional methods (manual measurements and resurvey bank lines) at Camp Cardinal.

Erosion length (cm) after the August 27th event (cm) at Site 2			
		PEEP SENSORS	
	Survey	Automated	Manual measurement with tape
PEEP A2	23.9	23.7	20.5
PEEP L231	4.3	5.7	6.2
PEEP A1	8.7	10.6	12.0
PEEP A4	16.6	11.6	11.5
Bank cross-section survey before the event : July 30th			
Bank cross-section survey after the event : September 30th			

CHAPTER 5. CONCLUSION

5.1 Summary

Cohesive streambank erosion is characterized by two main mechanisms, fluvial entrainment of individual particles and bank failure due to gravity (Thorne, 1980). In this study, the relative importance of fluvial erosion (compared to mass failure) was determined in two reaches from different locations of the Clear Creek Watershed (CCW). The first study reach (Site 1) was located in the agricultural headwater system of the watershed (i.e. downstream the confluence of two first order streams). Due to highly episodic, flashy flows, mass failure was expected to be the dominant erosion process. The second reach (Site 2) is a fourth-order stream and flows in an urban area near the mouth of the watershed. This site experiences more sustained, higher flows and frequent erosion events. Fluvial erosion was expected to be the main erosion process at Site 2.

Bank erosion was monitored between May 2009 and December 2009 using the continuously monitoring PEEPs and more traditional methods (e.g., geodetic channel surveys and standard erosion pins). This period contained two significant runoff events on June 19 and August 27, 2009. The PEEPs provided detailed time series of bank retreat during the study period. Statistical methods were applied to the time series data and included the application of a moving average complemented with Shewhart analyses and autocorrelation methods. The data statistics helped elucidate the dominant erosion processes occurring at both sites in CCW.

The main goal of the project was the identification of the key erosion process at each site. Beyond the distinguished flow conditions (hydraulic forces), different stream orders, and land-use, no further attempts were made to identify other key driving agents behind the erosion, such subaerial processes (e.g., seepage, freeze/thaw) acting at the cohesive riverbanks (Lindow et al., 2009).

At Site 1, the flash flood of June 19, 2009 produced significant, mass failure of the channel banks, especially at the bank crest and mid-section. Bank retreats of ~ 25 cm were measured with the highest erosion rate being observed at the mid-section of the bank. The high erosion at the bank midsection over-steepened the bank height making the bank more susceptible to mass failure and slumping. Similar findings were presented in the literature (Harden et al., 2009; Lawler et al., 1999).

At Site 2, flow was often higher than at Site 1 providing favorable conditions for more continuous fluvial erosion punctuated with irregular bank slumping. Erosion lengths up to 38 cm were detected at Site 2. The bank erosion monitoring at high resolution intervals due to the PEEPS allowed for better characterization the fluvial erosion occurring at this site and develop a correspondence between sedigraphs and hydrographs. .Similar statistical methods were used at both sites to support our findings. The moving average identified the dominant trend of the data and the variability of the erosion lengths at the two sites. Further, the use of the Shewhart Charts allowed us to detect the critical erosion events during the period of observation. For example, at Site 1 after the June 19th event, the PEEP data from the bank crest remained outside of the control limits supporting the high erosion lengths recorded by the PEEP at this location and corresponding visual observations. At Site 2 despite the relatively higher erosion lengths, all data remained in the control limits of the Shewhart Chart suggesting that no rare event occurred at Site 2. The autocorrelation techniques showed seasonality in the data at Site 2 while at Site 1 the autocorrelation showed non-stationarity in the dataset due to the flashy nature of the flow and bank geometry.

Finally the overall performance of the PEEPs was evaluated during this study. A correlation analysis was conducted between the direct measurements of traditional methods (e.g., erosion pins, geodetical surveys, measure tape) and the automated data recorded by the PEEP. The maximum error between manual and automated measurements of the exposed length of the PEEPs was observed at site 1 and this error

was less than 27%. The error between the channel survey and the automated PEEP measurements was less than 14%.

One key limitation of the PEEPs was their inability to record data while submerged. To our best knowledge, no statistical evaluation of this limitation has been published. The correlation between the submerged and unsubmerged data revealed that R^2 was higher for PEEPs at higher elevations above the free surface; i.e., the PEEPs located at the bank mid-section or crest performed better than the PEEPs near the bank toe.

Despite the above limitation, the PEEPs captured well the timing and magnitude of specific erosion events at both sites. The PEEPs present several advantages such as straightforward installation and application. Moreover, maintenance was limited to clearing debris, or leaves, that covered the photo-voltaic cells. Overall, the PEEPS appeared to be relatively robust instruments.

5.2 Future directions and recommendations

Still being relatively new, PEEPs need further development and more research to understand their full potential. PEEPs, which are driven by sunlight, are limited to daytime uses. The addition of thermistors on newer models may help solve the problem of nocturnal data. Lawler (2001) proposed the thermistors to overcome this limitation by using the Thermal Consonance Timing concept or to use an artificial light for the nocturnal data (Lawler, 2005a). The photovoltaic cells could be used during the day and the thermistors during night or even when the instrument is submerged.

Another hurdle in this study was the fact that the PEEPs were sensitive to any source that provoked a change in light intensity such as debris, snow, vegetation or submergence. Previous papers (Lawler, 2005b; Mitchell et al., 1999) have used the daily mean of the lateral erosion length measure. Developing thresholds for the light intensity

for all of these factors will facilitate the wider use of PEEPs by a broad range of applicants.

Lastly, proper calibration of the instrument was important in obtaining accurate erosion lengths. Calibration of the PEEPs within the banks nearby the study reach provided the most accurate erosion lengths. In addition, comparison with traditional, manual methods is recommended.

In conclusion, the capability of the instrument was remarkable. The PEEPs provided real-time monitoring of erosion events in terms of magnitude and frequency, which is not possible with the manual where only net changes from previous measurements are known. This real-time monitoring coupled with the automated nature of the instrument makes it ideal for certain sites that are not easy to access on a continuous basis. Automated and continuous real-time bank erosion data are in great needs. The PEEPs provide valuable data on the timing of individual bank erosion events, especially the time lag between the peak erosion and the peak of the hydrograph. This information is of great importance to the field of geomorphology, as well as to numerical model such as CONCEPTS (Langendoen and Alonso, 2008), which address contributions of bank erosion to the total sediment load of streams.

APPENDIX A PROGRAM SET-UP

Before running the calibration procedure (or in order to monitor the bank erosion data), a program was created and sent to the datalogger. Short Cut (version 2.5), a programming wizard, permitted to create the data logger program. Because of the different PEEP models used in this study, two different programs were completed. For the photovoltaic PEEPs, a differential voltage reading was used. It permitted voltage measurements between the high and the low inputs, into a differential channel. However, for the photo-resistance PEEPs, a half bridge program was used. It allowed an excitation voltage to be sent across the wires through the resistors (Campbell Scientific, 2006). The programs were entitled "PEEP_01" for the photovoltaic PEEPs and "PEEP_HB" for the photo-resistance PEEPs.

Following the steps below, the programs could be facilely created:

1. Open Short Cut
2. Select "new program" or "open a program" to edit
3. Select the appropriate data logger model (e.g., CR800 and CR1000)
4. Select the interval time (e.g., 15 minutes) at which the measurement will be made.
5. Choose the appropriate program for the sensors. For the photo-resistance PEEPs, the following selection was made: "Generic measurements"→"Half Bridge" → 2 Half Bridge sensors → Input the different parameters. For the photovoltaic PEEPs: "Generic measurements"→"Differential Voltage" → "3 Differentials voltage sensors" → Half Bridge sensors → Input the different parameters. Figures A.1 and A.2 show the specifications respectively for "PEEP_HB" and "PEEP_01".
6. Select and add the output table that will allow monitoring the data (Figure A.3). Click next.

7. Save the program, and click “Finish” if satisfied. Figures A.4 (a) and (b) give an example respectively of the wiring diagram and wiring text for the photo-resistance PEEPs. Figures A.5 (a) and (b) show the same information for the photovoltaic PEEPs.

The program has to be set up according to the expected data and the wiring panel available.

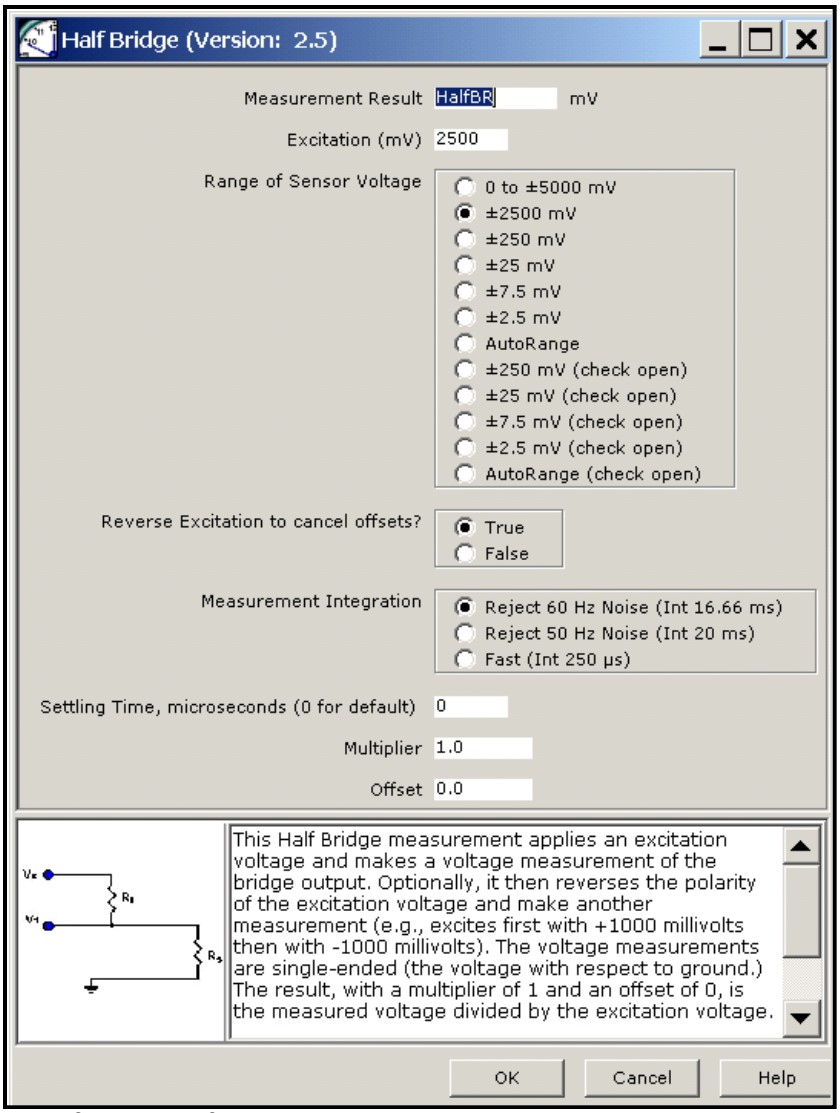

Figure A.1: Specifications of the program PEEP_HB

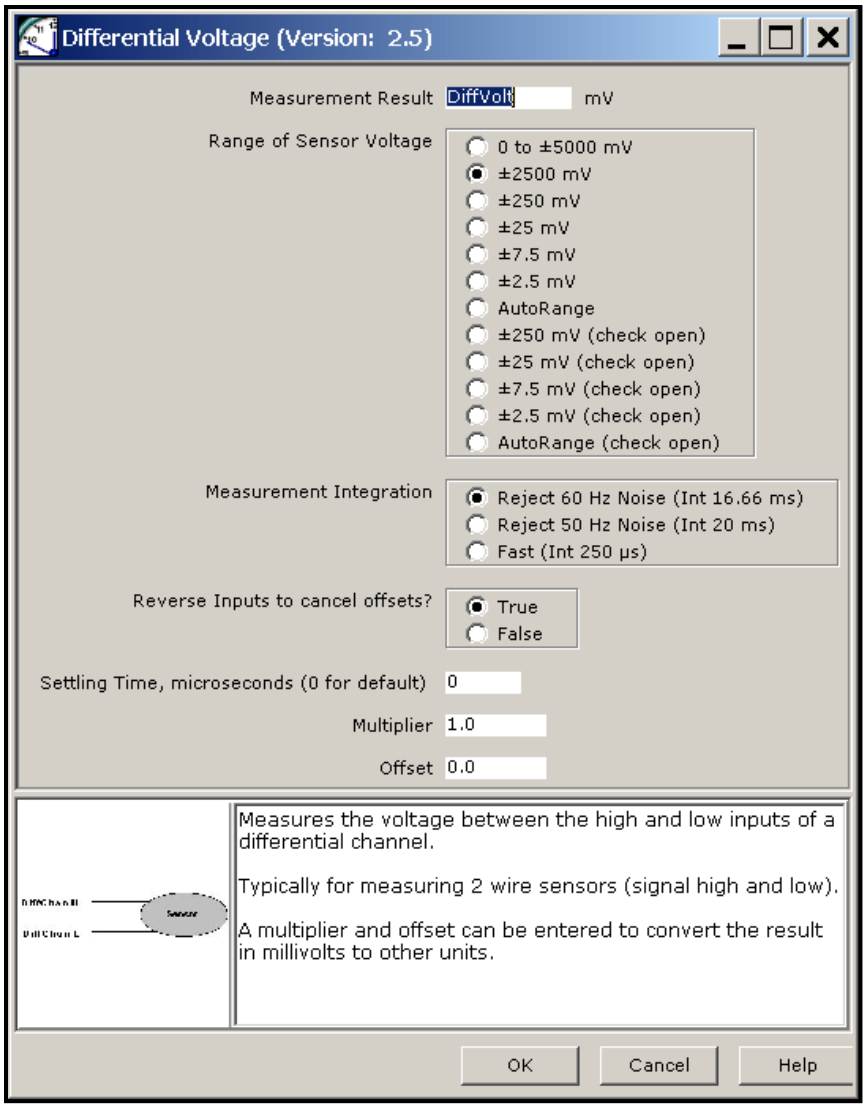

Figure A.2: Specifications of the program PEEP_01

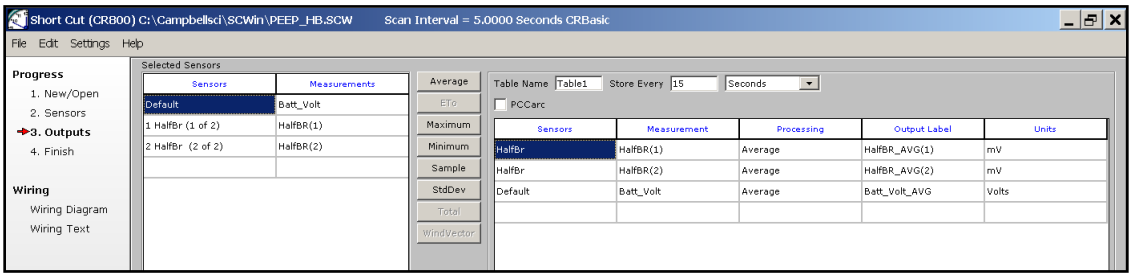

Figure A.3: Example of an output table of the data

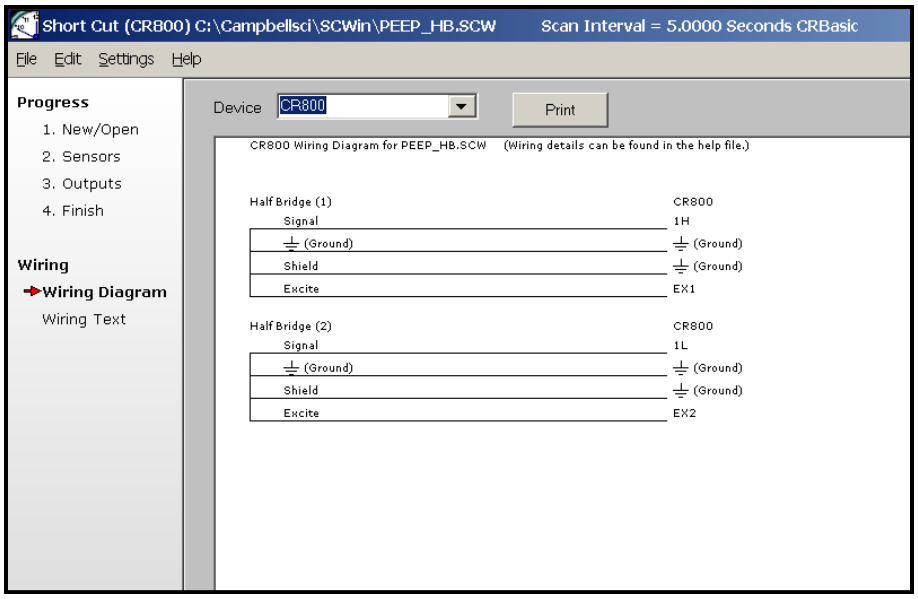

(a)

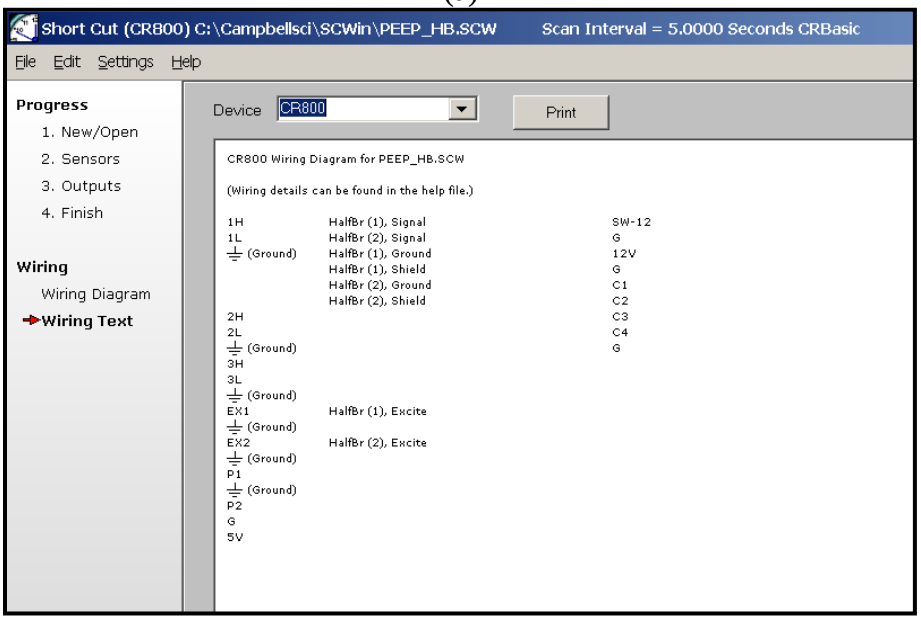

(b)

Figure A.4: Example of the wiring for the program used for the photo-resistance sensors (PEEP_HB)

(a) Wiring diagram
(b) Wiring text

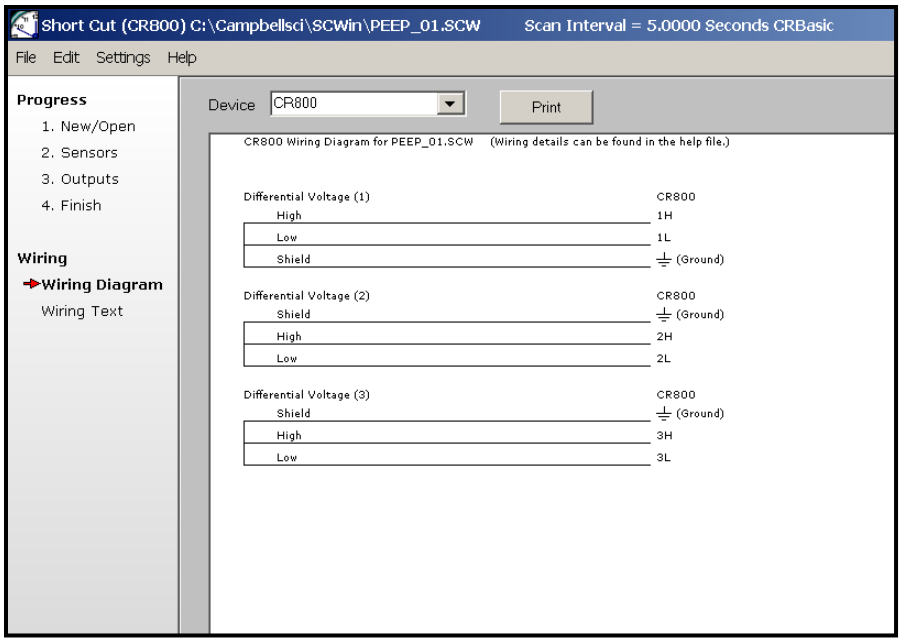

(a)

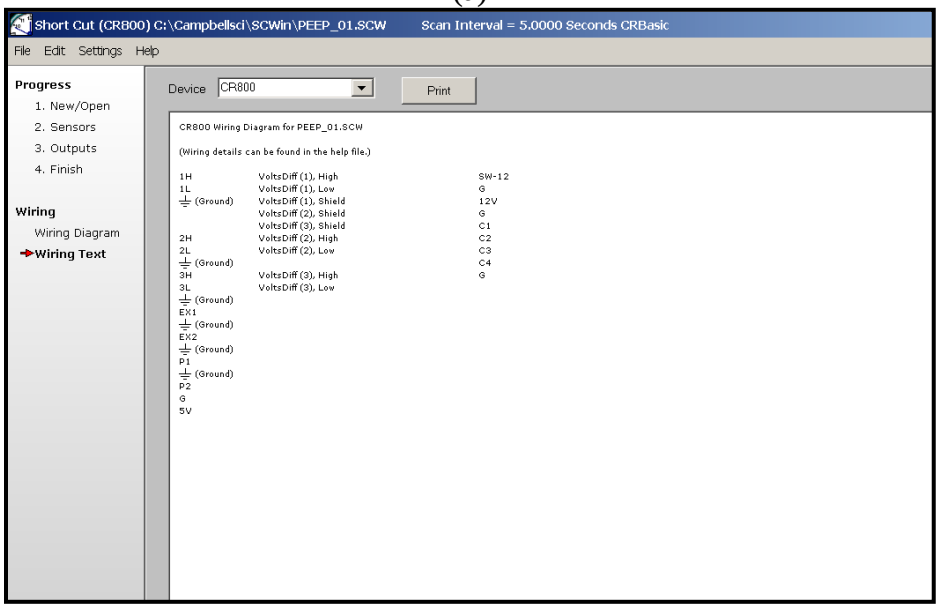

(b)

Figure A.5: : Example of the wiring for the program used for the photovoltaic sensors (PEEP_01).

(a) Wiring diagram

(b) Wiring text

APPENDIX B CODES

B1. CODE FOR THE PEEP_HB

```
'CR800
'Created by Short Cut (2.5)

'Declare Variables and Units
Public Batt_Volt
Public DiffVolt(3)

Units Batt_Volt=Volts
Units DiffVolt=mV

'Define Data Tables
DataTable(Table1,True,-1)
	DataInterval(0,15,Min,10)
	Average(1,DiffVolt(1),FP2,False)
	Average(1,DiffVolt(2),FP2,False)
	Average(1,DiffVolt(3),FP2,False)
	Average(1,Batt_Volt,FP2,False)
EndTable

'Main Program
BeginProg
	Scan(15,min,1,0)
		'Default Datalogger Battery Voltage measurement Batt_Volt:
		Battery(Batt_Volt)
		'Generic Differential Voltage measurements DiffVolt(1):
		VoltDiff(DiffVolt(1),3,mV250,1,True,0,_60Hz,1.0,0.0)
		'Call Data Tables and Store Data
		CallTable(Table1)
	NextScan

	EndProg
```

B2. CODE FOR THE PEEP_HB

```
'CR800
'Created by Short Cut (2.5)

'Declare Variables and Units
Public Batt_Volt
```

```
Public HalfBR(2)

Units Batt_Volt=Volts
Units HalfBR=mV

'Define Data Tables
DataTable(Table1,True,-1)
	DataInterval(0,15,Min,10)
	Average(1,HalfBR(1),FP2,False)
	Average(1,HalfBR(2),FP2,False)
	Average(1,Batt_Volt,FP2,False)
EndTable

'Main Program
BeginProg
	Scan(15,Min,1,0)
		'Default Datalogger Battery Voltage measurement Batt_Volt:
		Battery(Batt_Volt)
		'Generic Half Bridge measurements HalfBR(1):
		BrHalf(HalfBR(1),2,mV2500,1,1,1,2500,True,0,250,1.0,0.0)
		'Call Data Tables and Store Data
		CallTable(Table1)
	NextScan

	EndProg
```

APPENDIX C PROGRAMMING THE DATA LOGGER

Two Campbell Scientific data loggers (CR800 and CR1000), or DL, were used to store the data. The DL contains 6 single-ended (SE 1 – SE 6) or 3 differential (DIFF 1 – DIFF 3) analogs input. The accompanying software (PC200W) is designed for users dealing with simple data. It provides the connection between the DL and PEEPs allowing for instrument monitoring and data transfer. PC200W (version 3.3) runs on Windows XP, Vista and 2000 and can be downloaded for free on the company website using this link: http://www.campbellsci.com/2_716_14_1.

1. Turn on the PC and DL (ON-OFF button on battery)
2. Connect the PC to the DL using the RS232 Serial cable
3. Launch PC200W
4. Select "Connect" to make the connection with the datalogger (upper right of the PC200W window). Be sure the appropriate DL name has been selected. In this case, the desired DL is "5242"
5. Click on "Send program" and browse for the program created in the output location. Select it and send it to the DL. Hence, the DL has the program and will monitor and record the data according to the configuration of the program (Figure C.1).
6. Monitor tab
7. Collect data
8. Turn OFF

Once the program is sent to the data logger, it is not necessary to redo this procedure before any experiment unless a different program has been used with the DL.

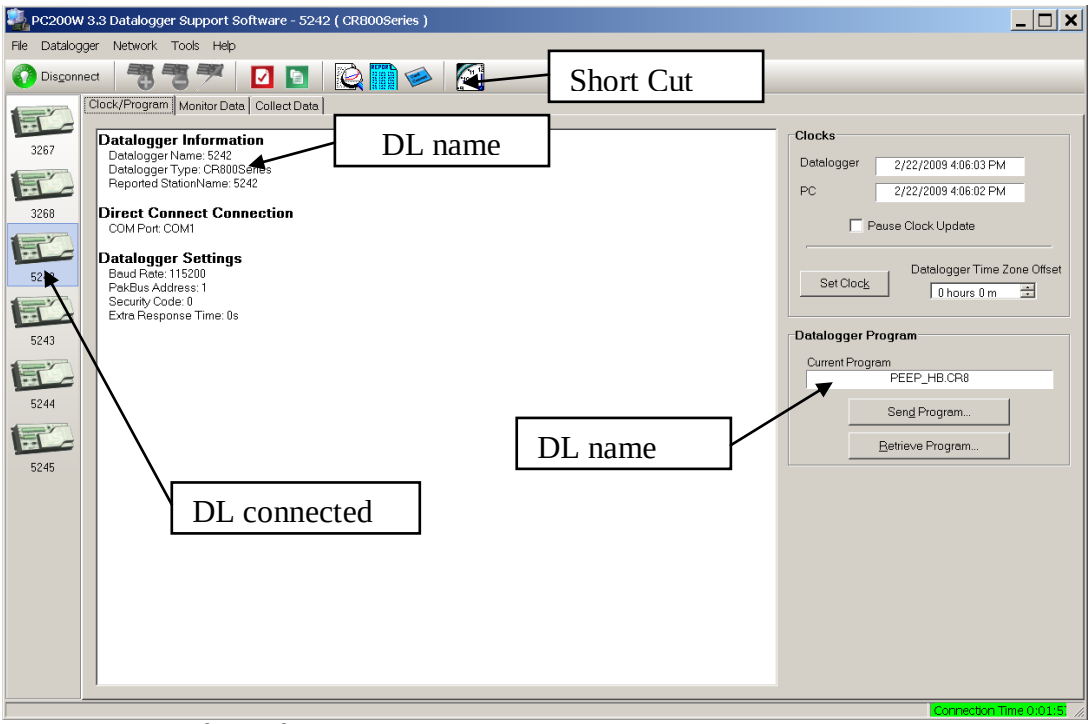

Figure C.1: : Interface of the Program PC200W

REFERENCES

Abaci, O., Papanicolaou, A.N.T., 2009. Long-term effects of management practices on water-driven soil erosion in an intense agricultural sub-watershed: monitoring and modelling. Hydrological Processes, 23(19): 2818-2837.

Aberle, J. et al., 2003. Straight benthic flow-through flume for in situ measurement of cohesive sediment dynamics. Journal of Hydraulic Engineering-Asce, 129(1): 63-67.

Abernethy, B., Rutherfurd, I.D., 1998. Where along a river's length will vegetation most effectively stabilise stream banks? Geomorphology, 23(1): 55-75.

Abernethy, B., Rutherfurd, I.D., 2000. The effect of riparian tree roots on the mass-stability of riverbanks. Earth Surface Processes and Landforms, 25(9): 921-937.

Amos, C.L., Grant, J., Daborn, G.R., Black, K., 1992. SEA CAROUSEL - A BENTHIC, ANNULAR FLUME. Estuarine Coastal and Shelf Science, 34(6): 557-577.

Arulanandan, K., 1975. FUNDAMENTAL ASPECTS OF EROSION OF COHESIVE SOILS. Journal of the Hydraulics Division-Asce, 101(NHY5): 635-639.

Arulanandan, K., Gillogley, E., Tully, R., 1980. Development of a quantitative method to predict critical shear stress and rate of erosion of natural undisturbed cohesive soils, Vicksburg, MS.

Bartley, R. et al., 2008. Bank erosion and channel width change in a tropical catchment. Earth Surface Processes and Landforms, 33(14): 2174-2200.

Black, K., Cramp, A., 1995. A DEVICE TO EXAMINE THE IN-SITU RESPONSE OF INTERTIDAL COHESIVE SEDIMENT DEPOSITS TO FLUID SHEAR. Continental Shelf Research, 15(15): 1945-1954.

Black, K.S., Paterson, D.M., 1997. Measurement of the erosion potential of cohesive, marine sediments: a review of current in situ technology. Journal of Marine Environmental Engineering, 4: 43–84.

Burkart, M.R., Oberle, S.L., Hewitt, M.J., Pickus, J., 1994. A FRAMEWORK FOR REGIONAL AGROECOSYSTEMS CHARACTERIZATION USING THE NATIONAL RESOURCES INVENTORY. Journal of Environmental Quality, 23(5): 866-874.

Campbell Scientific, I., 2006. Operator's Manual, CR800/CR850 Measurement and Control System.

Cao, S.Y., Knight, D.W., 1997. Entropy-based design approach of threshold alluvial channels. Journal of Hydraulic Research, 35(4): 505-524.

Cao, S.Y., Knight, D.W., 1998. Design for hydraulic geometry of alluvial channels. Journal of Hydraulic Engineering-Asce, 124(5): 484-492.

Casagli, N., Rinaldi, M., Gargini, A., Curini, A., 1999. Pore water pressure and streambank stability: Results from a monitoring site on the Sieve River, Italy. Earth Surface Processes and Landforms, 24(12): 1095-1114.

Chatfield, C., 1984. The Analysis of Time Series An Introduction. Chapman and Hall, London.

Clark, L.A., Wynn, T.M., 2007. Methods for determining streambank critical shear stress and soil erodibility: Implications for erosion rate predictions. Transactions of the Asabe, 50(1): 95-106.

Couper, P., Stott, T., Maddock, I., 2002. Insights into river bank erosion processes derived from analysis of negative erosion-pin recordings: Observations from three recent UK studies. Earth Surface Processes and Landforms, 27(1): 59-79.

Couper, P.R., Maddock, I.P., 2001. Subaerial river bank erosion processes and their interaction with other bank erosion mechanisms on the river arrow, Warwickshire, UK. Earth Surface Processes and Landforms, 26(6): 631-646.

Couperthwaite, J.S., Mitchell, S.B., West, J.R., Lawler, D.M., 1998. Cohesive sediment dynamics on an inter-tidal bank on the tidal trent, UK. Marine Pollution Bulletin, 37(3-7): 144-154.

Dapporto, S., Rinaldi, M., Casagli, N., 2001. Failure mechanisms and pore water pressure conditions: analysis of a riverbank along the Arno River (Central Italy). Engineering Geology, 61(4): 221-242.

Darby, S.E., Rinaldi, M., Dapporto, S., 2007. Coupled simulations of fluvial erosion and mass wasting for cohesive river banks. Journal of Geophysical Research-Earth Surface, 112(F3): 15.

Denn, K.D., 2009. Sediment Budget Closure During Runoff-Generated High Flow Events in South Amana Subwatershed, IA, The University of Iowa, Iowa City.

Diplas, P., 1990. CHARACTERISTICS OF SELF-FORMED STRAIGHT CHANNELS. Journal of Hydraulic Engineering-Asce, 116(5): 707-728.

Diplas, P., Vigilar, G., 1992. HYDRAULIC GEOMETRY OF THRESHOLD CHANNELS. Journal of Hydraulic Engineering-Asce, 118(4): 597-614.

Duan, J.G., 2005. Analytical approach to calculate rate of bank erosion. Journal of Hydraulic Engineering-Asce, 131(11): 980-990.

Effler, S.W., 1988. SECCHI DISK TRANSPARENCY AND TURBIDITY. Journal of Environmental Engineering-Asce, 114(6): 1436-1447.

Effler, S.W., Peng, F., Gelda, R.K., 2007. Size distributions and light scattering features of minerogenic particles in a stream during runoff events. Journal of Environmental Engineering-Asce, 133(9): 931-940.

Fox, G.A. et al., 2007. Measuring streambank erosion due to ground water seepage: correlation to bank pore water pressure, precipitation and stream stage. Earth Surface Processes and Landforms, 32: 1558-1573.

Fox, J.F., Papanicolaou, A.N., Kjos, L., 2005. Eddy taxonomy methodology around a submerged barb obstacle within a fixed rough bed. Journal of Engineering Mechanics-Asce, 131(10): 1082-1101.

Gilley, J.E., Elliot, W.J., Laflen, J.M., Simanton, J.R., 1993. CRITICAL SHEAR-STRESS AND CRITICAL FLOW-RATES FOR INITIATION OF RILLING. Journal of Hydrology, 142(1-4): 251-271.

Global Water Instrumentation, I., 2009. WL-16 Water Level Logger, Gold River, CA.

Glover, R.E., Florey, Q.L., 1951. Stable channel profiles, US Bureau of Reclamation, Washington DC.

Grissinger, E.H., 1982. Bank erosion of cohesive materials, Gravel-bed Rivers. John Wiley & Sons, Chichester, UK, pp. 273-287.

Guo, J., Julien, P.Y., 2005. Shear stress in smooth rectangular open-channel flows. Journal of Hydraulic Engineering-Asce, 131(1): 30-37.

Gust, G., Morris, M.J., 1989. Erosion thresholds and entrainment rates of undisturbed in situ sediments. Journal of Coastal Research, 5: 87-99.

Hancock, G.R., Murphy, D., Evans, K.G., 2010. Hillslope and catchment scale soil organic carbon concentration: An assessment of the role of geomorphology and soil erosion in an undisturbed environment. Geoderma, 155(1-2): 36-45.

Hanson, G.J., 1991. DEVELOPMENT OF A JET INDEX TO CHARACTERIZE EROSION RESISTANCE OF SOILS IN EARTHEN SPILLWAYS. Transactions of the Asae, 34(5): 2015-2020.

Hanson, G.J., Simon, A., 2001. Erodibility of cohesive streambeds in the loess area of the midwestern USA. Hydrological Processes, 15(1): 23-38.

Harden, C.P., Foster, W., Morris, C., Chartrand, K.J., Henry, E., 2009. RATES AND PROCESSES OF STREAMBANK EROSION IN TRIBUTARIES OF THE LITTLE RIVER, TENNESSEE. Physical Geography, 30(1): 1-16.

Harmel, R.D., Haan, C.T., Dutnell, R., 1999. Bank erosion and riparian vegetation influences: Upper Illinois River, Oklahoma. Transactions of the Asae, 42(5): 1321-1329.

Hilldale, R., 2001. Fluvial Erosion of Cohesive Banks Considering Turbulence and Secondary Flow, Washington State University.

Hooke, J.M., 1979. ANALYSIS OF THE PROCESSES OF RIVER BANK EROSION. Journal of Hydrology, 42(1-2): 39-62.

Hooke, J.M., 1980. MAGNITUDE AND DISTRIBUTION OF RATES OF RIVER BANK EROSION. Earth Surface Processes and Landforms, 5(2): 143-157.

Horn, D.P., Lane, S.P.H., 2006. Measurement of high-frequency bed level changes in the swash zone using Photo-Electronic Erosion Pin (PEEPS), International Conference on Coastal Engineering, San Diego, pp. 2591-2603.

Houwing, E.J., van Rijn, L.C., 1998. In Situ Erosion Flume (ISEF): determination of bed-shear stress and erosion of a kaolinite bed. Journal of Sea Research, 39(3-4): 243-253.

Hydro Scientific, L., 2004. The Photo-Electronic Erosion Pin (PEEP) system : User Guide, for Models PEEP 110, 200, and P-Lite 200. Hydro Scientific Ltd, Warwickshire.

Ikeda, S., 1981. SELFFORMED STRAIGHT CHANNELS IN SANDY BEDS. Journal of the Hydraulics Division-Asce, 107(4): 389-406.

Ikeda, S., Izumi, N., 1991. STABLE CHANNEL CROSS-SECTIONS OF STRAIGHT SAND RIVERS. Water Resources Research, 27(9): 2429-2438.

Ikeda, S., Parker, G., Kimura, Y., 1988. STABLE WIDTH AND DEPTH OF STRAIGHT GRAVEL RIVERS WITH HETEROGENEOUS BED MATERIALS. Water Resources Research, 24(5): 713-722.

Julian, J.P., Torres, R., 2006. Hydraulic erosion of cohesive riverbanks. Geomorphology, 76(1-2): 193-206.

Kandiah, A., 1974. Fundamental aspects of surface erosion of cohesive soils, University of California, Davis.

Keesstra, S.D., Bruijnzeel, L.A., van Huissteden, J., 2009. Meso-scale catchment sediment budgets: combining field surveys and modeling in the Dragonja catchment, southwest Slovenia. Earth Surface Processes and Landforms, 34(11): 1547-1561.

Kennedy, E.J., 1984. Discharge ratings at gauging stations, 59. United States Government Printing Office, Washington, D.C.

Korpela, I., Koskinen, M., Vasander, H., Holopainen, M., Minkkinen, K., 2009. Airborne small-footprint discrete-return LiDAR data in the assessment of boreal mire surface patterns, vegetation, and habitats. Forest Ecology and Management, 258(7): 1549-1566.

Langendoen, E.J., Alonso, C.V., 2008. Modeling the evolution of incised streams: I. Model formulation and validation of flow and streambed evolution components. Journal of Hydraulic Engineering-Asce, 134(6): 749-762.

Langendoen, E.J., Lowrance, R.R., Simon, A., 2009. Assessing the impact of riparian processes on streambank stability. Ecohydrology, 2(3): 360-369.

Lau, Y.L., Droppo, I.G., Krishnappan, B.G., 2001. Sequential erosion/deposition experiments - Demonstrating the effects of depositional history on sediment erosion. Water Research, 35(11): 2767-2773.

Lawler, D.M., 1991. A NEW TECHNIQUE FOR THE AUTOMATIC MONITORING OF EROSION AND DEPOSITION RATES. Water Resources Research, 27(8): 2125-2128.

Lawler, D.M., 1992. DESIGN AND INSTALLATION OF A NOVEL AUTOMATIC EROSION MONITORING-SYSTEM. Earth Surface Processes and Landforms, 17(5): 455-463.

Lawler, D.M., 1993a. NEEDLE ICE PROCESSES AND SEDIMENT MOBILIZATION ON RIVER BANKS - THE RIVER ILSTON, WEST-GLAMORGAN, UK. Journal of Hydrology, 150(1): 81-114.

Lawler, D.M., 1993b. The Measurement of River Bank Erosion and Lateral Channel Change - A review Earth Surface Processes and Landforms, 18(9): 777-821.

Lawler, D.M., 2005a. Defining the moment of erosion: the principle of thermal consonance timing. Earth Surface Processes and Landforms, 30(13): 1597-1615.

Lawler, D.M., 2005b. The importance of high-resolution monitoring in erosion and deposition dynamics studies: examples from estuarine and fluvial systems. Geomorphology, 64(1-2): 1-23.

Lawler, D.M., 2008. Advances in the continuous monitoring of erosion and deposition dynamics: Developments and applications of the new PEEP-3T system. Geomorphology, 93(1-2): 17-39.

Lawler, D.M., Couperthwaite, J., Bull, L.J., Harris, N.M., 1997a. Bank erosion events and processes in the Upper Severn basin. Hydrology and Earth System Sciences,: 523-534.

Lawler, D.M., Grove, J.R., Couperthwaite, J.S., Leeks, G.J.L., 1999. Downstream change in river bank erosion rates in the Swale-Ouse system, northern England. Hydrological Processes, 13(7): 977-992.

Lawler, D.M., Thorne, C.R., Hooke, J.M., 1997b. Bank erosion and instability. Applied Fluvial Geomorphology for River Engineering and Management: 137-172.

Lawler, D.M., West, J.R., Couperthwaite, J.S., Mitchell, S.B., 2001. Application of a novel automatic erosion and deposition monitoring system at a channel bank site on the tidal river Trent, UK. Estuarine Coastal and Shelf Science, 53(2): 237-247.

Lin, S.Y., Zou, T., Gao, H.W., Guo, X.Y., 2009. The vertical attenuation of irradiance as a function of turbidity: a case of the Huanghai (Yellow) Sea in spring. Acta Oceanologica Sinica, 28(5): 66-75.

Lindow, N., Fox, G.A., Evans, R.O., 2009. Seepage erosion in layered stream bank material. Earth Surface Processes and Landforms, 34(12): 1693-1701.

Loperfido, J.V., 2009. High-frequency sensing of clear creek water quality: mechanisms of dissolved oxygen and turbidity dynamics, and nutrient transport, Iowa City.

Loperfido, J.V., Just, C.L., Schnoor, J.L., 2009. High-Frequency Diel Dissolved Oxygen Stream Data Modeled for Variable Temperature and Scale. Journal of Environmental Engineering-Asce, 135(12): 1250-1256.

Maa, J.P.Y., Wright, L.D., Lee, C.H., Shannon, T.W., 1993. VIMS SEA CAROUSEL - A FIELD INSTRUMENT FOR STUDYING SEDIMENT TRANSPORT. Marine Geology, 115(3-4): 271-287.

McDermott, J.P., Sherman, D.J., 2009. Using Photo-Electronic Erosion Pins for Measuring Bed Elevation Changes in the Swash Zone. Journal of Coastal Research: 788–792.

McNeil, J., Taylor, C., Lick, W., 1996. Measurements of erosion of undisturbed bottom sediments with depth. Journal of Hydraulic Engineering-Asce, 122(6): 316-324.

Millar, R.G., 2000. Influence of bank vegetation on alluvial channel patterns. Water Resources Research, 36(4): 1109-1118.

Millar, R.G., Quick, M.C., 1998. Stable width and depth of gravel-bed rivers with cohesive banks. Journal of Hydraulic Engineering-Asce, 124(10): 1005-1013.

Mironenko, A.P., Willardson, L.S., Jenab, S.A., 1984. PARABOLIC CANAL DESIGN AND ANALYSIS. Journal of Irrigation and Drainage Engineering-Asce, 110(2): 241-246.

Mitchell, S.B., Couperthwaite, J.S., West, J.R., Lawler, D.M., 1999. Dynamics of erosion and deposition events on an intertidal mudbank at Burringham, River Trent, UK. Hydrological Processes, 13(7): 1155-1166.

Mitchell, S.B., Couperthwaite, J.S., West, J.R., Lawler, D.M., 2003. Measuring sediment exchange rates on an intertidal bank at Blacktoft, Humber Estuary, UK. Science of the Total Environment, 314: 535-549.

Mitchener, H., Torfs, H., 1996. Erosion of mud/sand mixtures. Coastal Engineering, 29(1-2): 1-25.

Notebaert, B., Verstraeten, G., Govers, G., Poesen, J., 2009. Qualitative and quantitative applications of LiDAR imagery in fluvial geomorphology. Earth Surface Processes and Landforms, 34(2): 217-231.

Odgaard, A.J., 1987. STREAMBANK EROSION ALONG 2 RIVERS IN IOWA. Water Resources Research, 23(7): 1225-1236.

Papanicolaou, A.N., Abaci, O., 2008. Upland Erosion Modeling in a Semihumid Environment via the Water Erosion Prediction Project Model. Journal of Irrigation and Drainage Engineering-Asce, 134(6): 796-806.

Papanicolaou, A.N., Dey, S., Rinaldi, M., Mazumdar, A., 2006. Research Issues for Riverine Bank Stability Analysis in the 21st Century, Iowa City.

Papanicolaou, A.N., Elhakeem, M., Hilldale, R., 2007. Secondary current effects on cohesive river bank erosion. Water Resources Research, 43(12).

Papanicolaou, A.N., Hilldale, R., 2001. Erosion of Streams with Cohesive banks, Pullman, WA.

Papanicolaou, A.N., Hilldale, R., 2002. Turbulence characteristics in gradual channel transition. Journal of Engineering Mechanics-Asce, 128(9): 948-960.

Papanicolaou, T., Wilson, C., Dermisis, D., 2008. The effects of headcut and knickpoint propagation on bridges in Iowa, Iowa City.

Parchure, T.M., Mehta, A.J., 1985. EROSION OF SOFT COHESIVE SEDIMENT DEPOSITS. Journal of Hydraulic Engineering-Asce, 111(10): 1308-1326.

Parker, G., 1978. SELF-FORMED STRAIGHT RIVERS WITH EQUILIBRIUM BANKS AND MOBILE BED .2. GRAVEL RIVER. Journal of Fluid Mechanics, 89(NOV): 127-&.

Parker, G., 1979. HYDRAULIC GEOMETRY OF ACTIVE GRAVEL RIVERS. Journal of the Hydraulics Division-Asce, 105(9): 1185-1201.

Partheniades, E., Kennedy, J.F., 1966. Depositional behavior of fine sediment in a turbulent fluid motion, Proc. 10th Conference on Coastal Engineering, Tokyo, pp. 707-724.

Paterson, D.M., 1989. Short term changes in the erodibility of intertidal cohesive sediments related to the migratory behaviour of epipelic diatoms. Limnology and Oceanography, 34(1): 223-234.

Pierce, T.J., Jarman, R.T., de Turville, C.M., 1970. An experimental study of silt scouring, Institution of Civil Engineers, pp. 231-243.

Pizzuto, J., 2009. An empirical model of event scale cohesive bank profile evolution. Earth Surface Processes and Landforms, 34(9): 1234-1244.

Pizzuto, J., O'Neal, M., Stotts, S., 2010. On the retreat of forested, cohesive riverbanks. Geomorphology, 116(3-4): 341-352.

Pizzuto, J.E., 1990. NUMERICAL-SIMULATION OF GRAVEL RIVER WIDENING. Water Resources Research, 26(9): 1971-1980.

Prosser, I.P., Hughes, A.O., Rutherfurd, I.D., 2000. Bank erosion of an incised upland channel by subaerial processes: Tasmania, Australia. Earth Surface Processes and Landforms, 25(10): 1085-1101.

Ravens, T.M., Gschwend, P.M., 1999. Flume measurements of sediment erodibility in Boston Harbor. Journal of Hydraulic Engineering-Asce, 125(10): 998-1005.

Rayburn, A.R., Schulte, L.A., 2009. Landscape change in an agricultural watershed in the US Midwest. Landscape and Urban Planning, 93(2): 132-141.

Rinaldi, M., Casagli, N., 1999. Stability of streambanks formed in partially saturated soils and effects of negative pore water pressures: the Sieve River (Italy). Geomorphology, 26(4): 253-277.

Rinaldi, M., Casagli, N., Dapporto, S., Gargini, A., 2004. Monitoring and modelling of pore water pressure changes and riverbank stability during flow events. Earth Surface Processes and Landforms, 29(2): 237-254.

Roberts, J.D., Jepsen, R.A., James, S.C., 2003. Measurements of sediment erosion and transport with the adjustable shear stress erosion and transport flume. Journal of Hydraulic Engineering-Asce, 129(11): 862-871.

Roca, M., Blanckaert, K., Martín-Vide, J.P., 2009. Reduction of Bend Scour by an Outer Bank Footing: Flow Field and Turbulence. JOURNAL OF HYDRAULIC ENGINEERING: 361–368.

Saynor, M.J., Erskine, W.D., 2006. Spatial and temporal variations in bank erosion on sand-bed streams in the seasonally wet tropics of northern Australia. Earth Surface Processes and Landforms, 31(9): 1080-1099.

Schilling, K.E., Wolter, C.F., 2000. Application of GPS and GIS to map channel features in Walnut Creek, Iowa. Journal of the American Water Resources Association, 36(6): 1423-1434.

Schünemann, M., Kühl, H., 1993. Experimental investigations of the erosional behaviour of naturally formed mud from the Elbe Estuary and adjacent Wadden Sea. Nearshore and Estuarine Cohesive Sediment Transport, 42: 314-330.

Simon, A., Collison, A.J.C., 2001. Pore-water pressure effects on the detachment of cohesive streambeds: Seepage forces and matric suction. Earth Surface Processes and Landforms, 26(13): 1421-1442.

Simon, A., Collison, A.J.C., 2002. Quantifying the mechanical and hydrologic effects of riparian vegetation on streambank stability. Earth Surface Processes and Landforms, 27(5): 527-546.

Simon, A., Curini, A., Darby, S.E., Langendoen, E.J., 2000. Bank and near-bank processes in an incised channel. Geomorphology, 35(3-4): 193-217.

Simon, A., Langendoen, E.J., Thomas, R., 2003. Incorporating Bank-Toe Erosion by Hydraulic Shear into a Bank-Stability Model: Missouri River, Eastern Montana, World Water & Environmental Resources Congress, Philadelphia, pp. 70-76.

Stebbings, J., 1963. The shape of self-formed model alluvial channels, Instn. Civ. Engrs., London, pp. 485-510.

Tamburrino, A., Gulliver, J.S., 1999. Large flow structures in a turbulent open channel flow. Journal of Hydraulic Research, 37(3): 363-380.

Tennekes, H., Lumley, J.L., 1972. A First Course in Turbulence. MIT Press, Cambridge, MA.

Thoma, D.P., Gupta, S.C., Bauer, M.E., Kirchoff, C.E., 2005. Airborne laser scanning for riverbank erosion assessment. Remote Sensing of Environment, 95(4): 493-501.

Thoman, R.W., Niezgoda, S.L., 2008. Determining Erodibility, Critical Shear Stress, and Allowable Discharge Estimates for Cohesive Channels: Case Study in the Powder River Basin of Wyoming. Journal of Hydraulic Engineering-Asce, 134(12): 1677-1687.

Thorne, C.R., 1980. Field measurements of rates of bank erosion and bank material strength, Erosion and Sediment Transport Measurement. IAHS, Florence, pp. 503-512.

Thorne, C.R., 1982. Processes and mechanisms of river bank erosion. In: Hey, R.D., Bathurst, J.C., Thorne, C.R. (Eds.), Gravel-bed rivers. Wiley, Chichester, UK, pp. 227-271.

Thorne, C.R., Hey, R.D., Newson, M.D., 1997. Applied Fluvial Geomorphology for River Engineering and Management. John Wiley and Sons Ltd, Chichester England.

Thorne, C.R., Osman, A.M., 1988. RIVERBANK STABILITY ANALYSIS .2. APPLICATIONS. Journal of Hydraulic Engineering-Asce, 114(2): 151-172.

Thorne, C.R., Tovey, N.K., 1981. STABILITY OF COMPOSITE RIVER BANKS. Earth Surface Processes and Landforms, 6(5): 469-484.

Tolhurst, T.J. et al., 1999. Measuring the in situ erosion shear stress of intertidal sediments with the Cohesive Strength Meter (CSM). Estuarine Coastal and Shelf Science, 49(2): 281-294.

Van Klaveren, R.W., McCool, D.K., 1998. Erodibility and critical shear of a previously frozen soil. Transactions of the Asae, 41(5): 1315-1321.

van Ledden, M., van Kesteren, W.G.M., Winterwerp, J.C., 2004. A conceptual framework for the erosion behaviour of sand-mud mixtures. Continental Shelf Research, 24(1): 1-11.

Westrich, B., Scharf, R., Schürlein, V., 1997. Measurement of cohesive sediment erodibility in a laboratory flume., IAHR Conference, pp. 184-188.

Widdows, J., Brinsley, M.D., Salkeld, P.N., Elliott, M., 1998. Use of annular flumes to determine the influence of current velocity and bivalves on material flux at the sediment-water interface. Estuaries, 21(4A): 552-559.

Wolman, M.G., 1959. FACTORS INFLUENCING EROSION OF A COHESIVE RIVER BANK. American Journal of Science, 257(3): 2042-216.

Wolman, M.G., Brush, L.M., 1959. EXPERIMENTAL-STUDY OF FACTORS CONTROLLING THE SIZE AND SHAPE OF STREAM CHANNELS IN COARSE NONCOHESIVE SANDS. Annals of the Association of American Geographers, 49(2): 220-220.

Wynn, T.M., Mostaghimi, S., 2006. Effects of riparian vegetation on stream bank subaerial processes in southwestern Virginia, USA. Earth Surface Processes and Landforms, 31(4): 399-413.

Young, R.A., 1977. Seaflume: A device for in-situ studies of threshold erosion velocity and erosional behaviour of undisturbed marine muds. Marine Geology, 23: M11-M18.

Yu, G., Knight, D.W., 1998. Geometry of self-formed straight threshold channels in uniform material. Proceedings of the Institution of Civil Engineers-Water and Maritime Engineering, 130(1): 31-41.

Yusoff, F.M.D., 1989. Light Availability for Phytoplankton Production in Turbid Tropical Fish Ponds. Pertanika, 12(3): 329-333.

Zreik, D.A., Krishnappan, B.G., Germaine, J.T., Madsen, O.S., Ladd, C.C., 1998. Erosional and mechanical strengths of deposited cohesive sediments. Journal of Hydraulic Engineering-Asce, 124(11): 1076-1085.